Black Start of an Offshore Wind Power Plant through an MMC based ES-STATCOM System

Master's Thesis

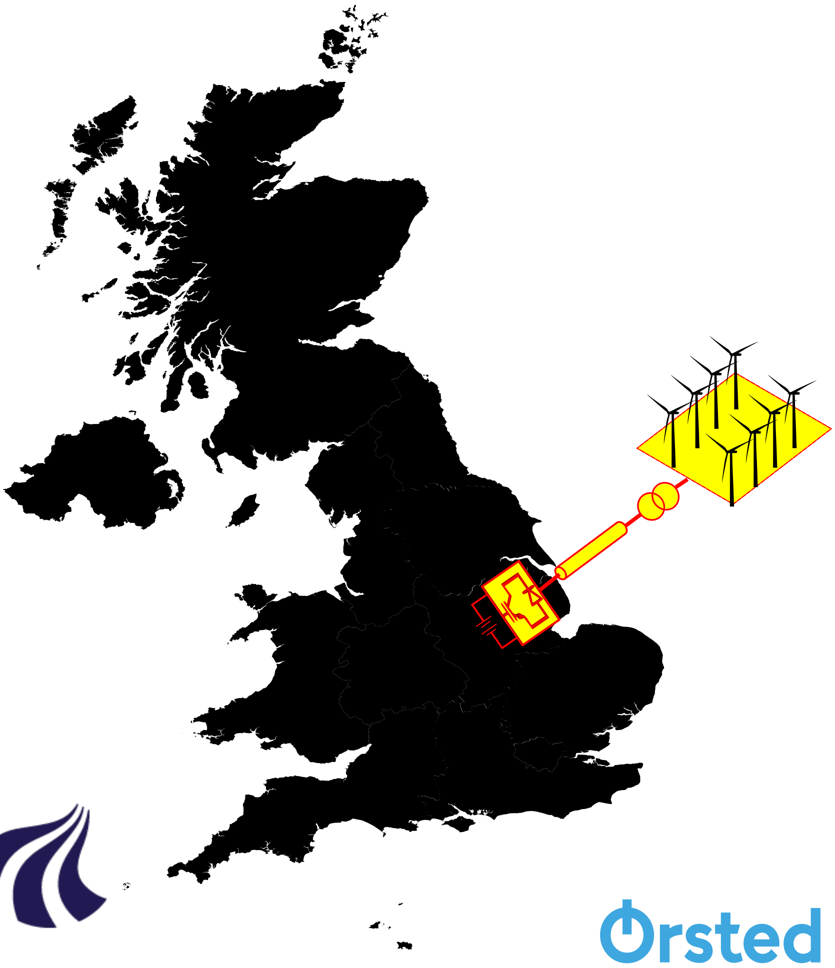

Written By:
Gustavo Matarazzo Zinoni

Group WPS4-1050
Department of Energy
Aalborg University

AALBORG UNIVERSITY
STUDENT REPORT

School of Engineering and Science (SES)
Energy Engineering
Pontoppidanstræde 111
9220 Aalborg Ø, Denmark
http://www.ses.aau.dk/

Title:
Black Start of an Offshore Wind Power Plant through an MMC based ES-STATCOM System

MSc semester project:
Master's Thesis.

Project period:
February 2021 - May 2021

Project group:
WPS4-1050

Participants:

Gustavo Matarazzo Zinoni

Supervisors:
Sanjay Chaudhary
Jayakrishnan Radhakrishna Pillai
Daniela Pagnani (Ørsted)
Lukasz Kocewiak (Ørsted)

Abstract:

A blackout is a highly unlikely, but impactful event that causes multiple socioeconomic difficulties. The power system must be restored rapidly to reduce the repercussion of the blackout. Conventional power plants have been traditionally responsible for Black Start (BS), while the majority of the renewable energy sources require an energized grid to be started. However, the gradual decommission of fossil-fueled power plants and the progress to a more sustainable power system raise the need of performing BS from non-conventional energy sources. In this project BS is achieved by an Offshore Wind Power Plant (OWPP) that is self-started with the help of an Integrated Battery Energy Storage and STATCOM (IBESS) System. The IBESS is able to energize the OWPP and enable the synchronization of the Wind Turbines (WTs). In this way, the OWPP becomes an islanded system ready to participate in the power system restoration. Connection of block-loads is then performed effectively, keeping voltage and frequency inside tight thresholds. This project demonstrates that the system formed by an IBESS and an OWPP is eligible as a BS unit.

Circulation: Uploaded digitally
Page count: 78
Appendix count: 2
Appendix pages: 10
Finished: 27/05/2021

By signing this document, each member of the group confirms participation on equal terms in the process of writing the project. Thus, each member of the group is responsible for the all contents in the project.

Resumé

Energisystemer i verden bevæger sig gradvist mod mere bæredygtige energikilder såsom vind- og solenergi. Denne tendens ledsages af en gradvis nedlukning af konventionelle kraftværker, især dem, der drives af fossile brændstoffer. I tilfælde af en blackout er sidstnævnte dog ofte ansvarlige for gendannelsen af elsystemet. I fremtiden forventes disse konventionelle black start (BS) udbydere ikke at være i drift. Så i tilfælde af en blackout, hvem skal gendanne elsystemet? Vedvarende energikilder kan være gode kandidater som BS enheder, og nogle transmissionssystemoperatører (TSO'er) har allerede skabt specifikke krav til ikke-konventionelle kraftværker. Desuden har offshore vindmølleparker (OVMP'er) flere fordele som BS-udbydere på grund af deres høje strømkapacitet, bæredygtige natur og hurtige opstart.

De største udfordringer ved at bruge en OVMP som en BS-enhed er den fluktuerende natur af vind, der truer forsyningens modstandsdygtighed og, vigtigere, behovet for en enhed, der selv kan starte OVMP'en, når systemet er slukket. Konceptualiseret af Aalborg Universitet, Ørsted og Hitachi-ABB Power Grids, kan det integrerede batterilagring og STATCOM system (teknisk navn: IBESS) give OVMP energi og danne et ø- strømssystem, der er klar til at deltage i genoprettelsen af elnettet. For selvstart af OVMP skal IBESS udstyres med en Grid-Forming (GFM) konverter for at danne en sinus spænding med en bestemt amplitude og frekvens. Derfor udvikles to GFM-controllere, den ene er baseret på Power Synchronization Control (PSC) og den anden er baseret på en Virtual Synchronous Machine (VSM). Udførelsen af IBESS evalueres for begge controllere for at forstå fordele og ulemper ved de to og beslutte, hvilken strategi der er bedre til BS-formål.

BS-simuleringerne kræver udvikling af en OVMP-model, der kan bruges til elektromagnetiske transiente (EMT) undersøgelser på grund af spændings- og strømtransienter, der vises efter omskifter kabler, transformere eller luftledninger. Referencekraftværket er baseret på Ørsteds Hornsea To OVMP som er placeret i Storbritannien. For udviklingen af modellen var samarbejdet mellem Ørsted og forskerne i IBESS-projektet afgørende, da de gav en detaljeret beskrivelse af de forskellige komponenter i OVMP.

Aktivering af lange eksportkabler eller kraftige transformatorer gennem en elektronisk konverter har den udfordring, at de genererede strøm- og spændingstransienter kan overbelaste og beskadige konverteringskomponenterne. I dette projekt løses dette ved gradvist at øge spændingsamplituden, indtil den nominelle værdi nås. Forbindelsen af vindmøller (VM'er) foretages imidlertid ved en normal omskift operation, så der forventes transienter. En lignende operation udføres til aktivering af landnetværket og forbindelse af blokbelastninger.

Dette projekt demonstrerer, at IBESS er i stand til at aktivere OVMP, tillade synkronisering af VM'erne, danne et ø-strømssystem og hjælpe med tilslutning af blokbelastninger. Projektets succes måles ved at analysere spændings- og frekvensbølgeformerne ved de forskellige busbarer i OVMP og landnet. BS-kravene er taget fra de netkoder, der leveres af NGESO, den britiske TSO; og ELIA, den belgiske TSO. Resultatet er, at systemet dannet af IBESS og OVMP er i stand til at opnå BS samt holde spænding og frekvens inden for de specificerede tærskler. Med hensyn til valget af den mest passende GFM-strategi konkluderes det, at VSM leverer lavere frekvens svingninger og en bedre spændingsregulering. Derimod involverer det længere afviklingstider end PSC.

Summary

Power systems throughout the world are gradually moving towards more sustainable energy sources such as wind and solar power. This trend is accompanied by the gradual decommission of conventional power plants, especially those powered by fossil fuels. However, in the event of a blackout, the latter are frequently responsible for the power system restoration. In the future these conventional black start (BS) providers are not expected to be under operation. So, in case of a blackout, who is going to restore the power system? Renewable energy sources can be good candidates as BS units, and some Transmission System Operators (TSOs) have already created specific requirements for non-conventional power plants. Moreover, Offshore Wind Power Plants (OWPPs) have several advantages as BS providers due to its high power capacity, sustainable nature and fast start-up.

The main challenges of using an OWPP as a BS unit is the intermittent nature of wind that threatens the resilience of supply and, more importantly, the need of a device that can self-start the power plant when the system is down. Conceptualized by Aalborg University, Ørsted and Hitachi-ABB Power Grids, the Integrated Battery Energy Storage and STATCOM (IBESS) System can energize the OWPP and form an islanded system ready to participate in the power system restoration. To self-start the OWPP, the IBESS needs to be equipped with a Grid-forming (GFM) converter to form a voltage waveform with a certain amplitude and frequency. Consequently, two GFM controllers are developed, one based on Power Synchronization Control (PSC) and the other based on a Virtual Synchronous Machine (VSM). The performance of the IBESS is evaluated for both schemes in order to understand the advantages and disadvantages of the two and decide which strategy is better for BS purposes.

The BS simulations require the development of an OWPP model that can be used for Electromagnetic Transient (EMT) studies due to the voltage and current transients that appear after switching cables, transformers or overhead lines (OHLs). The reference power plant is based upon Ørsted's Hornsea Two OWPP located in the UK. For the development of the model, the collaboration of Ørsted and the researchers of the IBESS Project was key, as they gave a detailed description of the different components of the OWPP.

Energizing long export cables or high power transformers through a power electronic converter has the challenge that the generated current and voltage transients can overload and damage the converter components. In this project this is solved by soft-charging the OWPP, which consists on gradually increase the voltage amplitude until the nominal value is reached. However, the connection of Wind Turbines (WTs) is done by a normal switching operation, so transients are expected. A similar switching is done for the energization of the onshore network and connection of block loads.

This project demonstrates that the IBESS is capable of energizing the OWPP, allow synchronization of the WTs, form an islanded power system, and aid the connection of block-loads. The success of the project is measured by analyzing the voltage and frequency waveforms at the different buses of the OWPP and onshore grid. The BS requirements are taken from the grid codes delivered by NGESO, the British TSO; and ELIA, the Belgian TSO. The outcome is that the system formed by the IBESS and the OWPP is capable of achieving BS, keeping voltage and frequency inside the specified thresholds. Regarding the selection of the most appropriate GFM strategy, it is concluded that the VSM deliver lower frequency oscillations and a better voltage regulation. On the other hand, it involves longer settling times than PSC.

Preface

This report is written by group *WPS4-1050*, formed by a 4$^{\text{th}}$ semester Master's student specialized in Wind Power Systems at the Department of Energy Technology at Aalborg University. The theme of this project is *"Master's Thesis on Black Start from an Offshore Wind Power Plant by means of GFM Converters"*.

The following software has been used to:

- **LaTeX** - Write and format the report.
- **Mendeley** - Sort and share the bibliography.
- **MATLAB** - Model and simulate the controllers, and general calculations and plots.
- **Inkscape** - Edit figures.
- **PSCAD** - Simulate the power system.

Reader's Guide:

On page vi, a table of contents is given. When viewing this report as a PDF, hyperlinks in the table of contents will allow fast navigation to the desired sections.
Page ix displays a nomenclature listing the abbreviations used in this report.

The bibliography on page 64 presents the literature used in this report. The references are given in the following format:

[Author][Title](Institution)(ISBN)[Year](URL)(Date Accessed)

Where fields in square brackets are mandatory, while regular brackets are only relevant for certain formats, i.e books or web pages. The bibliography entries are sorted after their appearance in the text. The references will be placed according to the text they are related to. This can be seen in the following example:

[1, p. 1].	*Before period*	Will add to the sentence before.
. [1, p. 1]	*After period*	Will add to the section before.

Table of Contents

Acknowledgments

I would like to show my gratitude to my supervisors from Aalborg University, Sanjay Chaudhary and Jayakrishnan Radhakrishna Pillai who supported me since the beginning of my Master's degree. They dedicated their time and effort to help me develop this thesis and become a competent Energy engineer.

In addition, I owe special thanks to Daniela Pagnani and Lukasz Kocewiak from Ørsted Wind Power. Their assistance and observations were important to improve the content of my thesis.

Finally, I thank all my teachers, colleagues and staff from Aalborg University for making of this academic experience the most exciting and enriching of my student life.

Nomenclature

Acronyms

AC	Alternate Current
AVC	Alternating Voltage Controller
BS	Black Start
DC	Direct Current
DPC	Direct Power Control
dPLL	Distributed PLL
EMT	Electromagnetic Transients
ES	Energy Storage
GFL	Grid Following
GFM	Grid Forming
HV	High Voltage
IBESS	Integrated Battery Energy Storage and STATCOM
IGBT	Insulated Gate Bipolar Transistor
MMC	Modular Multilevel Converter
MV	Medium Voltage
OHL	Overhead Line
OWPP	Offshore Wind Power Plant
PCC	Point of Common Coupling
PI	Proportional Integral
PLL	Phase Locked Loop
PMSM	Permanent Magnet Synchronous Machine
POC	Point of Connection
PSC	Power Synchronization Control
PWM	Pulse Width Modulation
SM	Submodule
TSO	Transmission System Operator
VSC	Voltage Source Converter
VSM	Virtual Synchronous Machine
WT	Wind Turbine

Chapter 1

Introduction

In this chapter the research carried out is contextualized. The relevance of achieving Black Start (BS) service from an Offshore Wind Power Plant (OWPP) is explained in the background. The problem formulation and the objective are stated providing a clear scope to the project. Afterwards, the following sections briefly describe the methodology and limitations of the project, ending with an outline of the report.

1.1 Background

BS is the process of re-energizing the the grid and restoring the power system operation at regulated nominal voltage and frequency after a highly unlikely, but highly impactful, event of a partial or total shut down of the system. Blackouts incur in a great social and economic costs; considering the United States, it is estimated that they cost to the country $20-$70 billion per year [1]. In Europe, the most recent blackout occurred in the United Kingdom in 2019 affecting 1 million consumers. Initiated by a lightning strike, Ørsted's plant Hornsea I failed to maintain its connection after the strike, which costed the company £4.5 million [2]. It must be mentioned that the socioeconomic consequences increase with the duration of the shutdown event. Therefore, it is critical to restore the power system as soon as possible.

BS still relies on conventional power plants, especially thermal and hydroelectric power generators. The former case is particularly characterized by its long start up times, [3], and the high fuel costs and generated emissions because of maintaining its operation to assure its availability for BS. Being the future European goals to gradually decommission conventional power plants to be substituted by renewable sources of energy, it is crucial to utilize them as BS providers. In fact, NGESO and ELIA, the British and Belgian Transmission System Operators (TSOs) respectively, already consider renewable sources as possible future BS providers [4],[5].

OWPPs are a promising source of BS because of their fast start up time and environmentally friendly conception [6]. The European Network TSOs (ENTSO-E) grid codes already included BS and islanded operation for OWPP as options, thus any relevant TSO can request these services to support the recovery of the system [7],[8]. Nevertheless, no OWPP in the world is yet able to perform BS [9]. The major challenge is the intermittent nature of wind that threatens the required availability and the resilience of supply of the BS service. The combination of the OWPP with Battery Energy Storage Systems (BESS) is an interesting solution to address this issue. Besides it could also aid other ancillary services such as frequency response or intra-day balancing of generation and load [10].

Aalborg University together with Ørsted and Hitachi-ABB has recently conceptualized the Integrated Battery Energy Storage and STATCOM (IBESS) System. Based on the Modular Multilevel Converter (MMC) technology, it accomplishes the functions of a battery energy storage and STATCOM (ES-STATCOM) device. With the help of a Grid Forming (GFM) control, it has the potential to self-start the OWPP. By this means, the IBESS would provide the start up power and set the reference voltage and frequency for the system. The in-built STATCOM would support the reactive power requirement during the energization of cables and transformers and would also stabilize the voltage. Afterwards, Grid Following (GFL) wind turbines (WTs) would be connected to meet the load demand.

Furthermore, IBESS could provide good inertial response to damp energization transients as well as allowing a smoother block-load connection [10].

1.2 Problem Formulation

As stated by ELIA, the main bottlenecks for the utilization of renewable sources as BS providers are the operation of Voltage Source Converters (VSCs) in weak grids, the significant reactive power that needs to be absorbed during energization and the lack of energy storage in most of renewable sources [5]. The IBESS System needs to account for theses bottlenecks and allow the use of an OWPP as BS provider. In addition, it intends to solve some other major challenges such as the energization of the long submarine cable and the smooth connection of block-loads keeping voltage and frequency between thresholds.

Consequently, the capability of the IBESS to self-start the OWPP must be primarily assessed. The first step consist on the energization of transformers and submarine cable. The former operation traditionally involves large inrush currents, while the latter, due to its large capacitance would produce large overvoltages. These transient phenomena is associated with the so called hard switching, that consists on the sequential energization of the different critical sections of the network. There are some methods to reduce these transients, such as the switching at the most convenient point of wave. However, it has some delay uncertainties because of the mechanical nature of the switches as well as the undetermined residual flux in the transformer windings. A first unknown would be if the IBESS System is able to withstand the transients that a hard switching procedure would generate in a worst case scenario.

Nevertheless, GFM converters would allow the soft-start the OWPP, which consists in connecting the network - cables, transformers, reactors, etc. - together with the self-start unit at a very low voltage and then ramp-up the voltage of the entire network, energizing it in one step [11]. Soft-start, or soft-charging, allows a faster and smoother energization of the system. However, it has the drawbacks of a delayed fault detection and clearing, as different settings for the under-voltage protection are necessary. It must be verified the capability of the IBESS to soft-start the OWPP by means of an appropriate GFM control. Furthermore, after modelling a realistic OWPP, the minimum power rating and State of Charge (SOC) of the IBESS System must be calculated so that it can assure the BS provision. This is crucial at it gives the required dimension of the Energy Storage and STATCOM system, as well as determining the minimum SOC that must be maintained during its normal operation - when it is providing other ancillary services.

GFM control enables a converter to work as an ideal Alternate Current (AC) voltage source with an specific amplitude and frequency. There has been a broad research on GFM control for WTs, especially considering their operation in microgrids, [12],[13], [14]. However, there is a lack of studies on the use of GFM converters for high power energization. Among the different GFM control concepts, it is key to analyze which is the most suitable considering the main challenges of a BS. Particularly interesting would be to analyze the voltage and frequency swings during the energization process and block-load connection.

After the energization, the IBESS and the OWPP will form an islanded system ready for participating on the restoration process. ELIA and NGESO have created a set of requirements for non-conventional BS providers. Some of the most important requirements are: self-start capability, limited time to connect the BS unit, voltage and frequency control during energization and block-loading, minimum block-loading capability, reactive power capability and minimum stored inertia [4], [15]. The compliance with these requirements is essential to assess if the system is eligible as BS unit.

Furthermore, recalling the IBESS being based on the MMC technology, it is relevant to account for the characteristics of this converter and, thereby analyze its internal behaviour during the BS procedure. An adequate model of the MMC is necessary to assess the internal dynamics and the design considerations, especially in terms of capacitors and semiconductors, in order to enable the self-start and block-loading.

Finally, it must be noted that another approach for BS from OWPPs is being discussed at the moment. It is mostly focused on High Voltage (HV) Direct Current (DC) connected OWPP, in which the energization of the Offshore AC network is made by GFM controlled WTs [11],[16]. The energized AC network is able to pre-charge the MMC based "rectifier" to obtain a specific DC link voltage. Especial attention is needed in the energization of the Onshore MMC "inverter", which operates as GFM converter and would create significant transients if it is not pre-charged previously. Even though this approach shows potential as a BS unit, it is out of the scope of this project.

1.3 Objectives

The main objective of this project is to design the IBESS System controller and demonstrate that it enables the BS capability of an OWPP. The objective is considered to be fulfilled when the IBESS is able to energize the different sections of the OWPP such as high voltage cables, collector-bus transformers, collector grid and, eventually, allow the synchronization of the WTs. In addition, after energization, the system has to accept block-loads keeping voltage and frequency between thresholds. In order to achieve the project objective, it is divided into several tasks:

- Develop an accurate and realistic model of an OWPP. It must contain all the components that are critical for the energization process.
- Control the IBESS System as a GFM unit. The performance of different GFM control schemes must be assessed to decide which is the best option for energization of OWPP and block-loading.
- Modelling the OWPP for Electromagnetic Transient (EMT) studies is also essential to perform accurate simulations of the energization process. In addition, the power rating of the MMC need to be considered for the purpose of BS. Relying in the soft-charging of the OWPP, high transients and stress to the converter are not expected during its energization. However, when a block-load is connected, it is probable that voltage and frequency swings happen. On the other hand, if hard switching is considered, then the performance of the converter during energization also needs to be assessed. Additionally, in this case, it is relevant to select the best energization procedure or sequence so as to reduce the transient phenomena.
- Once the IBESS and the OWPP form an islanded grid, the system is ready to accept loads and participate in the power system restoration. Therefore, the final task of the project is to evaluate whether the system is capable or not of performing BS.

1.4 Methodology

In order to fulfill the project ambitions, an extensive literature review should be accomplished first. Research on the state of art of the different components of OWPPs is key to develop an accurate power plant model valuable to assess the energization process and BS provision. In addition, the most important GFM control methods should be analyzed. It is relevant to capture the main challenges of a BS process and evaluate the performance of the different GFM controls in that scenario.

Having developed a proper OWPP model, simulations on the energization of the export cable and Offshore AC grid are performed. Accounting for the maximum capabilities of the IBESS System, the first simulation would concentrate on the energization of the OWPP. Having the complete system energized, its participation in the power system restoration process is simulated by the connection of block-loads. The switching of a section of the AC Onshore network consisting on a transmission line and a load would aid the evaluation of the system's ability to perform BS. The performance of the BS unit will be assessed based on the requirements from NGESO and ELIA. Critical metrics are, damping of frequency oscillations and ability to keep the voltage and frequency between given thresholds.

The main tool for performing the simulations is PSCAD because of its potential for EMT simulations. Besides, MATLAB is utilized for the controllers design and for plotting purposes.

1.5 Limitations

The present project involves several limitations that are stated in the following items:

- The IBESS System has the potential to perform different ancillary services such as: primary and secondary frequency response, intra-day balancing of generation and load, active filtering or voltage regulation [10]. However, this project only concentrates on its potential to energize the OWPP and conduct a BS.
- The internal dynamics of the MMC converter are not studied in this project. On the contrary, an averaged voltage source model of the IBESS converter is utilized. This means that dynamics faster the GFM controller bandwidth are left out of scope.
- The Battery Energy Storage model is simplified as it does not consider voltage variations due changes in the SOC. The battery voltage would fluctuate especially when the SOC is low. For the purpose of this project the SOC is considered to be at 50%, thus it behaves as a constant DC voltage source.
- Offshore WTs are equipped with GFL converters that synchronize to the formed AC voltage. Again, an average voltage source model of the WTs' converters is considered. This leaves the rotor's and DC link's dynamics out of scope.
- When analyzing the BS capability of the system, it is assumed that a sustained wind is flowing at the OWPP location. Therefore, the availability of the BS service and resilience of supply is presumed.
- In the event of low wind intensity at the OWPP location -considering low intensity the one sufficient to feed the OWPP auxiliary systems-, it would be interesting to analyze the ability of the IBESS System to maintain a stable islanded grid under wind fluctuations, ready to participate

in the restoration process once the wind intensity increases. This would assess the capability of the IBESS to support the voltage and frequency stability of the formed renewable energy based microgrid. Nevertheless, it is not certain if this is a realistic scenario for BS purposes, as the absence of sufficient wind would make the OWPP unavailable, thus this case is left out of scope.

- The present study does not consider possible faults during the restoration process. The designed BS procedure should ensure that the voltage and frequency stays between thresholds, but the performance of the system under an occasional fault is not studied.
- The time steps of the proposed BS procedure, i.e. the time instants at which the switching operations occur, is intended to reduce the computational burden, thus the events are separated by short time intervals. This means that the BS does not follow any grid code or requirements in terms of timestamps. In a real life scenario the BS procedure is expected to last significantly longer.

1.6 Outline of the Report

This report is divided into seven different chapters. Chapter 1 contains the background and motivation of this project, sets the objectives, describes the methodology and limitations. Then, Chapter 2 presents a literature overview on BS and the proposed regulations for non-conventional power plants. In addition, the main components of an OWPP are described, together with a brief overview of the IBESS. The concepts of GFM and GFL converters are introduced and some GFM implementations are briefly described.

Chapter 3 presents modelling guidelines for an OWPP. The main components of the OWPP are modelled for EMT simulations. Besides, the reference GFM and GFL controllers are explained.

Chapter 4 demonstrates the capability of the IBESS to energize the OWPP and operate in islanded mode. Then, in Chapter 5, the performance of the system during block-loading is assessed. An onshore network formed by a transmission line, a transformer and 3 loads is modelled to do the evaluation.

The reference GFM controller is not equipped with virtual inertia, thus in Chapter 6 a GFM converter with virtual inertia and damping is developed. Operating IBESS with this new control scheme, the BS process is repeated to evaluate if the voltage and frequency signals present lower oscillations after switching. Finally, Chapter 7 presents the conclusions and future work.

Chapter 2

Wind Powered Black Start

The present chapter aims to describe the state of art of the BS procedure and the relevant subsystems of the project. First, a brief overview on BS and its requirements for non-conventional power plants are given. Then, the characteristic components of OWPPs are described. This section is focused on HVAC connected OWPP because of being the most numerous. Consecutively, the IBESS System is presented so as to clarify the physical building blocks of the BS unit. Finally, an explanation on the most relevant GFM control strategies is given.

2.1 Introduction to Black Start

Wide area blackouts are highly unlikely and highly impactful events, which produce a relevant social and economic impact. Not only households are affected, but also industries, causing irreversible economic losses. The impact of the blackout increases with the restoration time, so it is crucial to have sufficient and fast BS units as well as an appropriate power system restoration plan.

Focusing on occidental Europe, there has been several blackout events. In September 2003 the Swedish/Danish system experienced a severe blackout due to the unrelated failure events of a 1200 MW nuclear power plant and a substation, which tripped another 1800 MW plant. It generated a high power flow from north to south systems, leading to voltage collapse and separation of the two regions forming two islanded networks that also suffered voltage and frequency collapse. A total power of 6550 MW was lost, affecting 4 million people. Also in September 2003, Italy suffered a nationwide blackout, which started with a flash-over hit in the Italy-Switzerland tie line that could not be reconnected. The frequency in the Italian system started decaying, loosing synchronism with the rest of Europe, causing the trip of its interconnection lines with France, Austria and Slovenia. It provoked the loss of 6400 MW, affecting 60 million people for 12 hours [17].

Other less important blackouts are the UCTE System disturbance, firstly generated by the intended opening of a 380 kV line due to marine ship transfer. Consequently a high power flow between two German areas produced the tripping of the East-West tie line, being the system divided into three islanded networks with significant power imbalance. In the Western area, frequency dropped causing interruption of supply to 15 million people for two hours. Finally, it was already mentioned in Section 1.1 the blackout in the United Kingdom in 2019.

2.1.1 The Black Start Process

Due to the high socio-economic impact of blackouts, one of the most important metrics of power system's resilience is the ability to quickly recover from them. The process involves multiple steps: power system status determination, plant preparation, generation restoration, transmission path energization, load restoration and system synchronization. Traditionally, BS has relied on Hydroelectric generators, Diesel generators and Thermal power plants. Hydroelectric generation is an ideal BS source as it needs very little initial power, it is reliable and has large capacity. Diesel generators can also be started with little power. Nevertheless, they have very low capacity and are powered by fossil fuels, generating important emissions. Finally, Thermal power plants can operate as BS units after they are started by a Diesel Generator. Although having large BS capacity, they are contaminant and have high stand-by costs [1].

Regarding the BS procedure, there are two main restoration strategies: build-down and build-up strategies [1]. The former consists on energizing the totality of the transmission system and then recover generation and load sequentially. This strategy needs significant BS power sources. On the other hand, build-up consists on the sectionalization of the power system into subsystems, energization of the transmission path of the individual subsystems, generation restoration and load pick-up within each section, and eventually, synchronization of the system. This second strategy is especially suitable for power systems with large share of non-conventional distributed generation.

2.1.2 Black Start from Non-Conventional Power Plants

Future power systems are expected to have an important share of renewable sources, being conventional power plants gradually decommissioned. Besides, many the regions in the world do not have sufficient hydroelectric resources. Consequently, it is key to provide BS service from non-conventional energy sources, being OWPPs excellent candidates due to its fast start-up and large capacity. Accordingly, some TSOs have already considered renewable energy sources as BS units. NGESO and ELIA have created extended requirements for BS to account for non-conventional sources [4],[15]. In addition, NGESO considers the need of some extra changes to account for the intermittency of the resource and the voltage level of the plant's Point of Connection (POC). Due to the growing interest of utilizing wind power plants as BS providers, several studies have addressed challenges and necessary functionalities of OWPP in the new scenario, such as [3], [6]. On the basis of these studies and the specifications from NGESO and ELIA, the main requirements for non-conventional BS suppliers are mentioned below:

- **Self-start:** ability to start the main generation plant without the use of an external electrical supply.
- **Service availability:** NGESO states that the BS provider should be able to provide the service at least 90% of the year. ELIA does not have and specific availability for the BS unit and would depend on the type of power plant and contractual terms.
- **Time to connect:** that is the time needed for the plant to start up and energize part of the network, since it receives instructions from the TSO. NGESO states a time to connect of less than 2 hours, while ELIA requires 1.5 or 3 hours, depending on whether the plant was operating or not before the black out.
- **Voltage control:** during energization and block loading NGESO requires to keep the voltage between a $\pm 10\,\%$ threshold. On the other hand, ELIA permits the voltage to lay in the range shown in Fig. 2.1.

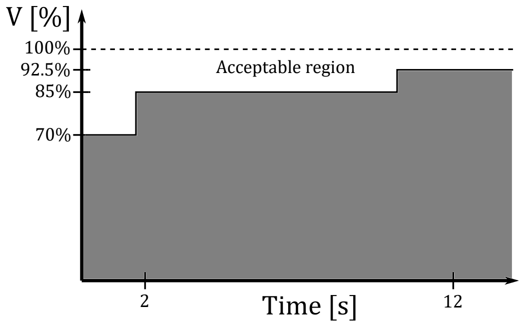

Figure 2.1: Acceptable voltage range after accepting block-loads, from [15].

- **Frequency control:** during block loading the frequency must remain between $[47.5, 52]$ Hz and $[47.5, 51.5]$ Hz for NGESO and ELIA respectively.
- **Block-loading size:** that is the capability of the BS unit to accept instantaneous loads. NGESO considered a minimum of 35 MW, but has changed to 20 MW to account for non-conventional sources. ELIA requires block-loads of 10 MW with an inductive power factor ≥ 0.8.
- **Reactive power capability:** consisting on the ability to energize part of the network. NGESO states a minimum of 100 Mvar (absorbing). ELIA present requirement is 30 Mvar, however it would be extended to 50 Mvar, depending on the zone. Additionally, both TSOs require that the BS unit has to withstand the inrush currents and transient overvoltages associated with the energization process.
- **BS Service resilience of supply:** NGESO states that the provider should assure that the BS service lasts for at least 10 hours. This requirement assures that BS providers can contribute to the later stages of the restoration process.
- **BS Auxiliary Units resilience of supply:** NGESO requires that the BS units run continuously at their rated output for at least 3 days.
- **Sequential start-ups:** during the system restoration, the system is unstable, so it is prone to faults/trips. Therefore, NGESO and ELIA states that the BS provider should be able to perform at least 3 sequential start-ups.

Table 2.1 shows a number of selected requirements that will be necessary to assess the BS capability of the system. Considering both NGESO and ELIA, the list captures the most strict specifications. Three of the categories mentioned above are not stated. First, it is difficult to assess the Service availability because of the intermittent character of wind. The same can be said about BS Service and BS Auxiliary Units resilience of supply. Moreover, NGESO is considering changing these requirements for non-conventional sources to account for the possible unavailability of the resource [4].

Table 2.1: List of requirements for Black Start. Based on [4] and [15].

Category	**NGESO**	**ELIA**	**Selected**
Time to connect	≤ 2 hrs	$\leq 1.5/3$ hrs	≤ 2 hrs
Voltage control	± 10 %	Fig. 2.1	± 10 %
Frequency control	$[47.5, 52]$Hz	$[47.5, 51.5]$Hz	$[47.5, 51.5]$Hz
Block-loading size	20 MW	10 MW	20 MW
Reactive power capability	100 Mvar	30 Mvar	100 Mvar
Sequential start-ups	≥ 3	≥ 3	≥ 3

2.1.3 IBESS and OWPP as Black Start Provider

The first challenge that an OWPP faces when it is considered as BS unit is its own start up. Export cables and transformers needs to be energized and GFL WTs require an established voltage waveform to which they can synchronize. IBESS is an ES-STATCOM system that enables bi-directional active and reactive power control. Besides, equipped with a GFM converter, it can generate a voltage waveform necessary for energization and WTs synchronization. The generated voltage should follow a ramp magnitude increase, to enable soft-charging. Hard switching transients of cables and transformers are expected to damage the converter as they involve high inrush currents and overvoltages.

IBESS should provide not only start up power, but also sufficient frequency and voltage controllability to allow the OWPP to work as an islanded system ready for accepting loads. An islanded OWPP would permit covering the demand of its own auxiliary loads. Besides, it could be useful to maintain the SOC of the IBESS' battery at an optimum level, by harvesting the wind that would be otherwise wasted - provided that the battery is not completely charged [18]. It must be mentioned that the WTs could be generating a low amount of active power, needing a significant use of pitch control, which would involve a limitation on the number of turbines that can be connected in islanded mode.

The islanded system formed by IBESS and the OWPP is maintained in stand by until the restoration process starts with the connection of the first block-loads. The fast controllability offered by IBESS is also and advantage, as it can damp the voltage and frequency oscillations that would appear when switching block loads. Nevertheless, the capability of IBESS and OWPP to provide BS is conditioned by the presence of wind. If there is not wind available, all the power should be provided by IBESS, leading to an uneconomical solution due to oversize of the ES-STATCOM system.

2.2 Offshore Wind Power Plants

The installations of OWPP are gaining great momentum worldwide as it presents advantages such as: higher wind intensity than onshore, which yields to an increase in power production; and steadier wind flow that makes the OWPP a more reliable source of power. Besides, countries like Denmark or Germany are lacking suitable and available onshore sites, together with the advantage that the water depth in their coasts increases very slowly with the distance to shore. The first OWPPs were installed in Denmark, the Netherlands, Belgium, Germany, Sweden, the UK, Ireland and China [19].

The main components of the OWPP are the WTs, their collection feeders, export cables and one or more substations. In addition, there might be reactive power compensation devices such as SVC, STATCOM or fixed reactors located offshore. The offshore substation is connected to the onshore one through a HVAC or HVDC transmission cable. It is also customary to have reactive power compensation onshore to comply with the grid codes regarding power factor or reactive power output from the OWPP. In the following, a brief description on the different components of the OWPP is given. It must be mentioned that the focus of these subsections are OWPPs with offshore AC networks. Nowadays, DC collection systems are also being considered as it has some advantages such as the elimination of the step up transformers, no need of reactive power compensation and the fact of using two-phase electric circuits [20]. However, this type of system is out of the scope of this project.

2.2.1 Type IV Wind Turbines

WT technology is divided in fours different configurations. Type I, also called fixed speed WTs were the first to be developed. Then, variable speed WTs were launched as Type II, III and IV. The first variable speed WT used a variable resistor connected to a wound rotor so as to achieve a 10% speed variation [20]. Type III and IV integrated the power converter to achieve a further variable speed and enable new control features such as the Maximum Point Power Tracking (MPPT). Type III, also called Double Fed Induction Generator (DFIG) WTs, are very extended, especially in the onshore market. In this case the converter is connected to the generator rotor, being a cost efficient solution. On the other hand, Type IV WTs are equipped with full scale converters connected between the generator stator and the grid. They enable full controllability, but they cannot achieve the power density and cost efficiency of DFIG.

The biggest offshore WT manufacturers such as Siemens Gamesa, Vestas or General Electric are relying on the Type IV WTs in their new developments for OWPPs [21], [22], [23]. The generator technology can vary from asynchronous, conventional synchronous or permanent magnet synchronous generators. They are electrically decoupled from the grid by means of the power converter, hence the frequency can vary on the generator side, keeping the grid side constant. Full scale converters enable reactive power support, smooth grid connection or virtual inertia provision. They also allow to remove the gearbox from the WT system, which reduces the cost. The main disadvantage is that the converter power rating has to be as big as the WT [20]. This makes them more costly than DFIG solutions, which are equipped with converters rated at approximately 30% of the WT power.

Figure 2.2 depicts a simplified schematic of a Type IV WT. It is equipped with a direct-drive permanent magnet synchronous generator (PMSG) and a VSC interfacing generator and grid. Between the grid side inverter and the grid there is also a filter, which objective is to mitigate the converter switching harmonics. It is normally accomplished by an LCL filter. Moreover, the transformer steps-up the voltage from the converter voltage level to the collector system voltage.

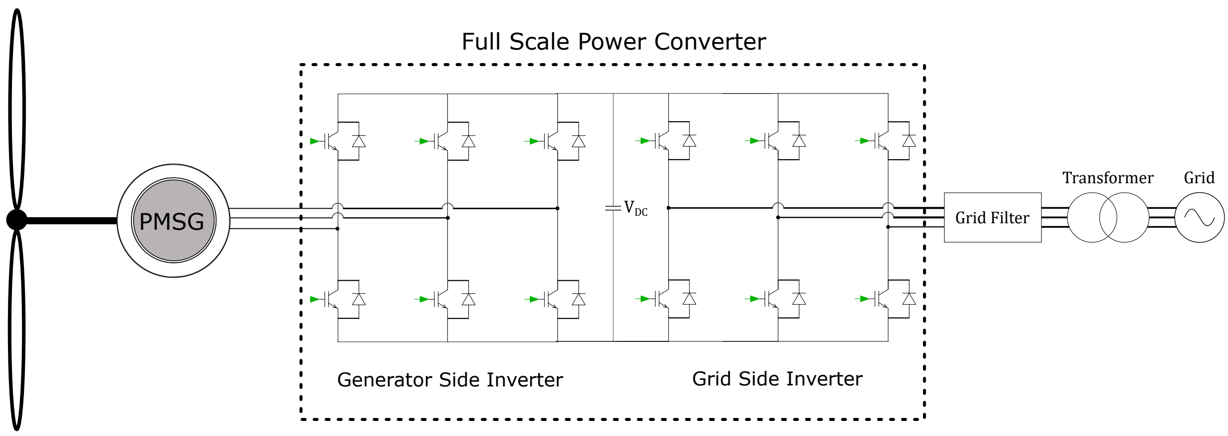

Figure 2.2: Schematic of an exemplary Type IV wind turbine

2.2.2 Offshore AC Network

At present most OWPPs use a radial configuration network due to its simplicity to control and protect, and the fact that it is cost efficient. The WTs are connected as a chain, where the feeder is taken to each wind turbine until the last one is reached [19] (see Fig. 2.3). Other network topologies involve loops in the feeders such as the single sided ring cluster or double sided ring cluster [19]. The looping enables to carry the generated power to the substation in case of a failure in any section of the feeder. The increased reliability and lower power losses compared to the radial topology is opposed to its significant cost because of the necessary higher cable ratings and longer cable run. Consequently, the extra investment needed to allow the ring clusters is not justified [19].

Offshore WTs are normally placed more separately than onshore ones because of the large wake effect that occurs at the sea. Additionally, a bulk amount of power needs to be collected, hence it is economically not viable to connect the turbines to the substation at the generator's voltage (typically 690 V even though General Electric is already commercializing WTs with generators rated at 3.3 kV) because of the consequent high power losses. Therefore, a transformer inside the WT steps up the voltage up to 36 kV or 66 kV. Power is taken to the substation through three-core cross-linked polyethylene (XLPE) insulated cables [20].

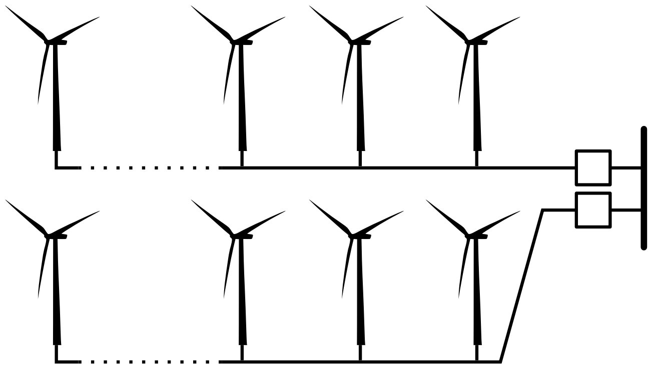

Figure 2.3: Radial topology, based on [20].

The characteristics of the offshore substation will be dependant on the transmission technology, that can be HVAC or HVDC. However, common to both are the circuit breakers and switches utilized to perform switching operations and clearing faults.

2.2.3 HVAC Transmission System

Most operational OWPPs adopt the HVAC transmission system because of being an economical solution [19],[20]. The main components of an HVAC connected offshore substation are a Medium Voltage (MV) and a HV switchgear, the transformer, reactive power compensation devices, the control system and the communication unit.

The major drawbacks of the HVAC transmission are that, over long distances to shore, there is a need of large reactive power compensation at both ends of the system. In addition, the OWPP is coupled with the grid, so any fault in it will be noticed in the wind farm, or vice versa. Concerning reactive power, long AC cables produce a relevant amount of capacitive power, so the charging current of the cable reduces the transmission capacity, needing inductive power to balance the former. Reactive power must be compensated depending on the load. Maximum compensation is needed at no-load condition, while only 50-60 % of the no-load situation is necessary at rated power. Therefore, it is convenient to mix fixed compensation, reactors, and controlled compensation, such as SVC or STATCOM. As the fixed compensation involves less space, then it would be located offshore. With such a configuration, the onshore dynamic reactive power compensator can control voltage levels at the grid connection point and contribute with short circuit fault currents [24].

As the key factors to select the transmission system are the distance to shore and the power rating of the OWPP, it was often suggested that an OWPP located 100 km from the coast and with a power transmission capacity of more than 200 MW, HVAC would be no longer convenient, being HVDC the preferred option [19]. Nevertheless, industry is still showing interest for HVAC for longer distances and higher capacities. Accordingly, Ørsted, in their Hornsea Project I, with a capacity of 1.2 GW and a distance to the Yorkshire (UK) coast of 120 km, applied HVAC at 220 kV compensating reactive power in the middle of the export cable. Figure 2.4 shows an schematic of a OWPP connected to shore through an HVAC cable.

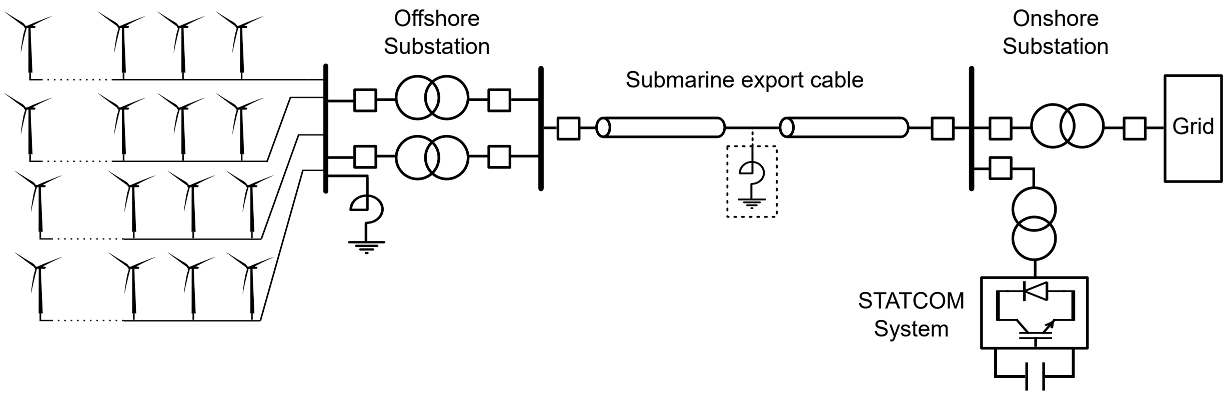

Figure 2.4: Single phase diagram of an exemplary HVAC connected OWPP.

2.3 The IBESS System

The IBESS System combines a Battery Energy Storage and STATCOM to achieve optimal operation and control of Wind Power Plants. STATCOM systems are VSC-based devices with a linear capacitor [20], connected in shunt to the network through a transformer. The AC ouput current of VSCs can be controlled in both magnitude and phase - leading or lagging the AC voltage, thus VSCs can be used to provide dynamic reactive power support. As the average active power drawn or fed by these converters is desired to be zero, only a small capacitor with little energy storage is necessary at the DC input [25]. However, the STATCOM system can be equipped with an active power source, like a Battery, in the DC terminals. This modification enables the creation of an ES-STATCOM system.

MMC is an appropiate converter topology for both VSC-HVDC interconnections and STATCOM systems. Indeed Siemens and ABB launched SVC Plus (STATCOM) [26] and STATCOM - SVC Light [27], respectively, as reactive power compensation devices based on the MMC technology, highlighting their lower footprint, lower harmonic content and faster response compared to traditional Static var Compensators (SVCs). In addition, Siemens has also launched SVC Plus Frequency Stabilizer that combines STATCOM and a 50 MW storage by means of supercapacitors [28]. Therefore, ES-STATCOM systems based on MMC are gaining momentum for future power systems with a large share of renewable sources as they can provide fast control of active power, emulate inertia as well as providing voltage stability and reactive power support.

Dedicated studies regarding the IBESS System can be found in [10] and [29]. The former concerns the Techno-economical feasibility of the system, highlighting the different revenue streams that the power plant owner can obtain by means of giving support to the power system. Moreover, the authors prioritize the different ancillary services to realize which are the most important services that the IBESS should provide. Key services are BS, frequency response, active harmonic filtering, intra-day balancing and synthetic inertia provision. An MMC based ES-STATCOM appears to be a good candidate to accomplish these tasks due to its fast active and reactive power response and high control bandwidth useful for harmonic filtering. New revenue streams, together with enhanced wind power plants designs, such as the use of Extra High Voltage (EHV) export cables, could reduce the total capital expenditure and the levelized cost of energy of OWPPs.

On the other hand, [29] benchmarks different MMC cell topologies for the ES-STATCOM implementation. Seven topologies are studied, mainly differentiated by the type of cell: bridge or chopper cell, and the installation of the Battery Storage: decentralized or centralized. Decentralized solutions involve a Battery packs in each cell, whereas centralized ones consist of a single Battery pack connected to the DC link. Optimizing total battery volume and converter silicon area, the authors select the best topology that consists on a Centralized Energy Storage and Double Star connection of Bridge cells (DSBC-CES). Figure 2.5 shows an schematic of the ES-STATCOM MMC.

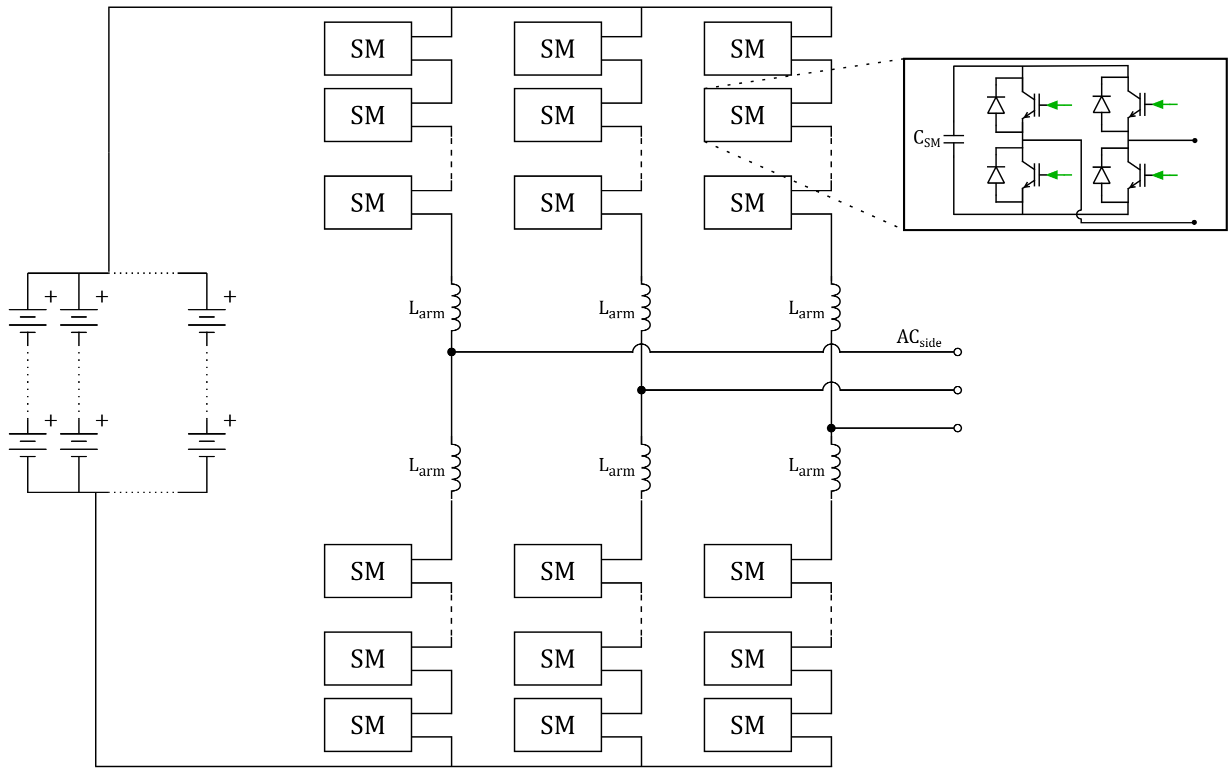

Figure 2.5: Schematic of the proposed MMC based ES-STATCOM System. The submodules have a Full Bridge configuration and the Battery Rack is centralized. Based on [29].

2.4 Grid Forming Control

Depending on the behaviour of the converter, they can be classified as GFL or GFM converters. The former are designed to deliver power to an energized grid and they can be represented by a current source in parallel with a high impedance. This current source needs to be synchronized with the AC voltage at the Point of Common Coupling (PCC), thus a Phase Locked Loop (PLL) is necessary. The utilization of the PLL indicates that there are other generators forming the grid, to which the GFL converter latches up. Therefore, these converters are suitable for operating in parallel in grid connected mode, but they cannot operate in islanded mode [12]. The regulation of their active and reactive power output is normally made by a high level controller as a MPPT or a plant controller.

On the other hand, GFM converters are intended to work as a voltage source. Hence, they present very low output impedance, which puts some challenges in their operation in parallel with other GFM converters as the output voltage has to be equal to avoid circulating currents between them. They are able to set a voltage and frequency of the local grid by an appropriate control loop. Considering that GFM converters are specifically used in an islanded system, the generated AC voltage will be used as reference for the rest of GFL converters present in it [12]. In the context of this project, the IBESS is the converter with GFM capabilities, while the rest are GFL and latch up to the AC reference created by the IBESS. In the following subsections, a number of GFM techniques are described.

2.4.1 Virtual Synchronous Machine

Traditional synchronous generators equipped with speed governors and excitation control, contribute to the system damping through their inertia and give frequency response through the droop of their governors; in addition to their voltage control and reactive power support capability. In the scenario of power electronic interfaced generation gradually substituting synchronous generators, Virtual Synchronous Machine (VSM) schemes intend to control the power converter emulating the performance of a synchronous generator. The main target is to add inertia to the power system and thus take advantage of its stabilizing effect [13].

Common to all VSM implementations are the inertia emulation and the damping of the electromagnetic oscillations [13]. These two aspects are correctly captured by the swing equation,

$$J\frac{d\omega}{dt} = T_m - T_e - D \cdot (\omega - \omega_g) \tag{2.1}$$

where T_m and T_e are the mechanical and electrical torque respectively. The rotor inertia is equal to J. ω is the rotational speed of the machine, while ω_g is the grid's angular frequency. Finally, D is the damping torque provided by the damping windings during transient phenomena. Equation (2.1) can be also expressed in terms of power by multiplying by ω_g at both sides of the equality, (2.2). Being, P_m the emulated mechanical power, while P_e is the electrical power. K_d is a constant associated with the damping torque, D.

$$J \cdot \omega_g \cdot \frac{d\omega}{dt} = P_m - P_e - K_d \cdot (\omega - \omega_g) \tag{2.2}$$

VSM implementations are classified as current, voltage or power reference. Power reference VSM does not have GFM capability, as they rely on a PLL which has to synchronize with a energized grid [13]. Moreover, based on [30], voltage reference VSMs can achieve better voltage quality than current reference applications. Besides, due to the wide utilization PWM controlled converters, voltage reference VSM are normally the preferred choice.

An example of the voltage reference VSM is the "Synchronverter", [14], where the voltage signal generated by the machine's model is directly fed into the PWM block to create the gate signals. The drawback of this implementation is that it does not involve saturation of the currents and voltages of the converter, which threatens the integrity of its components. A possible solution would be to apply cascaded voltage and current control that can involve protection strategies and saturation of the outputs.

Accordingly, in [31], the authors develop such a control strategy. The swing equation dominates the active power flow, while the reactive power is handled separately by a droop-based controller.

It is interesting that the internal loops do not rely on a PLL, but instead in the power balance synchronization mechanism given by the VSM inertia. Figure 2.6 show an schematic of this implementation.

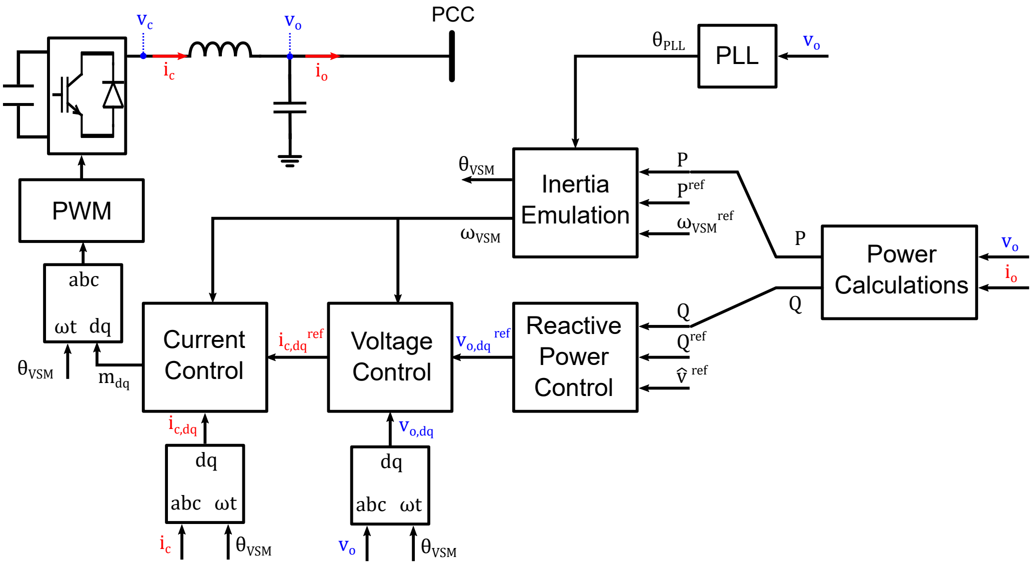

Figure 2.6: Simplified overview of the VSM implementation, based on [31]. The references for the AC voltage magnitude and frequency are $\hat{v}^{ref}$ and ω_{VSM}^{ref} respectively.

Note that there is an implemented PLL, but it is only used to account for the damping term of the swing equation. The virtual inertia and power control also includes an external frequency droop controller to emulate the speed governor of the synchronous generators. Finally, the cascaded voltage and current controllers are based on PI controllers in the *dq*-frame, with their corresponding decoupling terms, and possibility of adding an active resistance in the current control loop to limit the oscillations generated by the LC filter.

2.4.2 Power Synchronization Control

Another potential GFM stategy for the IBESS System is Power Synchronization Control (PSC), which was initially designed for VSC-HVDC systems connected to weak grids. The main features of the PSC implementation described in [32] are presented in this subsection.

The synchronization of VSC to the grid has traditionally relied in the PLL, which dynamics can have a negative impact in the performance of the VSC when operating in weak grids. To overcome this issue, the present method introduces a synchronization process by means of a transient power transfer. PSC employs a single integration to obtain the phase angle, thus improving the stability margin, being the synchronization law expressed by (2.3).

$$\frac{d\Delta\theta}{dt} = k_p(P_{ref} - P) \tag{2.3}$$

Where P_{ref} and P the reference and the measured output active power of the VSC respectively. k_p is the controller gain, while $\Delta\theta$ is its output, which provides the synchronization. Being active power controlled by increasing or decreasing the angle θ, or the frequency; the voltage control is achieved by an Alternating Voltage Controller (AVC) and a reactive power controller. The latter is accomplished by a PI controller and its output needs to be added to the former's reference. The AVC is designed to have a droop characteristic and will generate an output named V_0. This voltage is not directly fed to the PWM block because a high-pass filter is utilized to damp the grid frequency resonant poles [32]. Therefore,

$$v_{c,dq}^{ref} = V_0 - H_{HP}(s)i_{c,dq} \tag{2.4}$$

where, $v_{c,dq}^{ref}$ is the converter's reference voltage to be fed to the PWM block and $i_{c,dq}$ is the converter´s current - both magnitudes in the dq-frame. $H_{HP}(s)$ is expressed by (2.5), being R_a the filter's gain and ω_b the cutoff frequency.

$$H_{HP}(s) = \frac{R_a s}{s + \omega_b} \tag{2.5}$$

It must be mentioned that PSC also introduces a back-up PLL that is to be utilized during severe grid faults. Consequently, PSC has to decide through a Current Limiting Controller if $|i_{c,dq}|$ will exceed the maximum converter´s current, I_{max} and accordingly, limit this current and switch to synchronization via PLL. Failure to perform this operation would end in the acceleration of the "rotor speed", running into transient instability similar to a synchronous machine after a power system fault. In other words, the operation of the VSC under PSC has to be understood as a synchronous generator that limits the short circuit current contribution to I_{max} and runs with constant rotor speed during a fault. The equation ruling the Current Limiting Controller is given by (2.6), [32].

$$i_{c,dq}^{ref} = \frac{1}{\alpha_c L_c}(V_0 - v_{o,dq} - j\omega_1 L_c i_{c,dq} - H_{HP}(s)i_{c,dq}) + i_{c,dq} \tag{2.6}$$

Where α_c is the desired closed loop bandwidth and L_c is the converter's inductance. $v_{o,dq}$ is the voltage at the PCC, while ω_1 is the rated frequency. The voltage control law now becomes, [32],

$$v_{c,dq}^{ref} = \alpha_c L_c(i_{c,dq}^{ref} - i_{c,dq}) + j\omega_1 L_c i_{c,dq} + v_{o,dq} \tag{2.7}$$

By simple substitution of (2.6) into (2.7), it can be seen that is designed to turn into (2.4) during power synchronization operation. Exceeding I_{max} will also generate the signal C_{lim} that indicates the selector to switch to PLL synchronization. Figure 2.7 shows an schematic with the purpose of clarifying the different controllers of PSC.

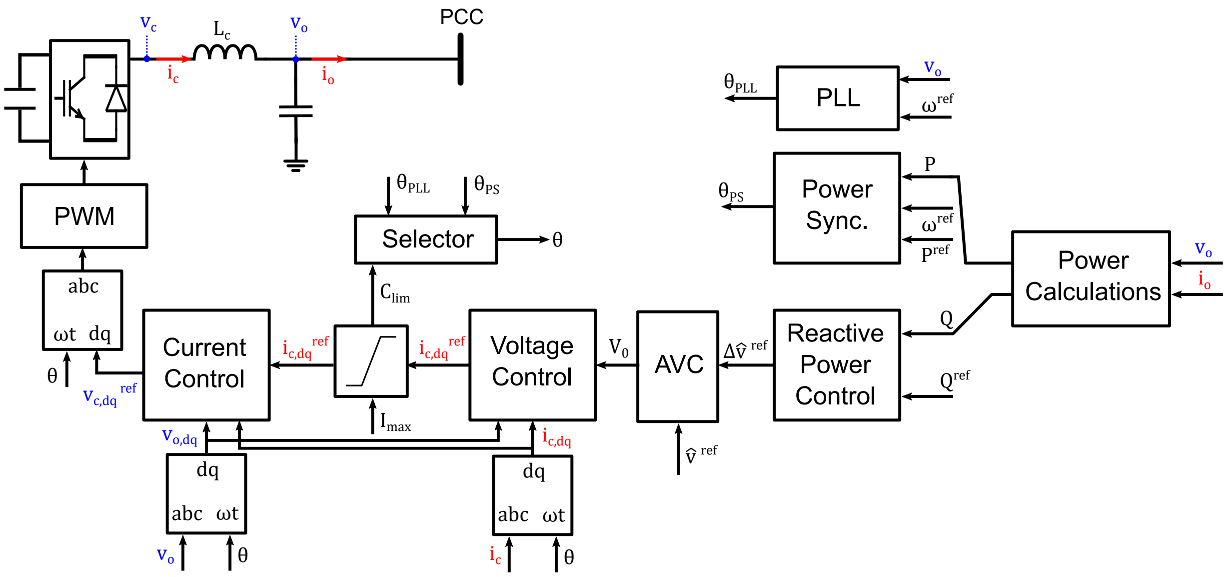

Figure 2.7: Simplified overview of the PSC implementation, based on [32]. The references for the AC voltage magnitude and frequency are $\hat{v}^{ref}$ and ω^{ref} respectively.

2.4.3 Overview of the GFM Control Methods

The previous subsections described two different GFM control strategies that can be applied for BS purposes. Nevertheless, the reference papers describing these schemes are not considering the BS provision. Instead, they are more mostly concerned with their operation in weak grids, [31], [32].

In [16] the authors present the utilization of four control strategies to provide BS from an MMC based VSC-HVDC connected OWPP: VSM, PSC, Distributed PLL (dPLL) and Direct Power Control (DPC). The WTs are equipped with GFM converters to energize the offshore AC network and charge a GFL offshore MMC. Consecutively, the onshore MMC is charged and set ready to operate. To be able to provide BS, the onshore MMC has GFM capabilities. To the author knowledge, it is the first study where several GFM control strategies are compared to assess the performance of the OWPP when providing BS. Thus, the main conclusions of [16] are presented in Table 2.2.

Table 2.2: Summary of the GFM controllers' attributes, based on [16].

GFM	Main features	Advantages	Disadvantages
VSM [31]	- Inertia emulation - Power synchronization method - Equipped with voltage and current cascaded controllers	- Provides inertial response and damping of oscillations	- Delayed response due to rigth hand zero - Low bandwidth cascaded control reduces the phase margin
PSC [32]	- Power synchronization method with a single integration - Converter current limitation	- No decoupling terms in voltage and current controllers: improved behaviour energizing capacitive sections - High pass filter damps resonant modes	- Delayed response due to right hand zero
dPLL [33]	- Q-f and P-V high level controllers - Equipped with voltage and current cascaded controllers	- Plug and play capability	- Low bandwidth cascaded control reduces the phase margin
DPC [34]	- No need of AC voltage sensors - Vector current control structure	- Straightforward implementation - No decoupling terms in voltage and current controllers: improved behaviour energizing capacitive sections	- Not mentioned

Note from the findings in Table 2.2 that power synchronization methods, VSM and PSC, have the disadvantage of presenting a delayed response. This is due to a right hand zero that appears in the $\frac{\Delta P(s)}{\Delta\theta(s)}$ transfer function as explained in [32]. Besides, those control strategies with low bandwidth cascaded voltage and current control, VSM and dPLL, suffer from reduced system damping due to their small phase margin, taking the system closer to instability. Therefore, virtual or real resistances in the system will be key to damp the possible synchronous oscillations [16].

However, the scenario presented in this project is different in many aspects. The IBESS System, located onshore, is the one equipped with a GFM converter and has to energize the AC network. Moreover, it should be able to energize the onshore substation, the submarine transmission cable and the offshore grid - dealing with an HVAC connected system. The combination of the IBESS with an

OWPP is a novel approach to BS, consequently, the performance of these control strategies needs to be investigated. For the purpose of this project, PSC and VSM are analyzed to assess the benefits of virtual inertia and the influence of implementing cascaded PI controllers in terms of stability and voltage regulation.

2.5 Summary

The present chapter established the framework of the project. Accordingly, Section 2.1 explained what is BS and how is performed at present, relying on conventional power plants. Moreover, it presents extended requirements that TSOs have developed so as to enable renewable energy sources to participate in the BS process. From them, a set of requirements is selected, which is going to be useful to assess whether or not the proposed system is eligible as BS unit.

The proposed BS procedure starts with the energization of an OWPP through a self-starter, constituted by the IBESS System. Therefore, Section 2.2 introduces the typical structure of an OWPP, highlighting its different components that need to be energized. Then, Section 2.3 briefly describes the IBESS that consists on an ES-STATCOM system. The combination of storage and wind power plants appear to be an attractive solution for BS units, as the battery compensates the intermittency of the resource. Besides, it is a good self-start unit for the wind power plant.

The IBESS has to be able to energize the OWPP to make it capable of participating in the BS. In order to achieve it, it must be equipped with a GFM converter that can create an AC voltage signal, energize the network and permit the connection of the offshore GFL WTs. Section 2.4 introduces a number of GFM control schemes that are appropriate to enable BS. Power synchronization methods, such as VSM and PSC, seem to be good candidates due to their inertial response and active power damping characteristics respectively. Consequently, their performance will be tested during energization of the OWPP and block-loading.

Chapter 3

Modelling of OWPPs for Black Start

This chapter presents brief modelling guidelines in order to study the energization of an OWPP. First the reference power plant is described, then the models of its key components are explained. The description of them is general, so that the modelling guidelines can be used to analyze any other wind power plant. The performance of the system is also dependant on the controllers. Therefore, the last part of the chapter is dedicated to the description of the implemented controllers, both for the IBESS and the WTs.

3.1 Overview of the OWPP

The reference wind power plant is Ørsted's Hornsea II, which will be fully operational in 2022 [35]. It has a power capacity of 1.4 GW and it is located at approximately 89 km from the Yorkshire coast in the UK. Figure 3.1 depicts an schematic of the modelled OWPP. It must be noted that the model does not involve the totality of the power plant, but only one third of it. This is a valid simplification as Hornsea II is formed by three identical systems [36]. The present model is the result of the coordinated work between Aalborg University, Ørsted Wind Power and Hitachi-ABB Corporate Research, which is detailed in [37].

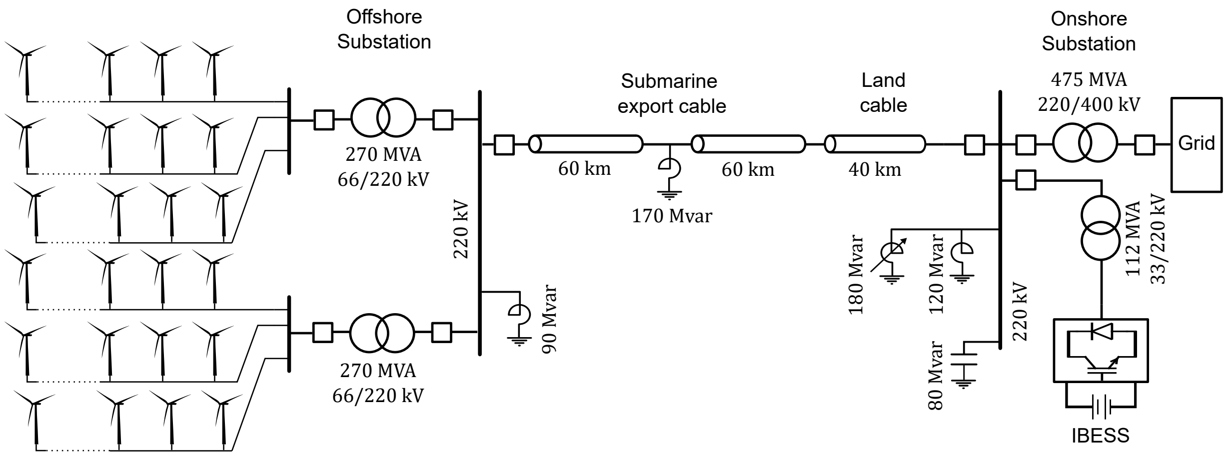

Figure 3.1: Offshore Wind Power Plant, based on Ørsted Hornsea Project II.

The test OWPP model is equipped with 54, 8 MW WTs, installed in a radial configuration. Each WT cluster is formed by 9 WTs, hence providing a total power of 72 MW. The offshore substation consists on two transformers and a 90 MVAr reactor for compensation of the capacitive currents. This substation is connected to the onshore grid through a 220 kV, 160 km long export cable, which is divided into three sections, two submarine sections and a land section. Due to the capacitive behaviour of cables, there is an intermediate substation for reactive power compensation that is sized to 170 MVAr. The onshore substation is equipped with a transformer that raises the voltage from 220 kV to the power transmission level of 400 kV. Reactive power compensation is considered at this bus in two different ways. There is a fixed reactor of 120 MVAr, and six 30 MVAr reactors that can be switched in order to correct the power factor at different load levels. All the reactors are assumed to have a quality factor of $Q = \frac{X}{R} = 200$. In addition, there is a 80 MVAr C-type filter for the attenuation of high frequency components.

To the onshore Bus, the IBESS System is connected through a transformer. The IBESS has been incorporated in the test OWPP model, as it is not originally in the Hornsea wind power plant. Such an option could provide self start, or voltage and frequency response in grid connected mode to any existing wind power plant. Besides, located onshore, the complexity of maintenance and installation costs are reduced.

3.2 Modelling of OWPP for EMT analysis

Having presented the reference OWPP, the modelling guidelines of its different components are given. First the export cable is explained, which have different characteristics in each section, so each of them should be modelled separately. Then the transformers key parameters are presented. WTs are not modelled individually, instead they are aggregated in 6 clusters of 72 MW. Thus, a simple way to find the collector equivalent circuit is described. Finally, a brief explanation on reactive power compensation of cables is given.

3.2.1 Export Cables

According to Cigre Tenchnical Brochure, [38], cable energization transients can lead to steep overvoltages that contain high frequency components, together with significant overcurrents at the sending end. Besides, due to travelling waves, there are overvoltages and reflections in the receiving end. These attributes of line energization transients raise the need of frequency dependant parameters for the cable models, which are normally not considered in other type of studies.

There are several mathematical models for cables and overhead lines (OHLs), mostly differentiated by whether they use lumped or distributed parameters. A clear representative of the former is the $\pi-$model, which is accurate for medium length lines at 50 Hz. The models taking into account distributed parameters normally consider travelling waves and are suitable for transient studies. In this group, the Bergeron's model consists on the representation of the distributed line capacitance and inductance through a Norton equivalent circuit based on the travelling wave theory. The resistance is considered as lumped. In addition, the characteristics of the line are evaluated at a single frequency, which limits its accuracy. Nevertheless, it provides conservative results and Cigre recommends its use when studying energization of cables [38].

Higher accuracy can be obtained by frequency dependant models, which consider the line capacitance, inductance and resistance as distributed. It is also based on the travelling wave theory and the characteristics are evaluated at all the frequencies. From the different frequency dependant models that have been developed, PSCAD utilizes the Universal Line Model developed by B. Gustavsen et.al [39]. In a cable energization simulation reported by Cigre, Bergeron's model gave similar overvoltage results to the universal model during the first 20 ms of simulation, delivering lower values after that period of time [38]. Nevertheless, there are two main reasons to select the frequency dependant model for the export cable. First, the energization of the OWPP is expected to take more than 20 ms. Secondly, transformers are also present in the power plant, which might generate inrush currents with rich harmonic content during their energization. This makes the frequency dependant parameters of the cable crucial to study possible overvoltages due to low order resonance excitation.

Having selected the mathematical model for the cable, the data describing the cable and its installation must be provided. Apart from the cable parameters, it is relevant to account for the bonding of the cable screens as it affects the wave propagation time and cable impedance; the cable layout (trefoil or flat configuration); and the earth resistivity. Regarding the cable parameters, it is in some cases necessary to convert the available cable data from the manufacturer to a new set of data that can be used in the cable model. In this project the approach showed in [40] is followed. Figure 3.2 show the differences between the physical characteristics of a cable and the simplified representation of it in PSCAD. Note that it is necessary to account for the discrepancies in the conductor core stranding, the semiconductor screens and the wire screen.

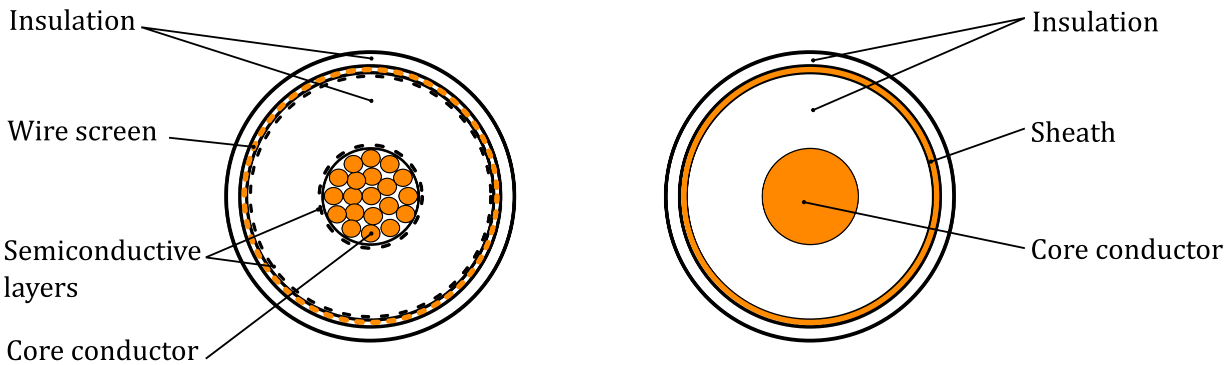

Figure 3.2: The cable section on the left represents a real cable, with a stranded conductor, semiconductor layers and wire screen. On the right, the simplified cable model provided by PSCAD.

Starting with the conductor core, the resistivity has to be reduced due to the fact that the real cable has a stranded conductor, being the modelled one solid. The new resistivity, ρ_c is calculated by,

$$\rho_c = \rho_c' \frac{\pi r_1^2}{A_c} \tag{3.1}$$

where, A_c is the nominal cross sectional area, r_1 is the external radius of the conductor and ρ_c' is the resistivity of the conductive material (for Copper: $1.7241 \times 10^{-8}\,\mathrm{m}$ and for Aluminium $2.8264 \times 10^{-8}\,\mathrm{m}$). The following correction that must be made is due to the lack of semiconductor screens in the simplified cable model. The relative permittivity, ε_{r1}, of the insulator must be corrected by, [40],

$$\varepsilon_{r1} = \varepsilon_{r-ins} \frac{ln(r_2/r_1)}{ln(b/a)} \tag{3.2}$$

being a and b the insulation inner and outer radius, and r_2 the sum of r_1 plus the thickness of the insulation and the semiconductor layers. ε_{r-ins} is the permittivity of the insulator -for XLPE, $\varepsilon_{r-ins} = 2.3$. It must be noted, that the utilization of these equations depend on the type of cable that the designer is implementing in the software, as some cable models already consider the semiconductor layers. Finally, regarding the wire screen, it is customary to replace it by a tubular conductor with a cross sectional area equal to the area of the wires,

$$r_3 = \sqrt{\frac{A_s}{\pi} + r_2^2} \tag{3.3}$$

where r_3 is the resultant radius of the screen and A_s is the actual screen cross sectional area. Other approach could be to keep the radius given by the manufacturer and correct the resistivity as with the core conductor.

3.2.2 Transformers

Appropriate modelling of transformers is crucial as their energization can be the source of RMS voltage drops and temporary overvoltages [41]. The former are caused by the high magnitude of the inrush current after energization and the latter are generated by the excitation of parallel resonances in the system due to the significant harmonic content of the transformer's inrush currents. This can be particularly problematic in OWPPs due to the utilization of long cables, which capacitance takes the resonant frequencies to low order harmonics ($\omega_{res} = \frac{1}{\sqrt{LC}}$).

The source of harmonic content is the non linearity of the magnetization current when the transformer core saturates. This can occur because of an abrupt change in voltage that is applied to it, which results in a variation in the flux, Φ (recall Faraday law, $V = -N\frac{d\Phi}{dt}$). Besides, the transformer may present residual flux that sums up to the induced one. Figure 3.3 depicts the relationship between flux and magnetization current. It is clear that if flux increases above the knee point, the relation enters in the non-linear region where a very small change in flux generates a large increase of the magnetization current.

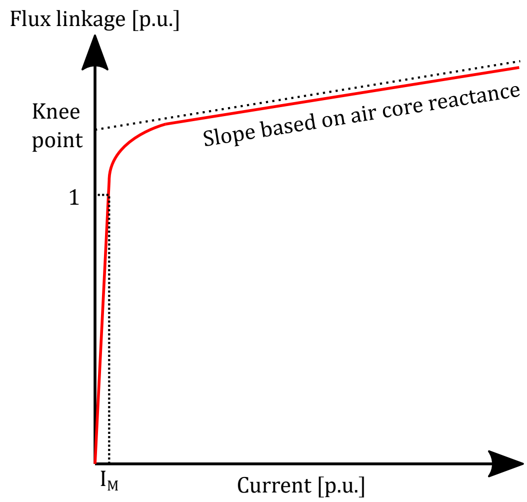

Figure 3.3: Transformer's saturation curve, based on [42]. I_M stands for magnetization current, that is expressed as a percentage of the rated current. For simplicity, the hysteresis loops are not shown.

There are main factors that affect the magnitude of the inrush currents. First, the residual flux at the instant previous to energization. Second, the point of wave at which the transformer is energized, being the energization at peak voltage the ideal case to avoid transients, whereas the energization at zero voltage would be the worst case. Besides, the difference in flux linkage between the nominal magnetization point and the knee point is of relevant importance. If they are close to each other, it is easier to take the core into saturation.

Due to the highly non linear behaviour of transformers during energization, Cigre Technical Brochure [41] gives some modelling guidelines for EMT analysis. The most important parameters that should be modelled are presented by order of importance:

- **Leakage inductance and winding resistance**, obtained from the short circuit test and gives the series impedance of the transformer.
- **Non linear saturation and core losses**, obtained from a no load test. The most important characteristics are the final linear slope of the saturation curve - air core inductance, defined as the coil inductance when there is no iron core - and the value where the core starts saturating, the so called knee point. Concerning core losses, they are related to the hysteresis of the ferromagnetic material.
- **Residual flux** which directly affects the first peak of the inrush current. If the remanent flux is close to the saturation region, a very small increase in flux can take the core into saturation. The residual flux remains in the transformer after it is disconnected from the power grid.
- **Frequency dependant winding resistance**, which is important to account for the damping of transients and resonant conditions.

Other parameters that are recommended to be modelled are magnetic phase coupling between phases as it affects simulations where phase unbalance or zero sequence currents may occur. Additionally it is advised to model the zero sequence impedance if unbalanced and/or fault conditions want to be tested, while hysteresis and frequency dependant core losses can be modelled if de-energizations are of interest. Nevertheless, these latter characteristics are not of relevance for the OWPP energization planned in this project, thus only the parameters highlighted in the items will be modelled.

3.2.3 Collector Cables

The power collection system of the OWPP consist on a radial arrangement of the WTs connected in a chain. For economical reasons, the cable cross-section along the radial cluster is not the same. In fact, it is customary to have several cable sections to optimize cost and power losses, being the cables that carry more power the ones with higher cross-section. The presence of multiple turbines and cable sections complicates the modelling and considerably increases the computational burden of the simulations. Therefore, each of the radial collectors are modelled as an equivalent circuit. Following the equivalence guidelines given in [43], the collector can be modelled as a π-circuit where the equivalent series impedance, Z_{eq}, and shunt admittance, Y_{eq}, are given by (3.4) and (3.5) respectively.

$$Z_{eq} = \frac{\sum_{i=1}^{n} Z_i \cdot S_i^2}{S_n^2} \tag{3.4}$$

$$Y_{eq} = \sum_{i=1}^{n} Y_i \tag{3.5}$$

Being Z_i the series impedance of each cable section and $S_i = \sum_{WT=1}^{i} S_{WT}$, where S_{WT} is the apparent generated power of each WT. Concerning (3.5), Y_i is the shunt admittance of each cable section. n is the number of cable sections.

It could be argued that a π-circuit does not account for distributed parameters or for their frequency dependence, especially necessary when studying transients. However, considering the collector cables to be relatively short ($\leq 10\,\text{km}$), while relying on soft-charging of the OWPP, and the fact that the the long export cables and transformers are modelled in detail, this simplification is considered appropriate in order to reduce the computational burden of the simulations.

3.2.4 Aggregated Wind Turbines

Following the same rationale as with the collector cables, the WTs in each radial feeder are aggregated into a single turbine. Being all of them similar, the total power of the aggregated WT is $S_{WT,eq} = n \cdot S_{WT}$. Regarding the parameters of the in-built transformer, its equivalent per unit parameters would be equal to the individual. Thus, the apparent power should be multiplied by the number of WTs in the cluster, $S_{tr,eq} = n \cdot S_{tr}$.

Figure 3.4 shows the actual implementation of the WT model, together with the collector equivalent circuit. Note that the WT is represented as an averaged voltage source model and an LCL filter. The LCL filter is formed by the converter side inductor, the shunt capacitance and the leakage inductance of the transformer. In series with the shunt capacitor, there is a damping resistor whose objective is to avoid oscillations that would appear due to the excitation of the LCL filter resonance frequency. The averaged voltage source model implies that the converter PWM is not taken into account, i.e. the converter output is a sinusoidal signal. Besides, the mechanical time constants related to the rotor side of the WT, or the converter DC link dynamics are not considered. Moreover, relevant for the controller, the voltage sensor is located at v_o, while the current is measured before the transformer, i_o.

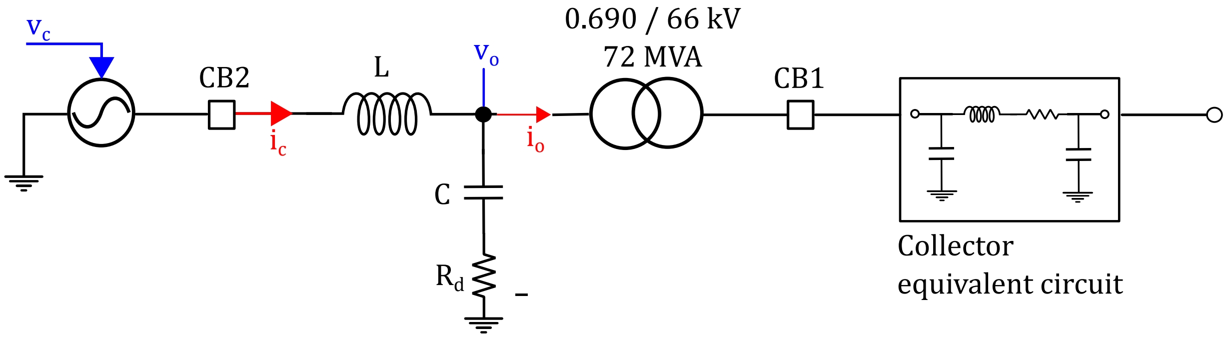

Figure 3.4: Single phase diagram of the implemented WT model.

3.2.5 The IBESS System

The IBESS is connected in shunt, through a transformer, to the onshore bus. Its implementation in the OWPP model is similar to the WT, as it is represented by an averaged voltage source model. Nevertheless, the LCL filter is substituted by a simple L filter. This is possible because of the MMC converter technology, which can create a voltage waveform with multiple levels. It reduces the switching harmonic content and, thereby, the filtering requirements. Due to the average voltage source model, the dynamics of the physical Battery ES are not considered. Figure 3.5 presents the implemented IBESS system. The voltage sensors are located at v_o and u_{PCC}, while the current is measured at the converter output, i_c.

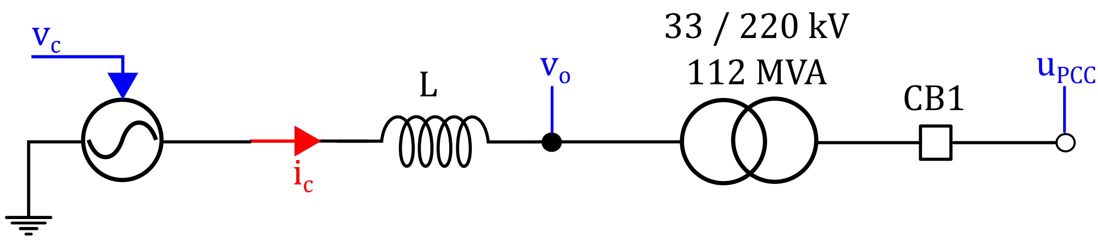

Figure 3.5: Single phase diagram of the implemented IBESS model.

3.2.6 Reactive Power Compensation

The OWPP test model is equipped with fixed and switched reactive power compensation. These reactors are modelled as three inductors in star connection. In series with the inductors, a resistance is placed to account for the losses ($\frac{X}{R} = 200$). In Fig. 3.1, the reactive power compensation is stated in power form. To calculate the inductance, L, and resistance, R, the following expressions are applied,

$$X = \omega_1 \cdot L = \frac{V_{LL}^2}{Q} \tag{3.6}$$

$$R = \frac{X}{200} \tag{3.7}$$

being ω_1 the nominal angular frequency, V_{LL} the RMS line to line voltage and Q the reactive power. The switching of reactors may give rise to transients in which the current waveform includes a DC component that decay with time. The existence of a transient when switching the reactor depends on the voltage point of wave at which the circuit breaker is closed. The situation is worst when the reactor is switched at zero voltage, while it is best when it is switched at peak, i.e. ideally no transient would occur. To avoid such transients, all the reactors are considered connected when the OWPP is soft-charged. Avoiding transients through soft-charging also facilitates the reactor model, as parameters such as iron losses, saturation or mutual coupling can be avoided.

Apart from the reactor, there is a C-type filter at the onshore bus. Its objective is the mitigation of high frequency components. This element is modelled as three capacitors in star connection and is also soft-charged with the rest of the OWPP. The expression to calculate the capacitance, C, is given below.

$$X = \frac{1}{\omega_1 \cdot C} = \frac{V_{LL}^2}{Q} \tag{3.8}$$

3.3 Control of IBESS

The reference control scheme utilized in the IBESS Project, [37], is PSC, which is described in [32]. The overview of it was shown in Section 2.4.2. It is mainly formed by: a Power Synchronization Loop, an AVC, and a Current Limiting Controller. The output voltage signal going out of the AVC is not directly fed to the converter because the system would be poorly damped. Instead an active resistance term, R_a is subtracted by means of high pass filtering the converter´s current, $i_{c,dq}$. In the following, the different building blocks of PSC are explained in detail.

3.3.1 Power Synchronization Loop

PSC achieves synchronization through the integration of the power difference multiplied by a gain K_p (2.3). Thereby, PSC inherently adds a frequency droop. The tuning process of this gain is explained in [44] for the operation of PSC in grid-connected mode. The objective is to obtain a sufficient stability margin irrespective of the Short Circuit Ratio (SCR) of the grid. By analyzing the closed loop dynamics of the Power Synchronization Loop, (3.9) is derived to obtain a gain margin of $g_m \geq 2$ [44]:

$$K_p = \frac{\omega_1 R_a}{\kappa V^2} \tag{3.9}$$

where ω_1 is the base angular frequency, $\omega_1 = 2\pi 50$; R_a is the active resistance value and V is the magnitude of the converter phase voltage. κ is the scaling factor, which for peak value vector scaling is equal to $\frac{3}{2}$. R_a cannot be selected arbitrarily as a high value would reduce the system's bandwidth, while a very low value would derive into a poor damping. In [44] the authors suggest $R_a = 0.2\,\mathrm{p\,u}$ and a negligible cutoff frequency for the high pass filter i.e. $\omega_b = 0.1\,\mathrm{p\,u}$; which means that $H_{HP}(s) \approx R_a$ [44]. Figure 3.6 shows the schematic of the power synchronization loop.

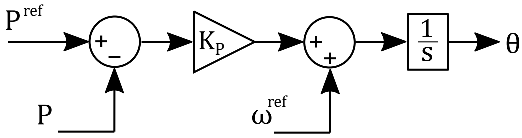

Figure 3.6: Power Synchronization Loop.

3.3.2 Alternating Voltage Controller

The objective of the AVC is to control the voltage at the IBESS PCC, in this case, the onshore substation bus. It is designed as a proportional controller, thus it has a droop characteristic. The output of the AVC feeds the voltage reference of the converter. Recalling (2.4), this reference is not directly fed to the converter modulator, instead the active resistance term is subtracted. Figure 3.7 depicts the schematic of the AVC.

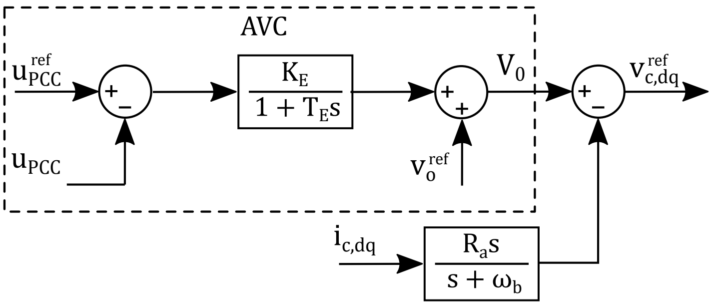

Figure 3.7: Alternating Voltage Control and active resistance term.

The reference signal of the AVC would change depending on the operation mode of the IBESS. The energization of the OWPP is made by soft-charging the AC network. Consequently, during this period the reference voltage signal is a ramp that goes from 0 to $\hat{v}_{ref}$. In grid-connected mode, or when the energization is over, the reference signal would remain constant.

3.3.3 Current Limiting Controller

The current limiting controller assures that the converter current does not exceed the semiconductor ratings. Therefore, the first step is to generate a current reference from the calculated converter voltage reference, $v_{c,dq}^{ref}$. The process is explained in [32] and the implemented control law was given in (2.6).

Once the reference current signal, $i_{c,dq}^{ref}$, is obtained, its module is limited to $1\,\mathrm{p\,u}$. The following part of the controller is the calculation of the new $v_{c,dq}^{ref}$ that avoids overloading the converter. This control law, (2.7), is similar to the ordinary utilized for proportional vector current controllers, consisting on a proportional gain that govern the system closed loop bandwidth (α), decoupling terms, and a feed-forward of the output voltage, i.e. the voltage at the grid side of the filter. Figure 3.8 shows the schematic of these controller. Note that, the output voltage is filtered to avoid introducing high frequency oscillations in the controller.

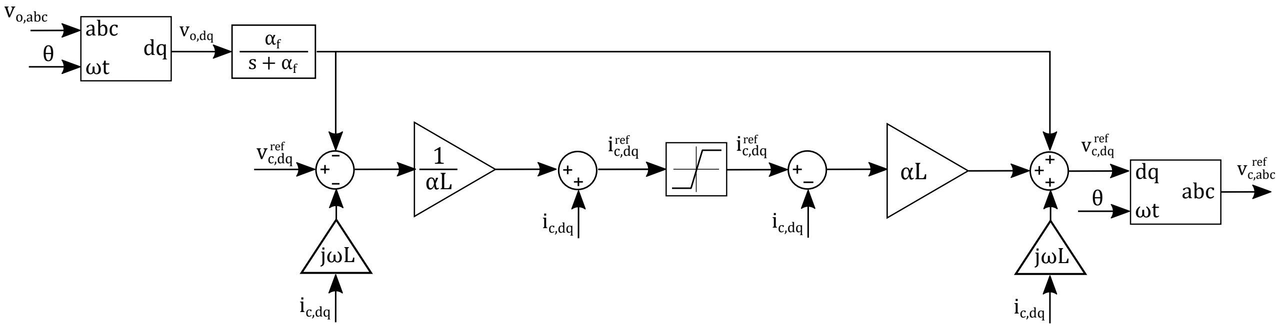

Figure 3.8: Current Limiting Controller.

3.4 Control of Wind Turbines

WTs utilize GFL control, hence the are synchronized to the AC grid by means of a PLL. The implemented current controller is based on vector current control in the dq-frame. In addition, they are equipped with $P - f$ and $Q - V$ droops to give frequency and voltage response respectively.

The current controller is developed following [45]. The current is regulated by PI controllers, and voltage feed-forward is implemented. Thereby, the proportional gain determines the closed loop bandwidth, while the integral gain should be negligible. Relying in voltage feed-forward, the proportional gain itself should be able to control the current without steady state error. However, due to resistive losses in the LCL filter, a small integral gain aids the reduction of the steady state error to zero. These gains can be calculated as:

$$K_p = \alpha_{WT,cl} \cdot L_f \tag{3.10}$$

$$K_i = \alpha_{WT,cl} \cdot R_f \tag{3.11}$$

where $\alpha_{WT,cl}$ is the desired closed loop bandwidth, while L_f is the filter inductance. R_f is a small resistors that account for the losses in the filter. They can be approximated as 10 % of the corresponding reactance.

Concerning the $P - f$ droop controller, it is designed to have a response similar to a synchronous machine governor. Hence, it is modelled as a simple gain, which account for the machine droop, R, and a time delay. Similarly, the $Q - V$ control is modelled as a gain and shorter time delay, as the excitation control of a synchronous machine has a faster response than the mechanical valves ruling the active power. Figure 3.9 shows the WT controller.

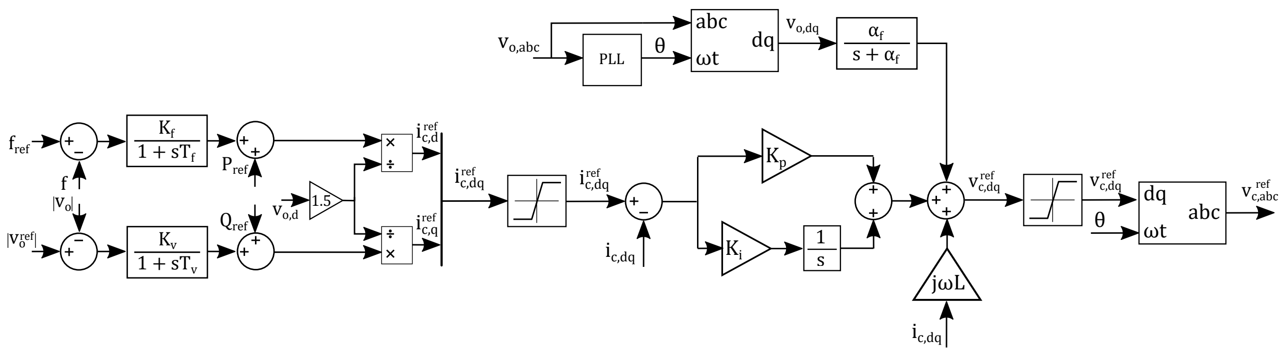

Figure 3.9: Wind turbine GFL controller.

Note that current and voltage limiters are implemented. The former would avoid that the converter current exceeds the semiconductor ratings. The latter is related to the converter DC link capability, which limits the achievable peak value of the AC voltage waveform.

3.5 Summary

The objective of the present chapter was to explain how to model an OWPP when a BS proceess needs to be designed or analysed. Section 3.1 presented the OWPP test model. It consists on a portion of Ørsted's HornSea II wind power plant located in the Yorkshire coast (UK). The modelling guidelines that explain how to implement appropriate models for EMT simulations are developed in Section 3.2. All the relevant components are considered: export cables, transformers, collector systems and wind turbines. The outcome of the modelling guidelines is a set of parameters that are presented in Appendix A.

In addition the IBESS system is incorporated to the OWPP at the onshore Bus. Modelled as an averaged voltage source, its key characteristic is the possibility to perform GFM control. Therefore, PSC is developed in detail in Section 3.3 as the reference control scheme for the IBESS. It will allow soft-charging the OWPP and create an AC voltage waveform to which the WTs can synchronize to. Concerning the WTs, they are equipped with GFL converters, thus traditional vector current control is implemented. A brief explanation on how to design this controller is given in Section 3.4.

The development of the OWPP test model enables to simulate the plant energization process, the switching of the WTs and their synchronization. Afterwards, the generated power of the WTs will be ramped-up to assess the islanded operation of the OWPP. The self-start process and islanded operation is presented in the following chapter.

Chapter 4

Black Start and Islanded Operation

In this chapter, the self-start process and islanded operation of the modelled OWPP is evaluated. The modelling guidelines for OWPPs were introduced in Chapter 3, and the specifications for Hornsea II wind power plant are given in Appendix A. There, the reader can find the parameters for the underground and submarine cable sections, the offshore collector equivalent circuit and the transformers data.

In the following sections the BS procedure is explained, highlighting the different steps and key performance metrics of the process. Then, the IBESS ratings and its controller parameters are presented. The same is done for the WT clusters, as both controllers are crucial for the correct operation during self-start, synchronization of wind turbines and eventual ramp-up of the WTs power. Finally, the performance of the system in each step of the process is explained and assessed.

4.1 The Black Start Procedure

By means of the IBESS operated as a GFM converter, the process start by ramping the converter voltage from 0 to 0.95 p u in 2 s. This is also called soft-charging and consists on gradually ramping-up the voltage in order to energize the OWPP components [11]. Therefore, all the circuit breakers are closed to enable the complete energization of the power plant (only the circuit breaker to the grid is kept open). The reason behind soft-charging the OWPP is the inability of the converter to withstand the high current and voltage transients that would appear if the different components are hard-switched. The expected result of soft-charging is the gradual ramp of the voltage in all the buses, avoiding transients in the voltage or current waveforms. The IBESS active power would increase to account for the losses in the circuit, while the reactive power would behave similarly, giving the required compensation in order to maintain the specified voltage level at the onshore bus.

At the 4 s time instant, the first WT cluster is energized. This is done by simply closing the WT circuit breaker, thus it consists on a hard-switching operation (CB1 in Fig. 3.4). At this instant, the WT transformer and the LC part of the filter is charged. The expected outcome is a high inrush current caused by the transformer energization. Besides, possible parallel resonances should be checked due to the nature of the transformer inrush current. It presents many harmonic components, being the second harmonic of relevance. Hence the presence of a parallel resonance at 100 Hz would provoke a sustained over voltage in the network. At 5 s the WT controller is enabled and the generator unblocked by switching a circuit breaker (CB2 in Fig. 3.4). At this point the WT cluster aids IBESS to regulate frequency and voltage as it presents P-f and Q-V high level droop controllers. The following WT clusters are connected similarly, separated by a 3 s time step.

Finally, after the six WT clusters are energized and synchronized, the total generated WT power is ramped-up to 50 MW. This happens from 23 to 24 s and it demonstrates the islanded operation of the OWPP. It is expected that the IBESS start absorbing the active power generated by the WTs. It must be noted that IBESS will not receive the exact 50 MW for two reasons: first, the resistive losses along the network; and second, the P-f droop controller will adapt the WT power reference set point depending on the frequency, reducing the generated power if the frequency exceeds 50 Hz. Figure 4.1 intends to clarify the self-start procedure, showing the different time instants at which each of the events occur.

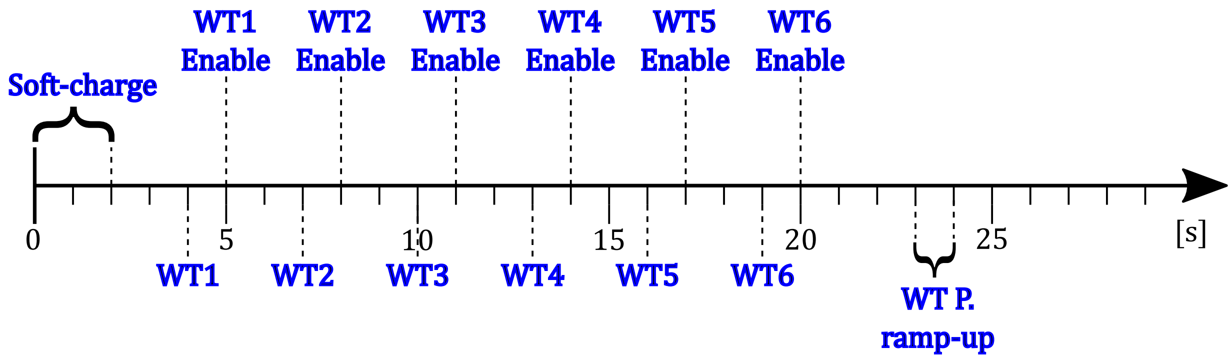

Figure 4.1: Timeline of the BS process.

It must be noted that the proposed procedure is not adapted to any standard process or grid code. In fact, there are still no regulations on how the BS of an OWPP should be performed. Furthermore, the duration of the process presented in Fig. 4.1 is intended to reduce the computational burden, hence it does not pretend to be the real time scale for the on-site course of action, which could take approximately 2 hours [4]. As an example, Energinet limits the active power ramp rate of grid-connected WTs to 100 kW/s, which would lead to longer ramp-up duration compared to the proposed timeline [46].

4.2 The Selft-start Unit: IBESS

Being the IBESS an ES-STATCOM system, it has the ability to self-start the OWPP. The STATCOM part consist of a 112 MVA converter, which operates at an RMS line to line voltage of 33 kV. However, the ES section is a battery rated at ±50 MW, limiting the active power capability to a level below the total converter rating. The ES-STATCOM is connected to the onshore bus by means of a 33/220 kV transformer and an inductor $L = 0.1\,\mathrm{p\,u}$, which represents the arm reactor of the MMC (see Fig. 2.5). The selection of $L = 0.1\,\mathrm{p\,u}$ corresponds to a typical impedance value.

Regarding the controller parameters, they are adjusted following the the guidelines given in Section 3.3 and checking the performance during the self-start process, achieving low voltage and frequency oscillations. In [44], the authors recommend to start the tuning process with the active resistance term. Recall that it is formed by a high pass filter, $H_{HP}(s)$, acting over the converter current that subtracts to the voltage reference in order to provide damping, $v_{c,dq} = V_0 - i_{c,dq} \cdot H_{HP}(s) = V_0 - i_{c,dq} \cdot \frac{R_a s}{s+\omega_b}$. Making ω_b negligible, $H_{HP}(s) \approx R_a$. Therefore, $\omega_b = 0.1\,\mathrm{p\,u} = 31.42\,\mathrm{rad/s}$ is selected. The following step is to set the value for R_a. High values would compromise the bandwidth of the controller, while very low ones would provide a poor damping of oscillations. In [44] a $R_a = 0.2\,\mathrm{p\,u}$ is recommended. However, in this application a shorter convergence time is desired, so $R_a = 0.075\,\mathrm{p\,u} = 0.73\,\Omega$ is chosen, achieving a suitable damping for the application.

The selection of the power synchronization loop gain, K_p is tied to R_a due to the stability of the closed loop system. As mentioned in Section 3.3.1, in order to obtain a sufficient gain margin, (3.9) should be applied, obtaining $K_p = 0.21 \frac{rad/s}{MW}$. This value is also affecting the P-f droop characteristic of the IBESS, so if it has a high value, power variations would result in higher frequency oscillations.

Concerning the AVC, it consists of a droop controller that regulates the voltage at the onshore bus,

$V_0 = v_o^{ref} + (u_{PCC}^{ref} - u_{PCC}) \cdot \frac{K_E}{1+T_E s}$ (recall Fig. 3.7). This controller is designed in per unit values, selecting a gain of $K_E = 0.75\,\mathrm{p\,u}$, which provides a good performance. Finally, the current limiting controller is tuned as a traditional proportional current controller. Its gain is calculated as:

$$K_p^{CLC} = \alpha_c \cdot L \tag{4.1}$$

being α_c the desired closed loop bandwidth, in this case equal to 1570 rad/s. An integral gain is not necessary as voltage feed-forward is implemented. The high frequency components of the voltage waveform are filtered with a low pass filter with cutoff frequency $\alpha_f = 2500\,\mathrm{rad/s}$. In summary, the controller parameters are stated in Table 4.1.

Table 4.1: Controller parameters for the IBESS system.

Controller	Parameter	Value	Unit
Power Synchronization Loop	K_p	0.21	$\frac{rad/s}{MW}$
Alternating Voltage Controller	K_E	0.75	p.u.
Alternating Voltage Controller	T_E	0.05	s
Active Resistance	R_a	0.73	Ω
Active Resistance	w_b	31.42	rad/s
Current Limiting Control	α_f	2500	rad/s
Current Limiting Control	α_c	1570	rad/s

4.3 Wind Turbines Clusters

WTs are aggregated into clusters with a total power capability of 72 MVA. The converter RMS line to line voltage is 0.690 kV, being stepped up to the collection voltage, 66 kV, by means of a transformer. Between the transformer and the converter, there is an LC filter consisting of a series inductor, $L = 0.1\,\mathrm{p\,u}$, a shunt capacitor, $C = 0.05\,\mathrm{p\,u}$ and a shunt damping resistor, R_d of similar order of magnitude that the shunt capacitor impedance at resonant frequency. These values are taken from the recommended design parameters for LCL filters given in [47]. The objective of the LC circuit is to attenuate the switching harmonics caused by the converter operation. Even though an averaged voltage source model is utilized for the converter (there are not switching harmonics), the LC branch is considered due to its effect during WT energization as well as during steady state performance.

Concerning the controller parameters, the PLL is tuned following [48], while for the current controller, the guidelines in [45] are adopted. The bandwidth of the PLL is chosen equal to $\alpha_c^{PLL} = 124\,\mathrm{rad/s} \approx 20\,\mathrm{Hz}$, achieving a settling time of 0.022 s and a sufficient oscillation rejection. On the other hand, the current controller bandwidth is selected assuming a converter switching frequency of 2.5 kHz. Thus, from [45], the recommended close loop bandwidth is:

$$\alpha_c \leq 0.2 \cdot 2500 = 500Hz \tag{4.2}$$

Then, the PI controller gains are calculated applying (3.10) and (3.11). Voltage feed-forward is implemented, being the voltage low-pass filtered with cutoff frequency of 5000 rad/s. Regarding the droops they are designed to resemble a synchronous generator, which implies that the P-f droop has a longer time response due to the mechanical nature of governors, while the Q-V is faster, resembling the voltage excitation control, with a gain of $K_v = 0.5\,\mathrm{pu}$. The P-f droop has a gain of $R = 5\%$, which is a typical reference value for synchronous generators, [49]. Overall, the controller parameters are presented in Table 4.2.

Table 4.2: Controller parameters for the WTs.

Controller	Parameter	Value	Unit
PLL	α_c^{PLL}	124	rad/s
P-f droop	R	5	%
P-f droop	T_f	0.5	s
Q-V droop	K_v	0.5	p.u.
Q-V droop	T_v	0.05	s
Current Control	α_f	5000	rad/s
Current Control	α_c	3141	rad/s

4.4 Soft-charging the OWPP

The process of soft-charging is performed by ramping-up the converter voltage from 0 to 0.95 p u in 2 s. The consequence is that voltage and current transients are avoided. It is depicted in Fig. 4.2 how the current waveform does not present any transient behaviour. For convenience, only phase "a" is shown, having the remaining phases a similar shape, but displaced 120º.

The voltage is ramped to 0.95 instead of 1 p u in order to have a voltage level closer to 1 p u at the offshore bus. This is due to the lower reactive power compensation at this bus, and the subsequent inability to reduce the voltage. In following steps, when the WTs are synchronized, they aid the reactive power compensation at the offshore network by means of their converters.

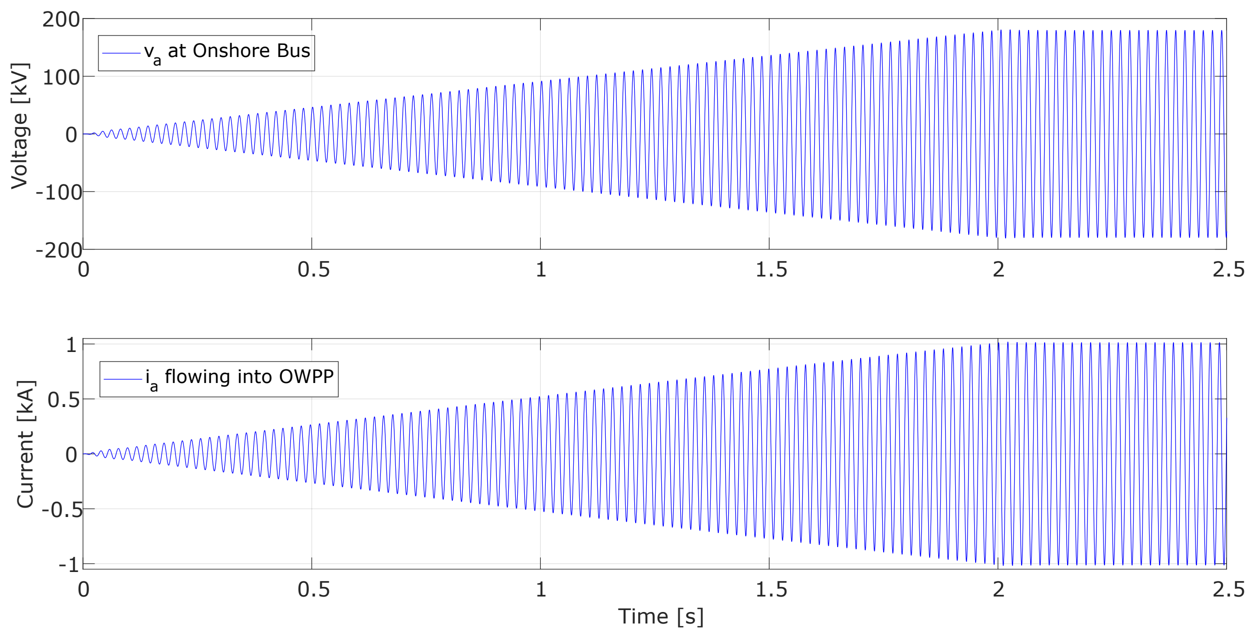

Figure 4.2: Phase "a" voltage and current waveforms at the onshore bus.

Figure 4.3 show the performance of the IBESS system during soft-charging. The active power increases and then settles to a stable point of 7.5 MW. This power is the combination of the losses in the cables and transformers, the shunt reactors, and a small leakage to the onshore gird. Due to the

Power Synchronization Loop, the frequency follows exactly the opposite behaviour, reducing its value because the network consumes power. Regarding reactive power, the IBESS absorbs 46 MVAr in order to maintain the desired voltage level at the onshore bus. It is natural that the IBESS absorbs reactive power because of the high capacitance of the export cable system. Finally, the RMS voltage of the converter and onshore bus is shown in the last graph. The IBESS presents a droop controller intended to control the voltage amplitude at the onshore bus. The inherent steady state error of proportional regulators cause that, even though the reference is 0.95 p u , the voltage at the converter is 0.93 p u , while achieving 1 p u at the 220 kV side of the transformer.

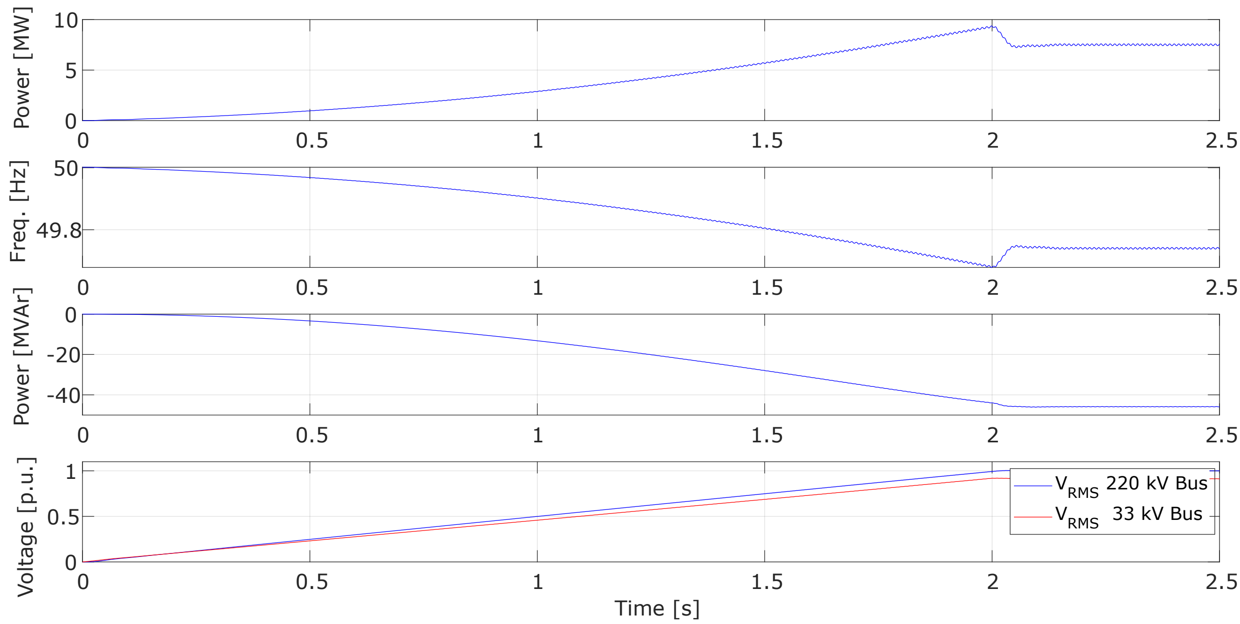

Figure 4.3: Performance of the IBESS during soft-charging.

4.5 Connection of Wind Turbines

At the 4 s time instant, the first WT cluster is switched. It consists in a hard-switching operation, thus transient phenomena is expected. The component causing the transients is the transformer, therefore its energization is analyzed first. After 1 s the control is enabled. At this point, the WT should be already synchronized by means of the PLL and ready to operate under GFL control. Finally, the performance of the IBESS GFM converter is also assessed, to check its ability to regulate voltage and frequency, together with the interaction between the IBESS and the WT cluster.

4.5.1 Wind Turbine Transformer Energization

Transformer inrush currents are characterized by being unidirectional, meaning that contain a DC component that takes the waveform to the positive or negative side of the $y-$axis. Moreover, it can be several times larger than the rated current and it presents all the harmonic components due to its non-symmetrical shape. Figure 4.4 shows the transformer inrush current when the WT cluster 1 is energized. The behaviour is the expected, being the peak current 1.5 times higher than the nominal current. Note how the DC component decays with time. The resistances along the circuit are the ones providing damping to the inrush currents.

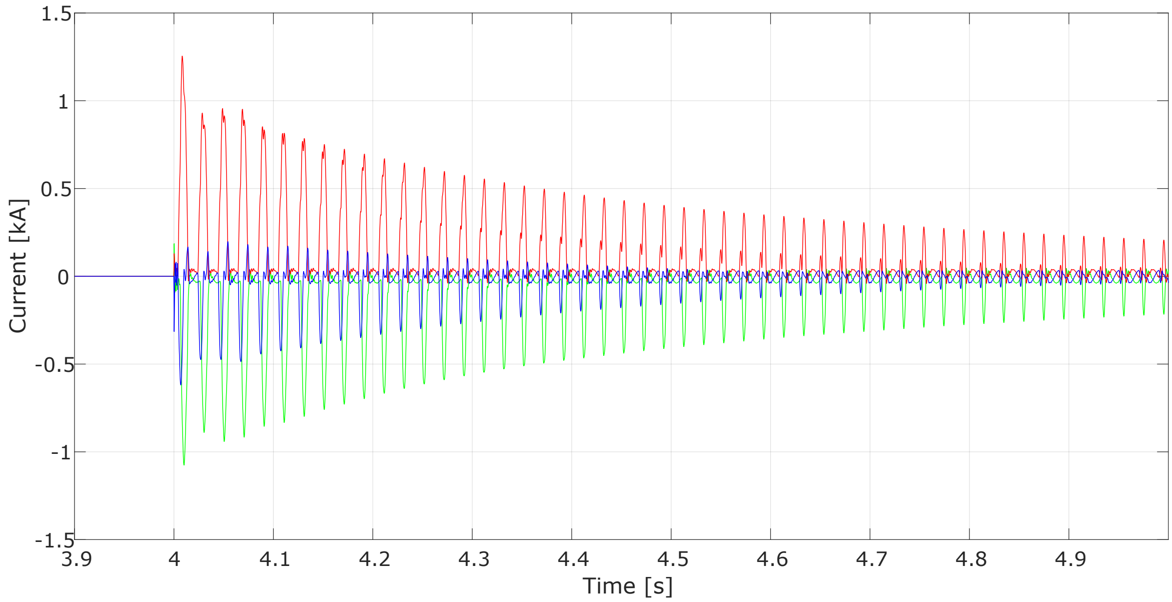

Figure 4.4: Three phase current waveforms measured at the HV side during WT transformer energization. Note the unbalance between phases. The first peak reaches 1.5 times the rated current.

Due to the presence of harmonic components in the current waveform, there is a risk of exciting a parallel resonance and generate a sustained overvoltage in the network. The main harmonic component is the second, having the rest lower magnitudes as the harmonic order increase. Consequently, it is valuable to perform a frequency scan at the WT bus and check if there are low order resonances (from 50 to 400Hz). Performing the frequency scan for frequencies between 0.1 to 2000 Hz, a parallel resonance at 1420 Hz is present. Fortunately, this resonance is at the 28$^{\text{th}}$ harmonic, which does not involves a risk of overvoltage. That can be seen in Fig. 4.5, where the voltage waveform at the WT bus is depicted. The waveform presents unbalanced phases, as a consequence of the unbalanced currents and a small amplitude reduction caused by the higher voltage drop, also due to the higher currents.

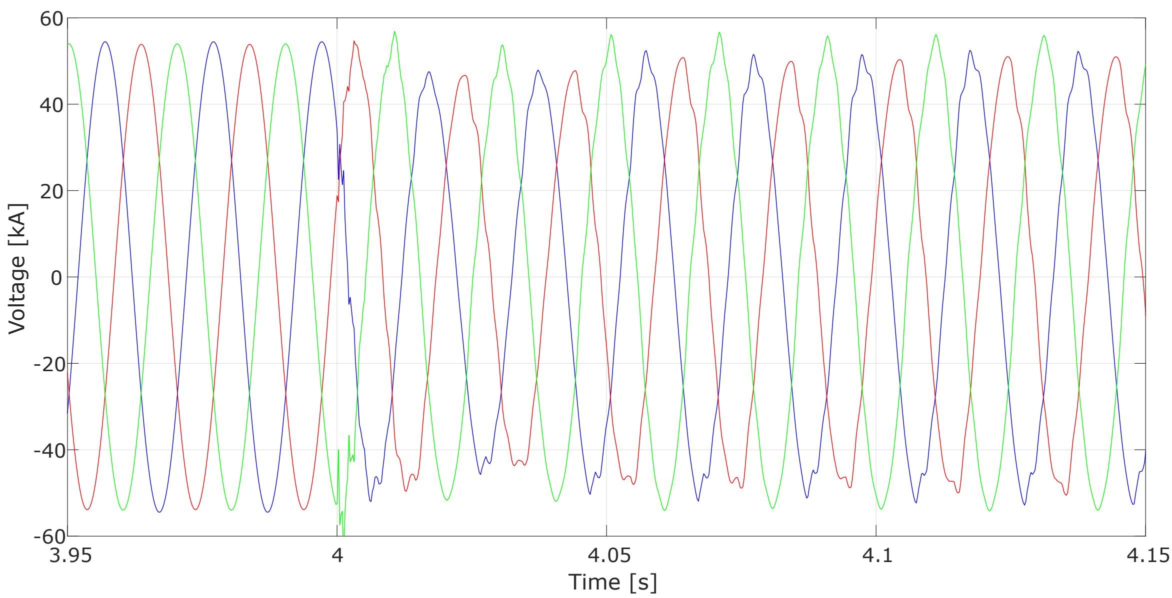

Figure 4.5: Three phase voltage waveforms measured at the HV side during WT transformer energization.

It was mentioned that the transformer energization is done together with the LC filter. This is an important observation as it affects the magnitude of the inrush current. If the transformer would be energized alone, the fundamental component of the inrush current would have been higher, whereas the low order harmonic components would not be affected. The reduction on the fundamental component can be explained by the compensation between capacitive and inductive currents that are drawn during energization of the transformer and the filter shunt capacitor. On the other hand, the low order harmonic components are tied to the transformer energization process, and are not influenced by the capacitor.

The simulated energization would not be performed so aggressively in a real scenario. In this case, a cluster formed by 9 WTs is being energized in a single switching. A real procedure would consist in the gradual switching of each WT, developing inrush currents of lower magnitude. However, the process would last significantly longer, increasing the computational burden of the simulation. The final objective of the project is to demonstrate the BS capability of the OWPP through the IBESS system, thus the progressive switching of the 9 WTs would not provide value to the assessment.

4.5.2 Synchronization of Wind Turbines

WT synchronization is highly dependant on the performance of the PLL. The PLL starts tracking the voltage since the energization begins, at 4 s. Its bandwidth is set to 19.7 Hz, which gives a good compromise between time response and oscillation rejection. Figure 4.6 shows the performance of the designed PLL. The *abc* voltage waveforms are transformed to the *dq*-reference frame by means of the tracked phase, θ_{PLL}, and Park's transformation. The *d*-axis component converges to the voltage amplitude, while the *q*-axis converges to zero. This is convenient for calculation of the current reference, being $i_d^{ref} = \frac{2P_{ref}}{3E_d}$ proportional to the reference active power, and $i_q^{ref} = \frac{2Q_{ref}}{3E_d}$ proportional to reactive power.

The oscillations caused by the transformer energization affect the PLL performance. After some time, they become negligible. The discontinuity at 5 s is caused when the WT control is enabled. Overall, the WT controller aids the stabilization of the voltage as it regulates the injected current.

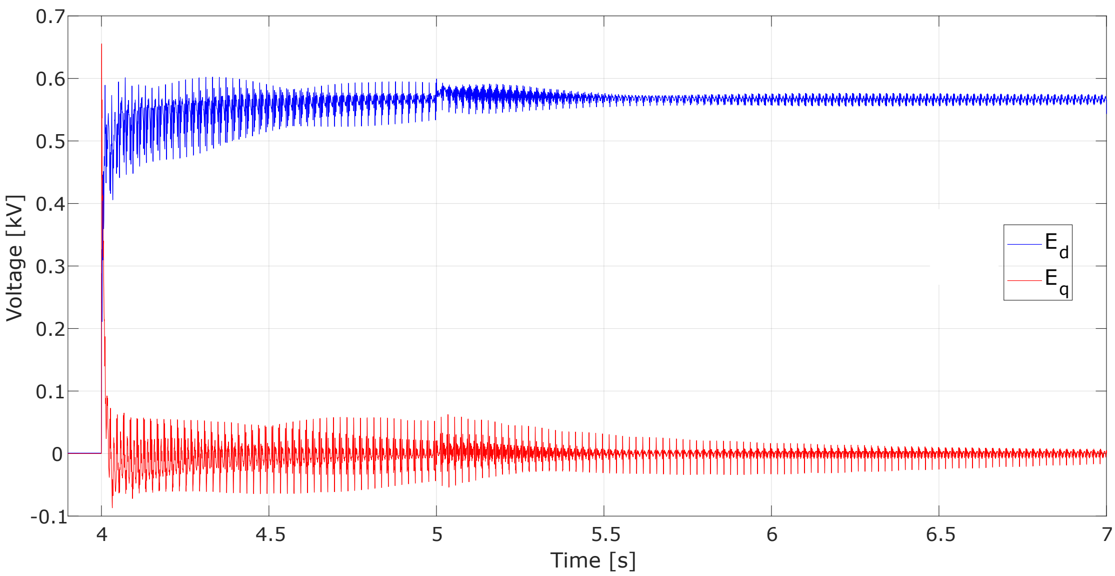

Figure 4.6: Performance of the PLL during synchronization of the WTs.

Figure 4.7 shows the reference and actual WT currents in the dq-frame. At 4 s the current references start building up, and at 5 s the control is enabled and the converter current follow the reference with a quick transition. Some oscillations remain in the current, which are due to the harmonic content of the transformer inrush current that are decaying with time.

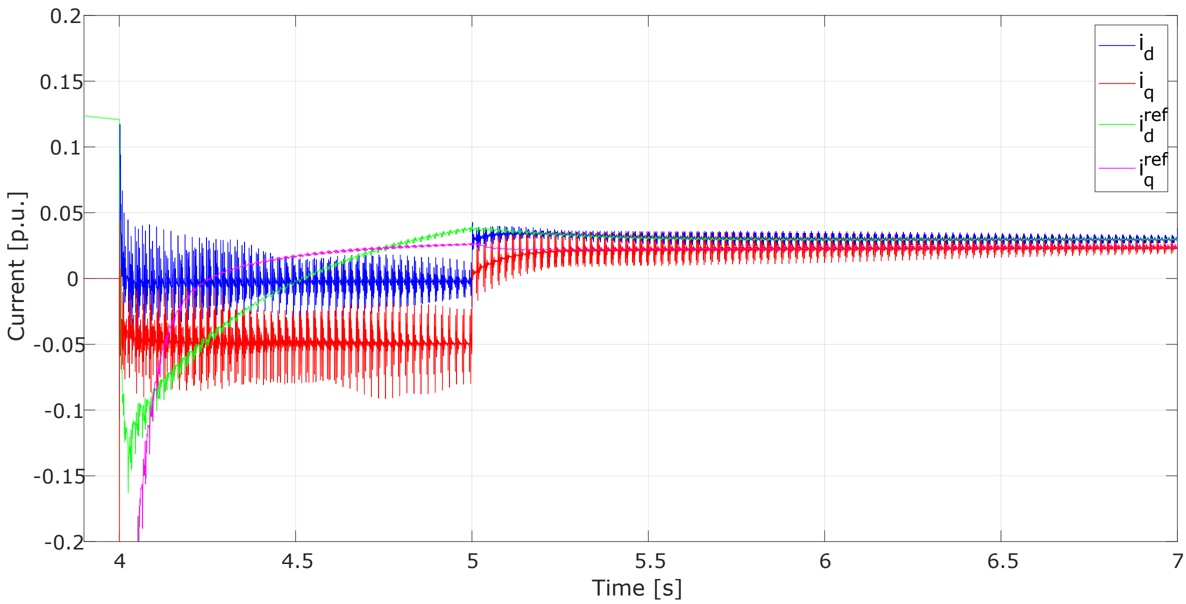

Figure 4.7: Performance of the WT current controller during synchronization.

4.5.3 Performance of IBESS

The IBESS is affected by the WT cluster energization and reacts to regulate voltage and frequency at the onshore bus. Besides, after the WT control is enabled, some interactions between the IBESS and the WTs occur, which affect the active and reactive power output of the ES-STATCOM system. Figure 4.8 shows the performance of the IBESS during the energization and synchronization of the WT cluster 1. There is an active power swing at the instant of energization, which stabilizes before the WT control is enabled. The opposite behaviour is seen in the frequency, due to the operation of the Power Synchronization Loop. The frequency swing is acceptable, with a maximum peak to peak amplitude of 0.7 Hz, while remaining between the [47.5,51.5] thresholds that were established in Table 2.1.

Concerning reactive power, there is a relevant transition from -46 to −7 MVAr after switching the WT cluster. This can be explained by the fact that the WT transformer enters into saturation. Because of this, the transformer absorbs a peak of 190 kA (measured at the LV side) of magnetizing current, i.e. reactive power, which compensates the one generated by the export cable. The reactive power absorption decays at the same pace as the DC component of the inrush current. Naturally, the voltage follows the opposite behaviour. However, note how the IBESS converter voltage increases in order to damp the voltage drop. The consequence is that the onshore bus voltage does not decay below the 0.9 p u voltage threshold.

After the WT control is enabled, the generated active power of the IBESS is reduced and the frequency gets closer to the rated, 50 Hz. Despite the WT active power reference is set to −0.05 p u to account for the WT auxiliary loads, the performance of the P-f droop control in an under-frequency situation makes the WT cluster 1 generate 2.2 MW, which causes the reduction on the generated power of the GFM unit, and also takes the frequency to a higher point. A similar interaction is seen on the reactive power. The Q-V droop controller of the WT aids the IBESS by absorbing 2.5 MVAr.

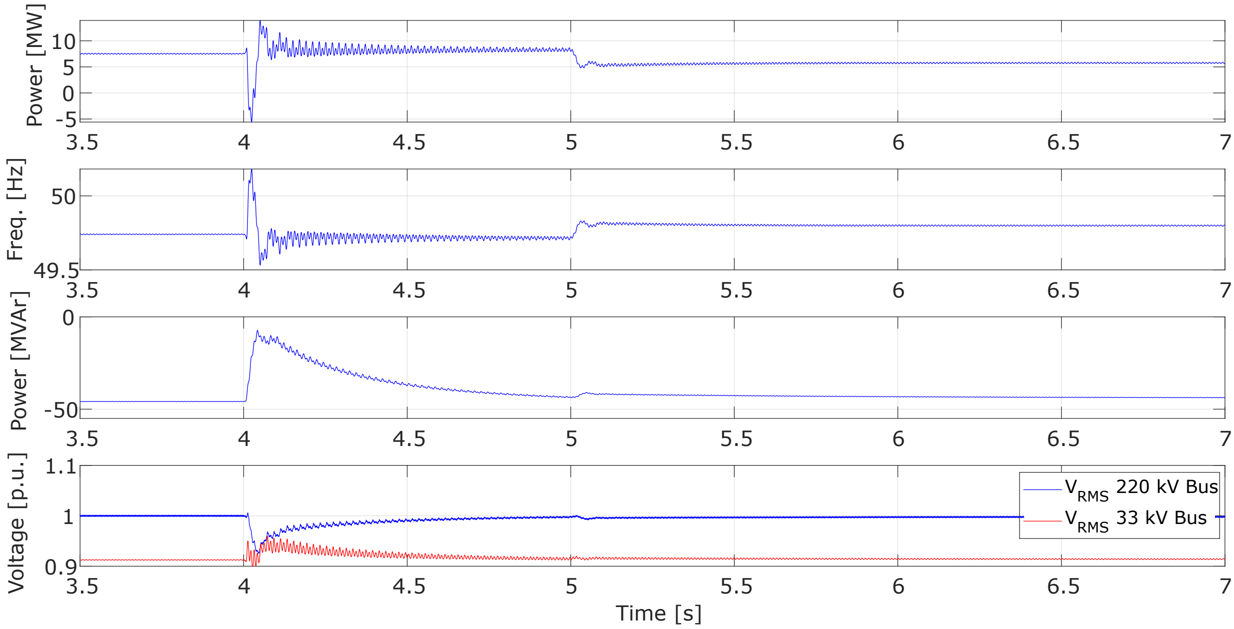

Figure 4.8: Performance of the system during the energization of WT Cluster 1.

4.5.4 Effect of Remanent Flux in the WT Transformer

In the previous WT cluster energization process, it was considered that there was no remanent flux in the transformer. The existence of a remanent flux is due to the hysteresis of the magnetic core, that opposes to the change in its magnetic induction when the winding excitation current has been reduced to zero. The effect of remanence may result in the aggravation of the transformer saturation. Therefore, the magnetization current that the transformers draw from the network becomes bigger. The situation can be worse because the remanent flux is summed to the change in the flux that the switching causes, saturating the core even more.

In order to study the effect that remanent flux has in the connection of WTs, the energization of the WT cluster 1 is performed with a remanence of 80% in phase "a", -80% in phase "b" and 0% in phase "c", which according to [50] corresponds to the worse case scenario. A new simulation is performed considering only the WT cluster 1. The WT1 circuit breaker is closed at 4 s, while the control is enabled at 6 s. This is a different scenario to the one presented before, and the reason behind delaying the WT generator unblocking is the longer settling time of the new transient. Figure 4.9 shows the magnetizing current after switching. Note how the peak values are higher than in Fig. 4.4, achieving a peak value of 3.5 p u during the first instants of energization. It must be mentioned that the unbalance between phases and the size of the peak also depends on the point of wave where the switching is done.

Concerning the performance of the IBESS and the voltage level at the onshore Bus, it is shown in Fig. 4.10. The active power and frequency swings are a 84 % higher after the switching, but they rapidly settle into a steady state value. Additionally, the reactive power presents an important difference with the previous energization. It undergoes a jump of 79 MVAr, going from the initial −46 MVAr to 33 MVAr. The higher change in reactive power is caused by the increased saturation, thereby increase in the reactive power absorption from the transformer. In fact, it absorbs a magnetizing current with a peak of 250 kA (measured at the LV side). Consequently, the voltage at the onshore bus is affected, experiencing a voltage drop down to 0.83 p u that the IBESS AVC cannot damp. In addition, the drop in voltage also causes that the generated reactive power from the cables shrinks. The reactive power compensation of the reactors is reduced as well, but this effect is less significant.

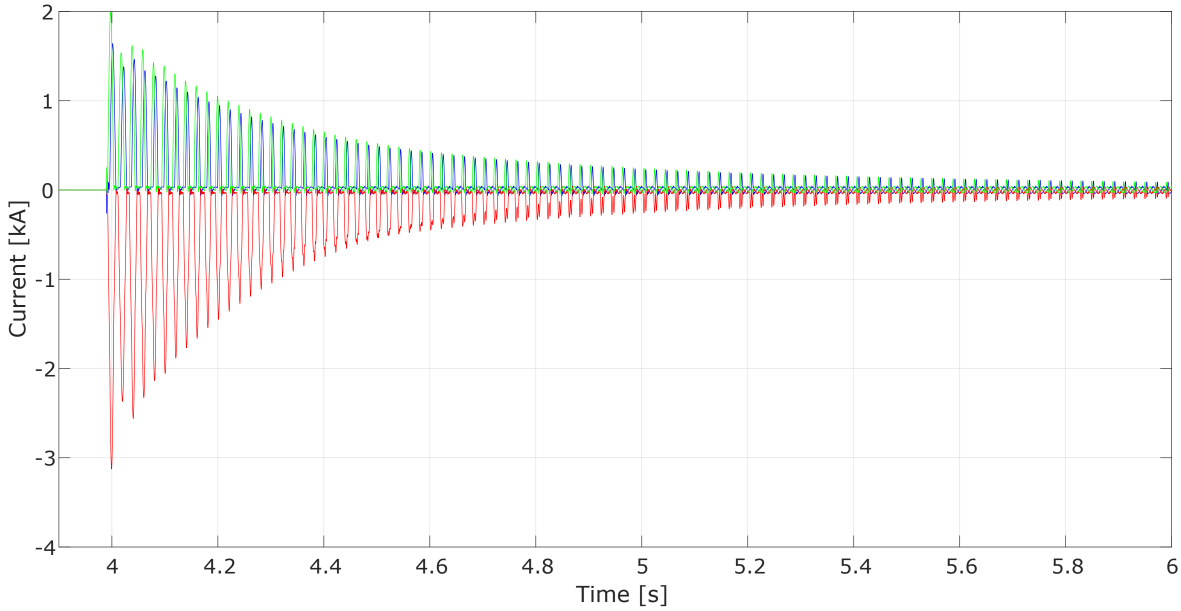

Figure 4.9: Three phase current waveforms measured at the HV side during WT transformer energization, when remanent flux is considered. Note the unbalance between phases. The first peak reaches 3.5 times the rated current.

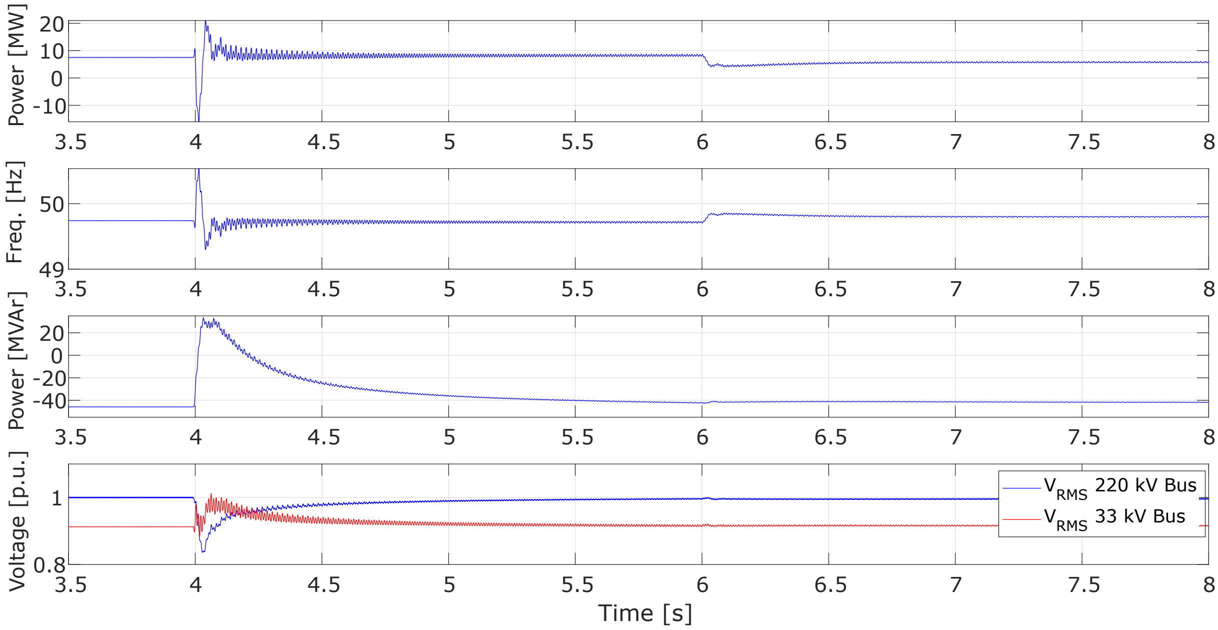

Figure 4.10: Performance of the system during the energization process, when remanent flux is considered.

A possible solution to this issue is the utilization of a pre-insertion resistor, which is connected during the switching, but gets bypassed when the WT generator is unblocked. A simulation was performed with a resistor of 0.2 p u for 0.2 s in the HV side of the WT transformer. The result is a magnetization current that has a peak of 2 p u and it is rapidly damped. The consequence at the onshore bus is a lower voltage drop, which does not fall below 0.92 p u . Please note that the rest of the results presented in the chapter are not considering the remanent flux. Hence, this analysis ends here. The reader interested in checking the transformer saturation curve can refer to Appendix A, Fig. A.1.

4.6 Overall Energization Process of the OWPP

The rest of the energization process follows a similar pattern to the switching of the first WT cluster. Separated by a 3 s time interval, the different WT clusters are connected and synchronized. As all the WTs are equipped with the same GFL controllers, their performance is equivalent. Nevertheless, the output of the P-f and Q-V droops differ because the frequency and voltage get closer to the reference values as more WTs are connected. This can be clearly seen in Fig. 4.11, where the IBESS generated active power and frequency present higher changes when the first WTs are enabled, but lower when the frequency is closer to 50 Hz and the effect of the P-f droop is not of relevance. It must be noted, that along the whole energization process the frequency remain in a tight interval of [49.5,50.2] Hz, which is considered successful.

Concerning reactive power, the performance is the same for all the energization instants, exhibiting a jump in reactive power consumption due to the transformer saturation. However, it is seen how the steady-state reactive power absorption from the IBESS gets reduced after each WT connection. This is due to the WT transformer, which can be seen as a series reactor that absorbs 2.7 MVAr, which compensates the leading reactive power provided by the export cable. Moreover, the WT converter also absorbs reactive power after its connection, thus it also contributes to the former behaviour. Concerning the voltage at the onshore bus (220 kV Bus), it presents similar drops at every WT switching, but its steady-state value is reduced. Recall the voltage reference at this bus was 0.95 p u , thus the reactive power consumption of the WTs due to the Q-V droops aid the IBESS in its voltage regulation task. It is positive that none of the voltage drops goes below 0.9 p u , which corresponded with the lower limit of the success criteria.

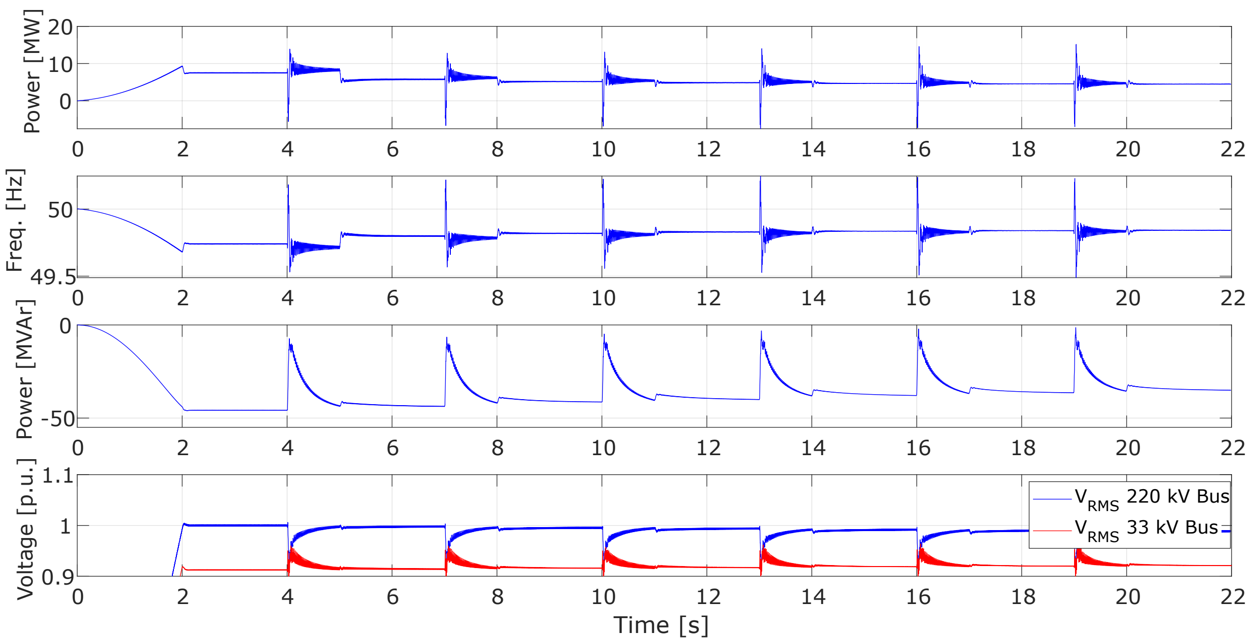

Figure 4.11: Performance of the system during the energization process.

4.7 Islanded Operation

During the previous analysis, the WTs were generating a limited amount of active power, mainly due to their droop controllers; whereas the IBESS was also supplying power to the OWPP. The IBESS System allows bi-directional power flow, which means that it can absorb active power and charge its 50 MW battery. Therefore, the islanded operation is demonstrated by ramping-up the WTs generated power. If the system behaves correctly, the IBESS should absorb the active power generated by the WTs, while the system frequency should increase as a consequence of the PSC synchronization loop.

Figure 4.12 shows the expected performance. Focusing on the WT active power, the power reference of the OWPP is set to supply 50 MW, i.e. 8.3 MW each cluster. However, the actual generated power only achieves 17 MW. This is due to the droop controllers, which, because of the 0.19 Hz over-frequency in the system, subtract 33 MW ($\Delta P_{droop} = \frac{\Delta f}{f_b}\frac{1}{R} \cdot S_b = \frac{0.19}{50} \cdot \frac{1}{0.05} \cdot 72 = 5.5$ MW per turbine) to the former power reference. The action of these droops is clear in the slow power transition after the 24 s time instant.

The IBESS generated power goes from 5 MW to −6 MW, thus it starts absorbing active power and charging its battery. Concerning the frequency, it moves from 49.8 Hz to 50.2 Hz following the same transition as the active power.

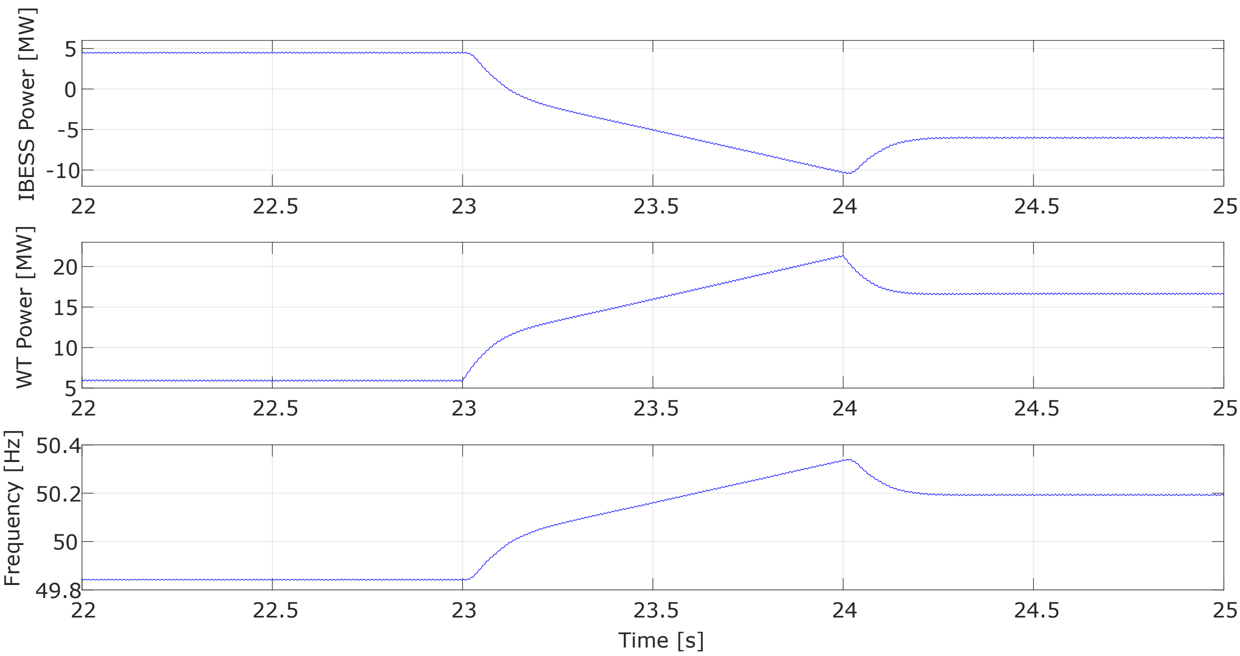

Figure 4.12: Active power and frequency during WT power ramp-up. Demonstrates the islanded operation of the OWPP

4.8 Summary

The present chapter has demonstrated the capacity of the IBESS to self-start the OWPP. This is the first necessary step to enable a wind powered BS. The OWPP is initially de-energized, and needs a power source to achieve the charge of the export cable and the substations transformers. The IBESS is controlled as a GFM converter, and it is able to form a voltage waveform that gradually increases its amplitude. This is known as soft-charging, and enables energization without experiencing transients.

After soft-start, the different WT clusters have to be connected and synchronized. The connection of the WTs is a hard-switching operation, thus a transient inrush current is developed. The OWPP experiences frequency swings and voltage drops after the switching, but they are rapidly regulated by the GFM controller. All the WTs connections are considered satisfactory, as the frequency and voltage success criteria -introduced in Table 2.1- is never violated.

Once the OWPP is energized and the turbines synchronized, the islanded operation is demonstrated. Up to this moment the IBESS was supplying power to the OWPP. However, if the WTs ramp-up their generated power, it is possible to invert the power flow and charge the battery of the ES-STATCOM system. After ramping-up the generated power, the IBESS successfully absorbs the surplus power. Consequently, the self-start and islanded operation of the OWPP is satisfactory; being ready to take part of the power system BS.

Furthermore, during the chapter, the effect of remanent flux in the WT transformer was analyzed. It was demonstrated how remanence increases saturation of the magnetic core, thus developing a higher inrush magnetization current. In addition, it was found that the use of a pre-insertion resistor of 0.2 p u for 0.2 s at the HV side of the WT transformer effectively damp the transient and avoids the violation of the success criteria even during the transient.

Nevertheless, the self-start and islanded operation of the OWPP is not enough to evaluate whether Hornsea II can be eligible as a BS unit. In next chapter simulations, the OWPP is going to take active part in the power system restoration. A simple onshore network will be modelled and energized. Then, three 20 MW block-loads are connected in steps. This would allow the assessment of the wind powered BS.

Chapter 5

Block-load Connection

This chapter demonstrates the BS capabilities of the system formed by IBESS and the OWPP. The energization of the onshore grid and the connection of block-loads is simulated and assessed. First, an introduction of the proposed onshore network is done, then the system performance during energization is described, highlighting the specific features of an OHL energization. The next step is the connection of block-loads, which is followed by a fast frequency response given by the IBESS. Finally, the restoration of the frequency to its nominal value is also accomplished to evaluate the performance and interaction between IBESS and the OWPP.

5.1 The Onshore Network

The proposed onshore network consists of a transmission line, a transformer and 3 resistive loads of 20 MW. Figure 5.1 shows the single phase diagram of the grid. Recall that the 475 MVA transformer was already soft-charged in the previous steps. The selection of the block-load size equal to 20 MW follows the requirements from NGESO, which were highlighted in Table 2.1. The transmission line does not have any reactive power compensation, which will affect the reactive power absorption from the IBESS, as it is forced to consume an amount of reactive power to maintain the voltage close to the reference value. If the IBESS is not able to compensate the line capacitance, a higher voltage in the onshore Bus will result.

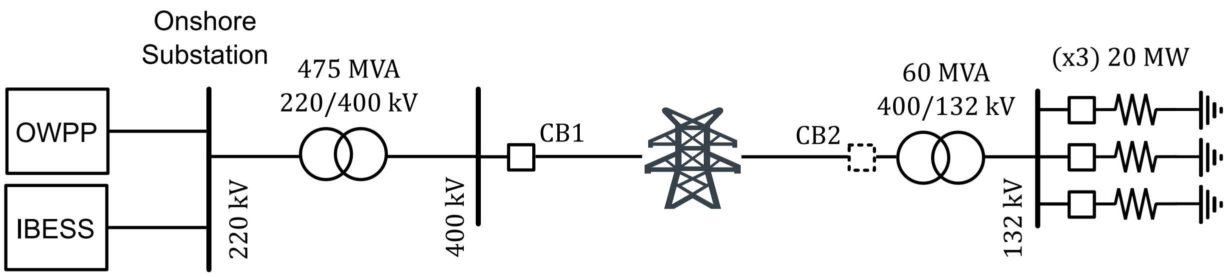

Figure 5.1: Single phase diagram of the onshore network.

The HV transmission line consists on a 100 km OHL. In the original IBESS project, [37], this line is developed with the data from NGESO. Unfortunately, this data only allows to model the OHLs as $\pi-$sections. Therefore, for this analysis, the transmission line specified in [51] is utilized, which represents a real 400 kV OHL located in Denmark. Figure 5.2 represents the geometry of the tower and cable positions. In addition, Table 5.1 represents the parameters of the conductors.

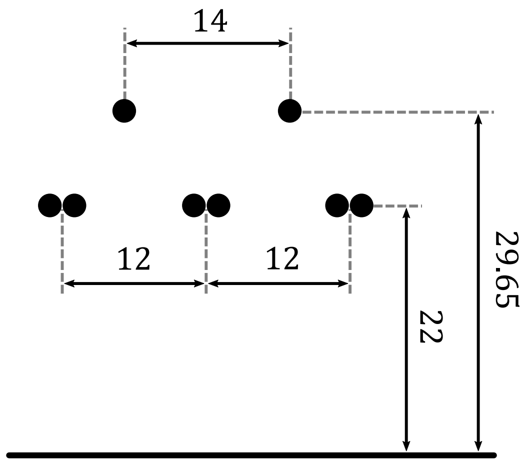

Figure 5.2: Geometrical representation of the position of the conductors and ground wires. Values given in meters. Taken from [51].

Table 5.1: Parameters of the OHL, from [51].

Parameter	Value	Unit
Voltage	400	kV
Length	100	km
Conductor data		
Outer radius	14.89	mm
R_{DC}	0.0514	Ω
Bundling distance	0.4	m
Ground wires data		
Outer radius	7.3	mm
R_{DC}	0.298	Ω

The detailed description of the OHL enables the creation of a frequency dependant model that deliver accurate results in EMT simulations. The following component is a 240 MVA transformer that reduces the voltage to 132 kV. Its parameters are detailed in Table 5.2. The loads are connected at the 132 kV Bus.

Table 5.2: Onshore grid transformer parameters.

Parameter	Value	Unit
Voltage	400/132	kV/kV
Configuration	YYn	
Power rating	240	MVA
Series resistance	0.005	p.u.
Series reactance	0.1	p.u.
Core losses	0.007	p.u.

Saturation of this transformer is not enabled. The reasons behind it is the appearance of numerical problems in the PSCAD calculations that would obligate to reduce the simulation time step or to increase the copper and core losses of the device. When following these recommendations, the switching generates a transient that takes a significant time to decay, making the simulations extremely long without adding value to the purpose of the project.

5.2 Transmission Line Energization

The energization of the onshore network is simulated by energizing the 400 kV OHL. Figure 5.3 shows the induced transient current waveforms at the sending end of the transmission line. The reason behind this transient can be explained by the travelling wave theory. When the line is energized, it is subjected to a voltage impulse, which generates an inrush current. The value of the current depends on the line surge impedance, Z_0 that is defined as:

$$Z_0 = \sqrt{\frac{R_{OHL} + j\omega L_{OHL}}{j\omega C_{OHL}}} \tag{5.1}$$

being R_{OHL}, L_{OHL} and C_{OHL} the resistance, inductance and capacitance of the OHL. The bigger the surge impedance, the lower the first current peak will be. In addition to this first magnitude of the inrush current, note that there are several peaks in a single fundamental cycle. They are caused by the reflections at the sending and receiving ends. The wave needs some time to reach the receiving end, and when it arrives it is reflected back to the sending end. The resistance of the line damps these reflections, and that is why they appear to be less significant after a couple of fundamental cycles.

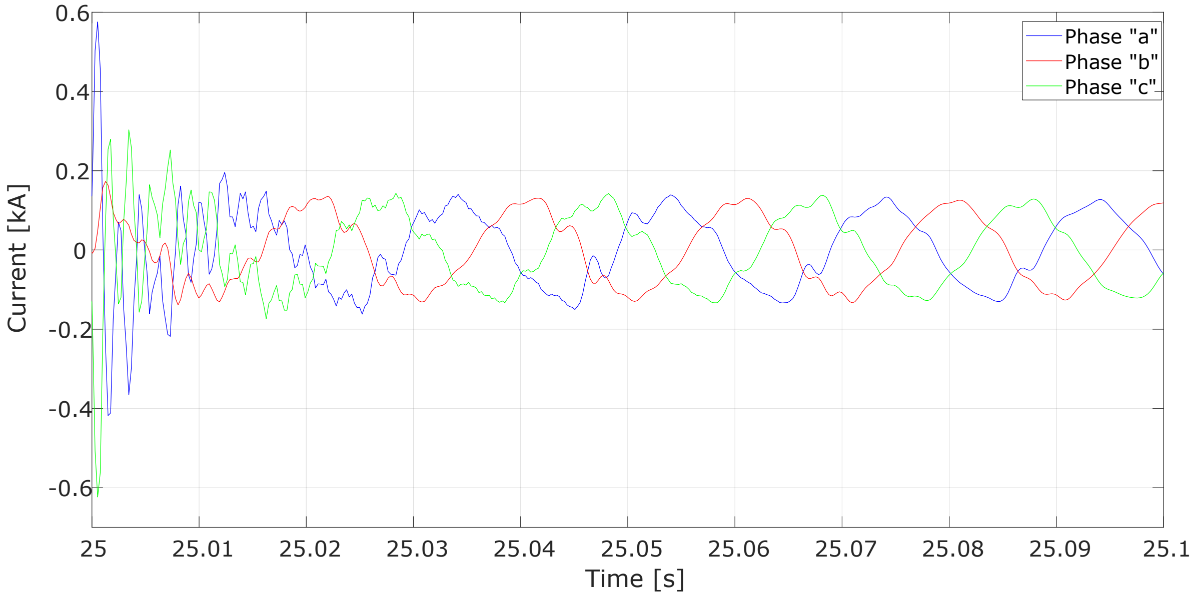

Figure 5.3: Transient current waveforms after OHL switching.

Even though the line is open at the receiving end, the current reaches a steady state value after several cycles. Recall, there is no reactive power compensation, so it corresponds to a capacitive current. Figure 5.4, shows the behaviour of the IBESS during the energization. The active power experiments a small and properly damped transient, which returns to steady state in 10 fundamental cycles. Besides, the absorbed power and frequency level are very similar to the ones before the switching instant, what denotes that the line resistance is negligible ($R_{OHL} = 0.17 \times 10^{-2}$ p u for a $S_b = 100$ MVA). On the other hand, there are relevant changes in the reactive power and voltage profile. The shunt capacitance ($C_{OHL} = 0.547$ p u for a $S_b = 100$ MVA) introduced by the transmission line causes that the IBESS has to absorb 50 MVAr more in order to avoid an overvoltage at the onshore Bus. Finally, the voltage at the 220 kV Bus reaches 1.05 p u , while the converter voltage reduces its magnitude in order to absorb reactive power.

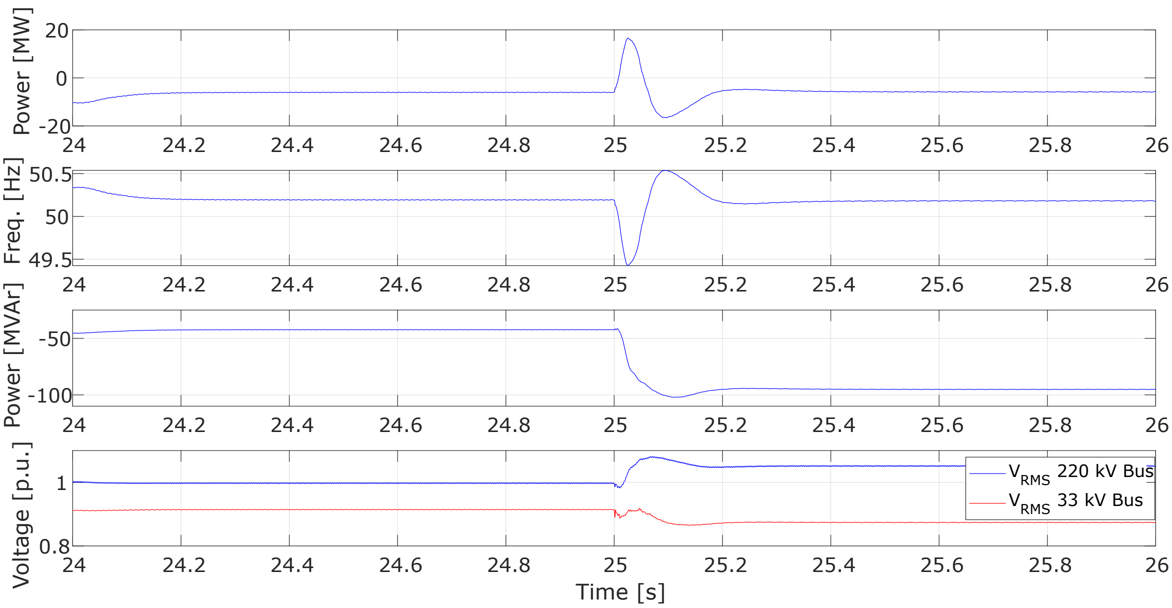

Figure 5.4: IBESS Performance at the switching instant

Overall, the energization of the onshore network can be considered successful. The peak of the generated inrush current achieves a value of 0.89 p u when compared against the rated current of the 475 MVA transformer ($S_b = 475$ MVA and $V_b = 400$ kV), which can be withstood as it does not exceed its ratings. Regarding the performance of IBESS, it reacts to the OHL charging damping an active and reactive power transient in 0.2 s. After this short oscillation, frequency and voltage achieve a stable steady state point. Besides, the converter current does not exceed its overload limit at any instant after the switching.

5.3 Connection of Block-loads

Once the onshore network is charged, it is time to assess the capability of the system during block-loading. Three pure resistive loads of 20 MW are connected separated by a 2 s time step. A frequency drop is anticipated, to which the IBESS should react. In addition, due to the droop controllers, the WTs are expected to contribute with active power in order to restore the frequency to a new steady state point ($\Delta P_{droop} = \frac{\Delta f}{f_b}\frac{1}{R} \cdot S_b$).

5.3.1 Frequency response of IBESS

The connection of the block-loads generates a 0.64 Hz frequency drop that is depicted in Fig. 5.5. It corresponds to a typical response, as it suddenly drops with a high Rate of Change of Frequency (RoCoF), down to a nadir of 49.55 Hz. The magnitude of the drop depends on the system damping and the action of the power synchronization loop. Additionally, the very fast RoCoF is also facilitated by the lack of virtual inertia in the proposed PSC scheme. After the frequency drop, frequency is raised to a new steady state point. This is known as primary response and is due to the droop characteristic of both IBESS and the WTs.

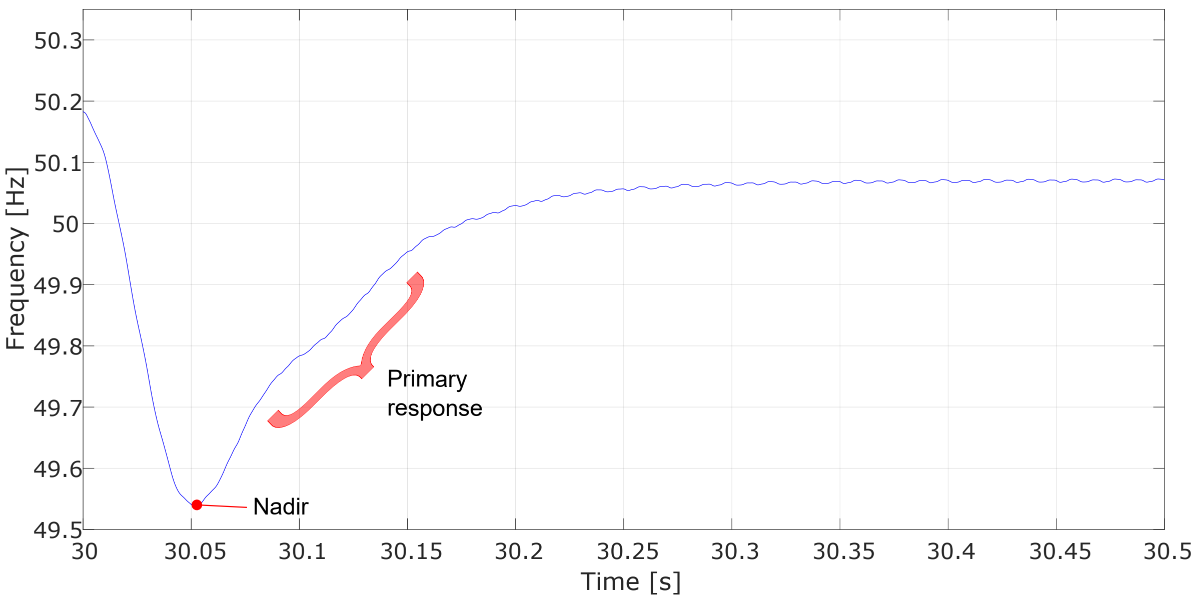

Figure 5.5: Frequency sag after switching the first block-load.

The performance of the IBESS is depicted in Fig. 5.6. Note how the frequency sag is accompanied by the fast response of the generated power. At the switching instant, the IBESS is the only device capable of reacting to the frequency change because the system´s frequency depends upon the power synchronization loop. In addition, the response of the WTs is much slower. Hence, the IBESS has to provide the 20 MW on its own. After each block-load connection, the output power settles at a new steady state value $\Delta P_{IBESS} = 3.5\,\text{MW}$ higher. This is due to the performance of the power synchronization loop and the interaction with the WTs, which are supporting the active power generation with $\Delta P_{droop} = \frac{0.11}{50} \cdot \frac{1}{0.05} \cdot 72 = 3.17\,\text{MW}$ per WT, due to their droop characteristic.

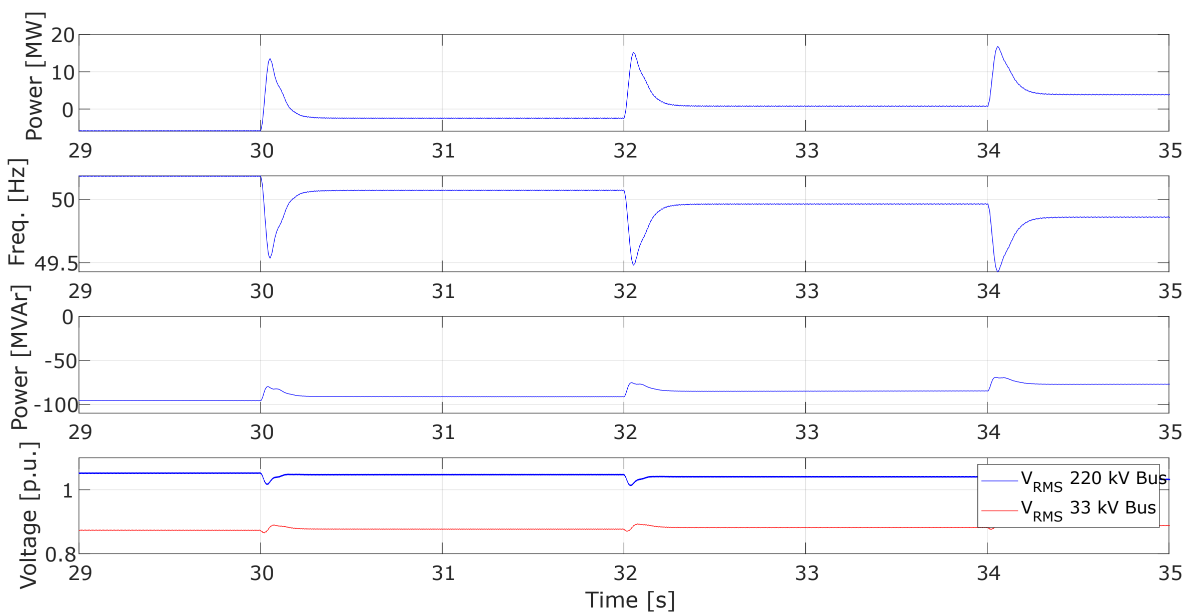

Figure 5.6: IBESS Performance during the connection of block-loads.

Concerning reactive power, the connection of the block-loads causes a relaxation of the reactive power absorption. The transmission line was behaving as a shunt capacitor in the state previous to block-loading. However, after a sustained current starts flowing through the line, the effect of the series resistance and inductance becomes relevant, generating a voltage drop. Besides, the reduction of the voltage also contributes to the reduction of the reactive power generated by the shunt capacitors.

The active power support given by the WTs due to its droop controllers was mentioned in the previous paragraphs. Figure 5.7 shows this performance. Note how the generated power of the WT cluster increases from 3.05 to 6.22 MW ($3.05 + \Delta P_{droop} = 6.22$) in order to feed the load. All the WT clusters are equipped with similar droops, so the power depicted in the graph should be multiplied by six to realize the total generated power by the OWPP. Regarding reactive power, the changes are not so relevant as the voltage at the WT cluster bus does not vary significantly. However, it is clear how the droop reacts by changing the reactive power reference in order to support the voltage regulation.

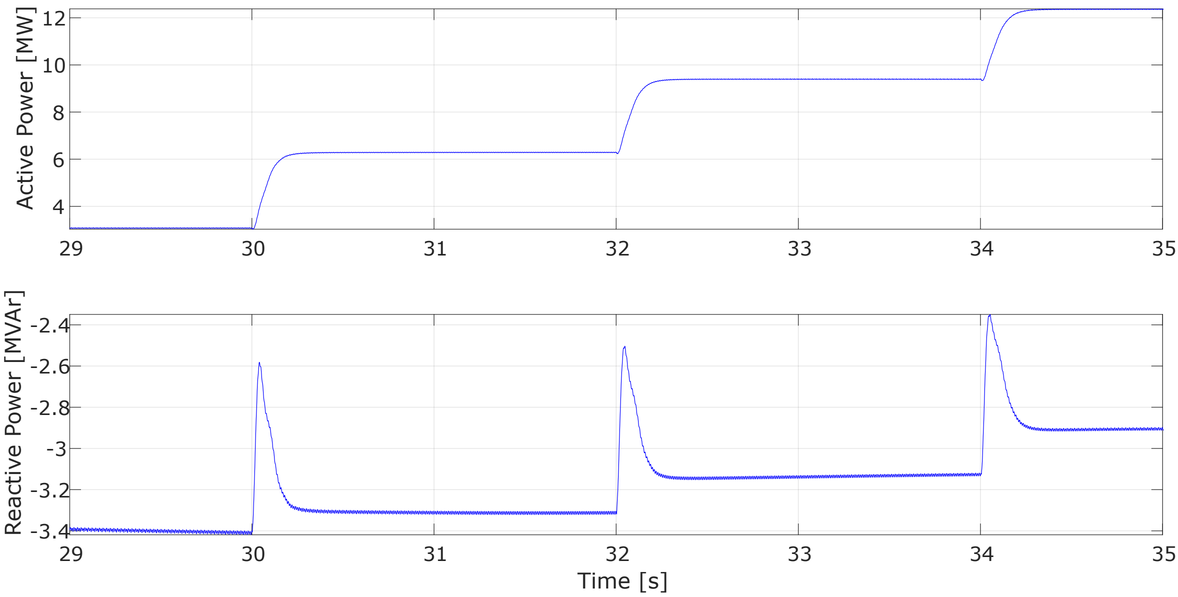

Figure 5.7: WT Cluster 1 generated power due to P-f and Q-V droops.

In summary, the block-loading procedure is considered successful. The frequency drops are not outside the normal operation thresholds [46], which goes between [49.5,50.5] Hz. In addition, they do not exceed the NGESO and ELIA requirements for BS, which were stated in Table 2.1. The same can be said for the voltage level at the onshore bus, that remains between ±10 % of the rated value during the whole process.

5.3.2 Restoration of Nominal Frequency

Even though the BS capability has been already demonstrated, it is interesting to briefly analyze the frequency restoration process up to 50 Hz. From Fig. 5.6 it is seen that after block-loading the frequency has a steady state value of 49.86 Hz. The regulation process to restore the frequency to its nominal value is called secondary control and consists on a centralized and automated system that computes a power reference variation, ΔP, by following the changes in frequency, $\Delta\omega$. It is then added to the active power reference set-points of the different generators of the system taking into account several factors such as size and type of power plant in order to divide the power allocation [49]. In this project, the six WT clusters are similar to each other, so the allocation is made by an equal increment of the power reference of each turbine, $\Delta P_{WT,i}^{ref} = \frac{1}{6}\Delta P$.

As the purpose of this project is not to develop an automatic generation controller, it is designed as a simple integrator which acts over the frequency difference as, $\Delta P_{WT,i}^{ref} = \frac{1}{6}\left(\frac{K}{Ts}\Delta\omega\right)$. The time constant is $T = 1$ s and the gain is $K = 30$, being ΔP and $\Delta\omega$ in per unit. The secondary control is activated manually, and it is disconnected after the frequency has settled at 50 Hz. Figure 5.8 shows the active power of the OWPP and the IBESS, together with the system frequency. Note how the frequency moves to 50 Hz, following the WT generated power. In addition, the effect of the P-f droop decays, due to the fact that Δf is becoming smaller, until it reaches 0 Hz. The IBESS follows the opposite behaviour than frequency, reducing its power generation until it reaches a 0 MW power level.

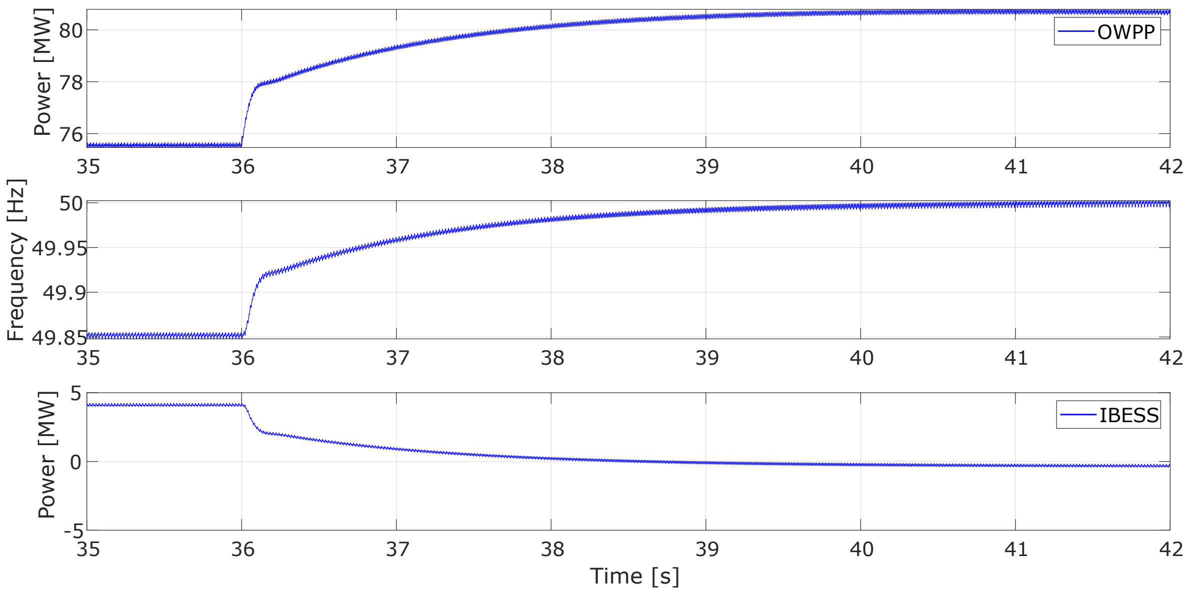

Figure 5.8: Generated power and system frequency

This experiment demonstrates the proper interaction between the IBESS and the OWPP. The controllers are responding as expected, delivering positive results at different scenarios.

5.4 Summary

This chapter has demonstrated the BS capability of the system formed by the IBESS and the OWPP. To assess the power system restoration process, an onshore network is modelled first. It consists in an OHL, a transformer and 3 block-loads. The OHL is modelled with frequency dependant parameters in order to obtain accurate results for transient studies. On the other hand, saturation of the transformer is not enabled due to PSCAD numerical problems. Regarding the block-loads, they consist of 20 MW resistive loads, which is what NGESO requires for BS units [4].

The energization of the onshore network generates an inrush current at the sending end, which did not exceed the onshore transformer ratings. However, charging the capacitance of the line generated a relevant amount of reactive power. It obligates the IBESS to absorb 100 MVAr in order to regulate voltage at the onshore bus. Even so, the voltage level does not exceed 1.05 p u , which is considered successful.

Having energized the onshore network, the block loading is simulated. It involves a typical frequency response, with an immediate sudden drop and a gradual restoration to a new steady state value. The high RoCoF is influenced by the fact that virtual inertia is not implemented in the proposed power synchronization loop. The primary response is achieved by the combined operation of the IBESS and the WTs P-f droop controllers. Nevertheless, primary control is not able to restore the frequency to the nominal value; instead a steady state error is introduced. In order to restore the frequency to its nominal value, the generated power of the OWPP is ramped-up through an integrator acting over the frequency difference until it settles at 50 Hz. Overall, block-loading is also considered successful as the frequency varies between 50.2 to 49.4 Hz, which is inside the thresholds specified by ELIA and NGESO.

BS capability has been demonstrated operating the IBESS under PSC. Virtual inertia and damping were not implemented, which would damp the frequency sags that appear in several steps of the procedure. Consequently, in the next chapter a VSM will be developed in order to compare the performance of both GFM schemes in BS operation.

Chapter 6

Virtual Synchronous Machine for Black Start

During previous chapters all the different subsystems needed to simulate the BS of an OWPP and the following block-load connection were developed. One of these subsystems was the GFM converter, which was modelled following the PSC control scheme. The results showed that the system was capable of performing BS fulfilling the requirements given by NGESO and ELIA.

Nevertheless, both the voltage and frequency presented oscillations during energization of the WT clusters or during the block-load connection. Therefore, in this chapter a new GFM control strategy is developed for the purpose of BS. First the controller design is presented and then the BS procedure is repeated to compare the performance against PSC. Specific behaviour at the WT buses is not presented again, such as transformer energization or WT synchronization, because they do not present significant differences with the previous process. However, it is the focus of the chapter to assess the voltage and frequency performance at the onshore buses. It must be highlighted that the only change of this new model is the IBESS controller, keeping the OWPP and the WT controllers identical to what was developed in previous chapters.

6.1 The Black Start Procedure with VSM

The use of VSM implies to imitate the characteristics of a real synchronous machine. This brings several advantages such as the inertia and damping effect that aids the reduction of oscillations. On the other hand, being the synchronous machine an electromechanical device, its response time is slower if compared to a power electronic converter. As an example, the inertia effect corresponds to the opposition of a big rotational mass to change its velocity, which involves longer time to slow down, but also to speed up. Consequently, simulations have shown the need of changing the BS procedure timescale in order to enable the stabilization of the VSM after each step.

Figure 6.1 depicts the new timescale. The sequential energization of the WT clusters is maintained. However, the WT power ramp-up in order to demonstrate islanded operation is performed in three seconds. Then, after voltage and frequency have settled, the onshore network is energized at the 27.5 s time instant. The block-load connection starts at 30 s, but leaving a time span of 4 s between the three switching operations due to the longer settling time of the VSM active power.

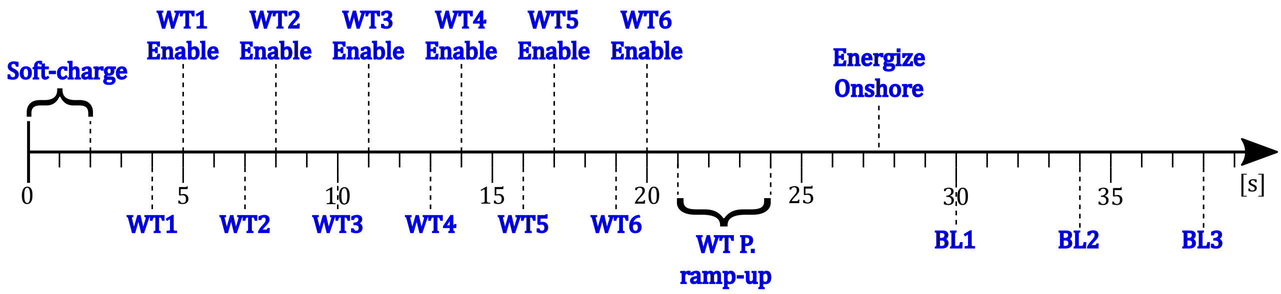

Figure 6.1: Timeline of the BS procedure with VSM.

6.2 Controller Modelling

The controller is designed following the guidelines given by [31]. Nevertheless, some changes and adaptations are made taking some useful block-sets from PSC, such as the AVC, and removing some of the proposed by [31] due to the differences between the two converter models.

First the power synchronization loop is designed. It is based on the swing equation and its implementation is taken similar to the one presented in [44]. The loop follows the same theory as [31], but the application is more intuitive in the former case. Besides, the latter relies on a PLL to implement the damping term because it is designed for grid connected operation. It computes the damping term by multiplying a damping constant, K_D, by the difference between the VSM frequency, ω_{VSM}, and the actual grid frequency, ω_{PLL}, chased by the PLL. As during BS there is no grid, the approach in [44] is preferred, which consist in multiplying K_D by the difference between the VSM frequency and the same signal low pass filtered.

In a second step, the cascaded voltage and current control is designed. It involves the implementation of a virtual impedance in order to damp oscillations, similar to the high pass filter that was applied for PSC. Cascade voltage and current control enables the use of current limiters in order to avoid the converter damage, thus imitating the functionality of the current limiting controller. Finally, it is noted that compared to the control scheme proposed by [31], the designed controller does not involve active damping of the LC filter resonance as, in the IBESS model, there is no shunt capacitor (recall Section 3.2.5). The main difference between the VSM implementation with cascaded voltage and current control and the PSC presented in former chapters is the PI voltage and current controllers that are added in [31]. In PSC, the current limiting controller is based on proportional (P) control.

6.2.1 Power Synchronization Loop

The implementation of the power synchronization loop is based on the swing equation presented in (2.2). It determines the acceleration of the rotor considering the power imbalance between mechanical and electrical power together with the damping term. An extra term can be added to (2.2) to take into account the P-f droop of the synchronous machine governor, as seen below in (6.1).

$$M \cdot \frac{d\omega_g}{dt} = P_{ref} - P - K_d \cdot (\omega_g - \omega_f) - K_g \cdot (\omega_1 - \omega_g) \tag{6.1}$$

Being K_g the P-f droop constant. Note there is no time delay for this term, as it would be expected if a mechanical governor of a synchronous machine is actuated. This is possible because of the fast response of power converters. In addition, ω_g is the VSM and network angular frequency, while ω_1 is the reference angular frequency. ω_f is the result of low pass filtering ω_g. Finally, M is the virtual inertia scaled by ω_1, and can be expressed as

$$M = \frac{2S_bH}{\omega_1} \tag{6.2}$$

where H is the inertia constant in seconds. Regarding the damping term, the development of its expression $K_d \cdot (\omega_g - \omega_f)$, delivers the following transfer function, $D(s)$:

$$D(s) = K_d \left(\omega_g - \omega_g \frac{\alpha_f}{s + \alpha_f} \right) = \frac{K_d s}{s + \alpha_f} \tag{6.3}$$

being α_f the filter cutoff angular frequency. Finally, the droop term, K_g is calculated as it would be done for a traditional synchronous machine, (6.4), where R is the droop in percentage.

$$K_g = \frac{S_b}{R\omega_1} \tag{6.4}$$

Figure 6.2 depicts the implemented controller. See that it consists on the translation of (6.1) into the Laplace domain. The first integration is done to obtain $\Delta\omega$, while the second results from the known relation, $\frac{d\theta}{dt} = \omega$. The main difference between this implementation and the traditional PSC is the use of double integration to obtain θ that may bring the reduction of the stability margins.

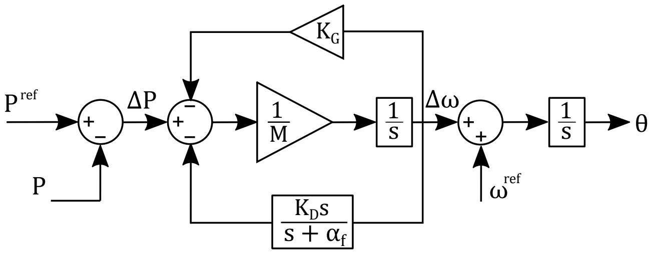

Figure 6.2: Power synchronization loop, with virtual inertia and damping terms.

It must be noted that the power synchronization loop is not restricted to the VSM developed in [31]. Instead, it could be well applied to the PSC scheme, keeping the AVC and the current limiting controller as it was developed in the previous chapters.

6.2.2 Cascaded Voltage and Current Controllers

The input of voltage and current controller is a converter voltage reference named V_0 that is aligned with the d-axis. This reference is generated by an AVC that is designed identically to the one used for PSC (please refer to Section 3.3.2). Hence, the new implementation consist of two cascaded PI regulators.

The converter voltage reference, $v_{c,dq}$ is generated by subtracting an virtual resistance to V_0 with the objective of damping oscillations and reduce the sensitivity to disturbances at the PCC. Then, $v_{c,dq}$ enters a PI controller that creates converter current reference, $i_{c,dq}^{ref}$. Note there is no feed-forward implemented. The reference current goes through a current limiter to avoid overloading of the converter. The next step is the current controller, that also consists of a PI regulator, but in this case it involves voltage feed-forward and the inductance decoupling term due to the abc to $dq0$ transformation. Figure 6.3 depicts the voltage and current controller implemented for BS purpose.

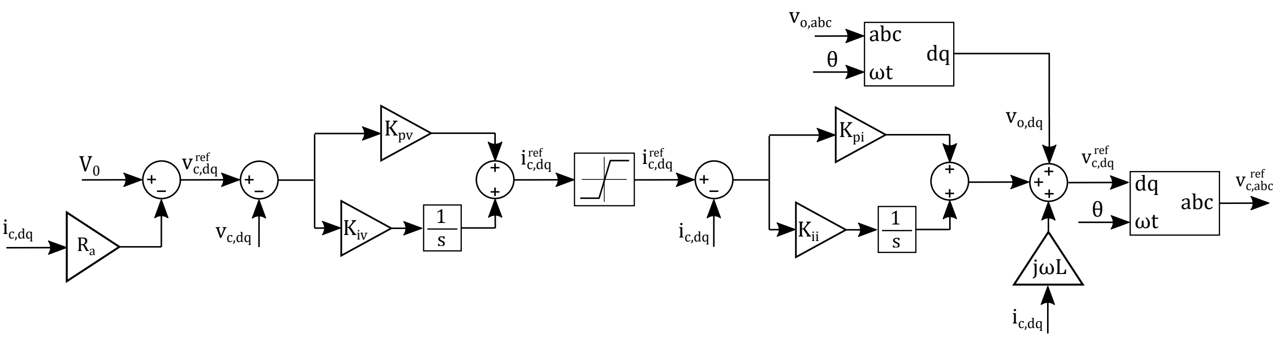

Figure 6.3: Cascaded voltage and current controllers.

The tuning of the cascaded PI controllers is done following the "Modulus Optimum" method presented in [52], which can be also named pole cancellation technique. The process starts with the faster controller, that is the current regulator. Considering the plant an inductor L and its equivalent resistance R, its transfer function is:

$$G(s) = \frac{I(s)}{V(s)} = \frac{1}{R + Ls} \tag{6.5}$$

Thus, the open loop transfer function considering the PI regulator is:

$$G_{ol,i}(s) = \left(K_{pi} + \frac{K_{ii}}{s}\right)\left(\frac{1}{R + Ls}\right) \tag{6.6}$$

The objective of the pole cancellation technique is to achieve critical damping on the closed loop transfer function, so it has a response similar to a first order system. Hence, the form of the pursued open loop transfer function is:

$$G_{ol}(s) = \frac{\alpha_{cl}}{s} \tag{6.7}$$

being α_{cl} the closed loop bandwidth, which is limited by the converter switching frequency:
$\alpha_{cl} \leq 0.2 \cdot 2\pi f_{sw}$, [45]. Inspecting (6.6), the desired response is obtained for:

$$K_{pi} = \alpha_{cl,i} \cdot L \tag{6.8}$$

$$K_{ii} = \alpha_{cl,i} \cdot R \tag{6.9}$$

The voltage controller is then tuned following the same principle, but considering a lower bandwidth. A difference of one decade is recommended to avoid unwanted interactions, [53]. For the IBESS model presented in Section 3.2.5, the plant of the voltage controller consists simply on the closed loop transfer function of the current inner loop. This transfer function can be approximated by a first order system of time constant T_e. Hence, the open loop transfer function of the voltage controller is:

$$G_{ol,v}(s) = \left(K_{pv} + \frac{K_{iv}}{s}\right)\left(\frac{1}{1 + T_e s}\right) \tag{6.10}$$

If an open loop transfer function equal to (6.7) is pursued, the PI gains are selected as:

$$K_{pv} = \alpha_{cl,v} \cdot T_e \tag{6.11}$$

$$K_{iv} = \frac{K_{pv}}{T_e} = \alpha_{cl,v} \tag{6.12}$$

This tuning method is similar to the one applied for the WT controllers in Section 3.4. However it is elaborated here for convenience and to enhance the understanding of the VSM tuning process.

6.2.3 Controller parameters

The previous subsections gave the means to tune the VSM control scheme. Now, it is time to propose the values for the different gains and set the controller parameters. Starting from the power synchronization loop, when considering a base active power of $P_b = 50\,\text{MW}$, a reference angular frequency of $\omega_1 = 314.16\,\text{rad/s}$ and an inertia constant of $H = 5\,\text{s}$, (6.2) gives a $M = 1.59\frac{MWs^2}{rad}$. Then, the P-f droop is calculated by selecting an $R = 0.02$, which is not standard in synchronous generators, but it shows to give lower oscillations and higher stability margins than a more traditional $R = 0.05$. The utilization of $R = 0.02$ could lead to saturation of the battery for grid connected mode, as a change in frequency of 1 Hz would generate a 50 MW change in power. Nevertheless, dealing with a power electronic converter, this parameter can be changed depending on the operation, BS or grid connected. Finally, the damping constant is chosen as $K_d = 8$ as it gives a good compromise between low RoCoF and fast settling time. The filter cutoff frequency is taken as $\alpha_f = 20\,\mathrm{rad/s}$ to assure the damping of all oscillations at fundamental frequency and above.

Concerning the AVC and the virtual resistance, its values are kept similar to those utilized for PSC, as the two block-sets pursue the same objectives in both control schemes. Regarding the cascaded voltage and current controllers, the current control bandwidth is selected to be $\alpha_{cl,i} = 6283\,\mathrm{rad/s}$, which means that a switching frequency of $f_{sw} = 5000\,\mathrm{Hz}$ is assumed. This assumption is based on the higher effective switching frequency of MMC if compared with a 2 level converter, [54]. On the other hand, the voltage controller bandwidth is selected as $\alpha_{cl,v} = 314\,\mathrm{rad/s}$, more than one decade lower than the inner loop. In summary, the controller parameters are stated in Table 6.1.

Table 6.1: VSM Controller Parameters

Controller	Parameter	Value	Unit
Power Synchronization Loop	M	1.59	$\frac{MWs^2}{rad}$
Power Synchronization Loop	K_g	8	$\frac{MWs}{rad}$
Power Synchronization Loop	α_f	20	rad/s
Average Voltage Controller	K_E	0.75	p.u.
Average Voltage Controller	T_E	0.05	s
Active Resistance	R_a	0.73	Ω
Voltage Controller	K_{pv}	0.051	1/Ω
Voltage Controller	K_{iv}	314	1/Ωs
Current Controller	K_{pi}	36.8	Ω
Current Controller	K_{ii}	609.9	Ω/s

6.3 Energization of the Offshore Wind Power Plant

The capability of VSM to BS the OWPP is simulated and compared with the PSC performance. The first step is the soft-charge and energization of the WT cluster 1. Figure 6.4 shows the active power and frequency of the IBESS operating under PSC and VSM. It is clear that both GFM strategies are capable of soft-charging the OWPP, settling at approximately the same power, but at different frequency. The difference in power is mainly generated by the lower losses in the shunt reactors, which because of being subjected to a lower voltage at the terminals, a lower current flow through them. The energization of the first WT cluster is successful for VSM, presenting a smoother frequency profile after switching. When the WT control is enabled and the generator unblocked, the WT P-f droop does not create such an aggressive step in power and frequency, because the frequency is at 49.84 Hz, being the effect of the droop of $\Delta P_{droop} = 4\,\mathrm{MW}$. The performance of VSM is superior than PSC during WT switching due to its capacity to damp the frequency oscillations. The power signal is similar, as it is dominated by the dynamics of the energization and network characteristics.

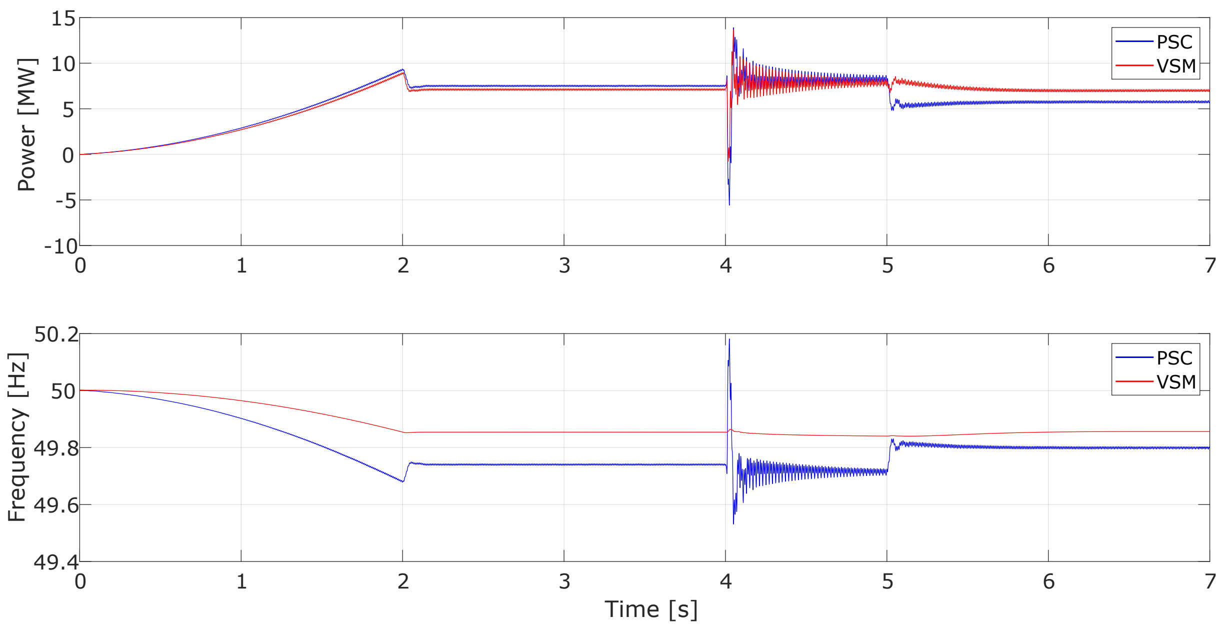

Figure 6.4: Active Power and frequency during soft-charging and first WT cluster switching. The figure shows the performance of PSC and VSM.

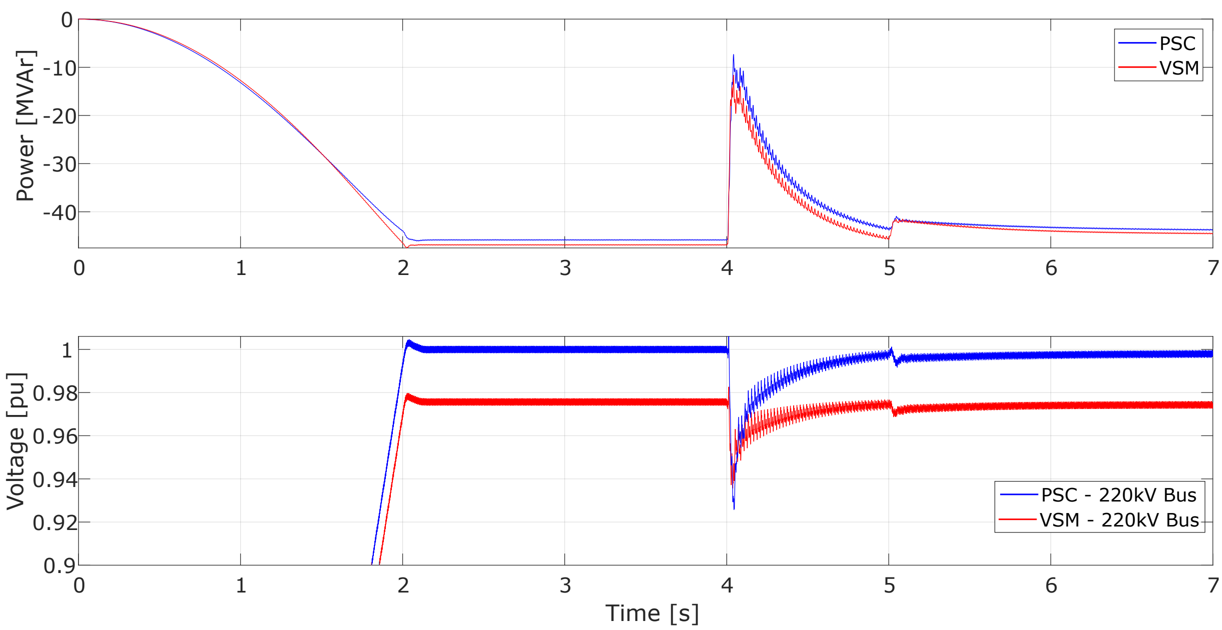

Figure 6.5: Reactive Power and onshore Bus voltage during soft-charging and first WT cluster switching. The figure shows the performance of PSC and VSM.

On the other hand, Fig. 6.5 shows the reactive power and RMS voltage at the onshore bus. After soft-charge, the reactive power settles at a lower level for VSM, meaning that the converter absorbs more reactive power. This is due to the better capability of VSM to set the voltage level at the onshore bus. Recall, that the reference voltage was 0.95 p u . The VSM sets a voltage closer to 0.95 p u than PSC, so it needs to absorb more reactive power to achieve this. After the WT cluster switching, the converter experiments a reactive power sag due to the saturation of the WT transformer. This is followed by a voltage drop in the onshore bus. The voltage drop when the converter is operated under

PSC is 0.078 p u , while is of only 0.04 p u for VSM. Again, the performance of VSM is improved as the voltage experiments smaller changes during energization.

Finally, Fig. 6.6 shows the performance of the IBESS during the whole OWPP energization, when it is operated under VSM. It depicts active power, network frequency, reactive power, and RMS voltage at the converter terminal and the onshore bus. It is noted the lack of oscillations in the frequency signal, settling at an average value of 49.85 Hz. Concerning reactive power, every switching generates a similar variation. The gradual reduction in the amount of reactive power that the IBESS is absorbing is generated by the Q-V droops of the WT converters, which makes them absorb $\Delta Q = 0.75\,\text{MVAr}$ reactive power, reducing the burden of the IBESS. The voltage profile at the onshore bus is kept in a tight interval of [0.936,0.98] pu, whereas the converter voltage is lower to enable the reactive power absorption. The voltage at the onshore Bus is also showing a decay after every energization. The reduction of the voltage causes that the reactive power generation of the export cable gets cut down.

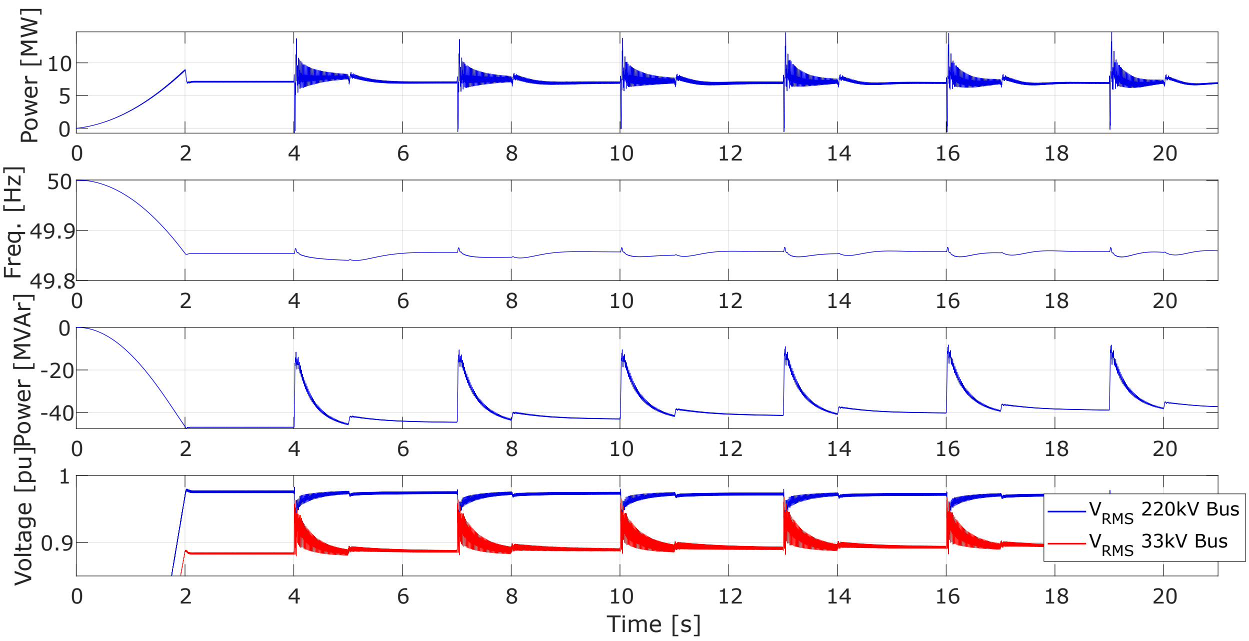

Figure 6.6: IBESS Performance during overall energization process. IBESS is operated under VSM.

6.4 Islanded Operation

In a similar way as it was done in Section 4.7, the islanded operation of the system is assessed. Because of the longer settling time of the frequency when the GFM converter is a VSM, the power ramp-up is made in 3 s. This avoids the frequency oscillations that would appear due to the integration of the power difference in the power synchronization loop. The WT power reference is raised up to 8.3 MW per cluster, summing a total power of 50 MW. However, the final delivered power is only 19.8 MW due to the effect of the P-f droops, which subtract $\Delta P_{droop} = \frac{0.175}{50}\frac{1}{0.05}72 = 5.03\,\text{MW}$ per WT cluster. Figure 6.7 shows that the IBESS was generating 6.7 MW before the WT power ramp-up, and ends absorbing 9.3 MW. The frequency follow the opposite behaviour moving from 49.86 to 50.175 Hz.

This experiment demonstrates the islanded operation of the IBESS and the OWPP as the GFM converter is capable of responding to changes in the WT generated power. When the power output of the OWPP is low, the battery of IBESS is being discharged. However, when the WT power increases, the power flow direction changes, charging the battery.

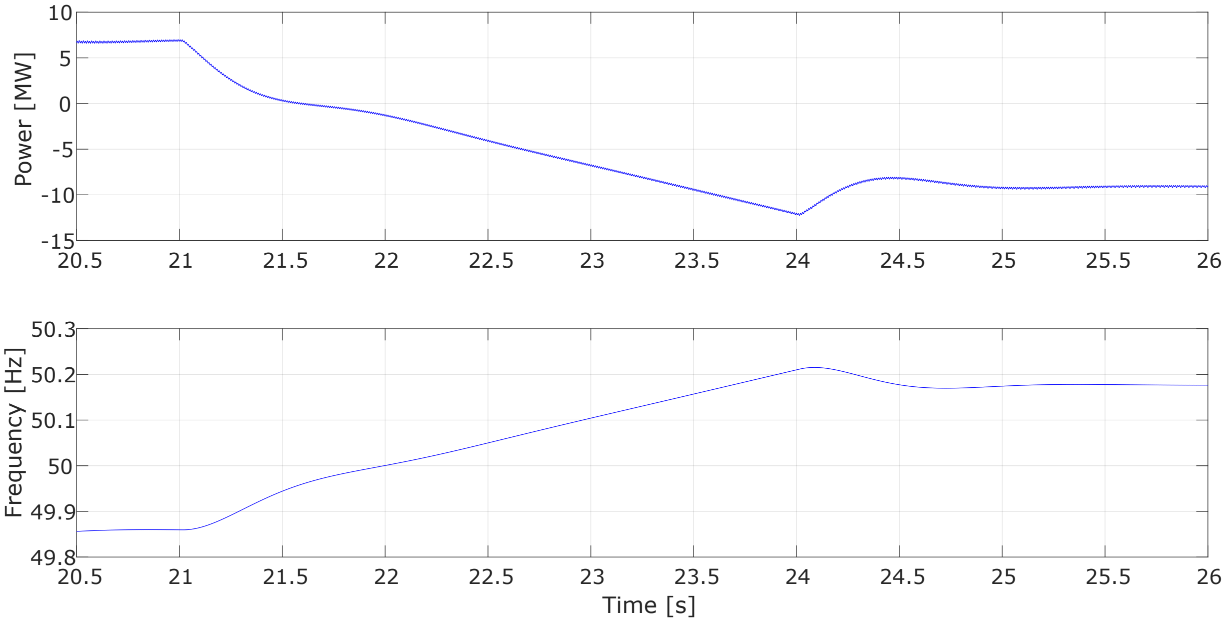

Figure 6.7: Active power and frequency during WT power ramp-up. IBESS is operated under VSM.

6.5 Energization of the Onshore Network

The energization of the onshore network consisted in the switching of a 100 km OHL. Even though the switching instant is different for the simulations with PSC and VSM, their performance is compared. Recall that, when operating under PSC, the energization was done at 25 s, whereas utilizing the VSM, it was delayed until 27.5 s, because of its longer settling time after WT power ramp-up. The current profile at the sending end of the OHL - 400 kV Bus - was depicted in Fig. 5.3. This behaviour does not change between PSC and VSM because it is driven by the OHL electrical parameters and the voltage point of wave of the switching instant; not on the type of controller. However, the response of the GFM converter is different for the two control schemes. Figure 6.8 shows the active power and frequency during energization. Equipped with PSC, the converter exhibits a 33 MW peak to peak power change, which is directly translated into frequency oscillations due to the fact that the power synchronization loop consists of a single gain. On the other hand, VSM introduces power oscillations that are 33 % smaller than in the case of PSC. The frequency change has a peak of only 0.04 Hz, which is a significant improvement respect to the PSC performance.

Regarding reactive power and voltage at the onshore bus - 220 kV Bus - the results are shown in Fig.6.9. Note that the switching of the OHL generates the absorption of 43 MVAr more than in the previous state. This is due to the shunt capacitance of the transmission line, that it is not compensated by shunt reactors. VSM presents a short ringing, while PSC does not. This is due to the cascaded voltage and current controllers that introduces some oscillations when the current reference is created by the first PI controller. PSC gives a smother performance in both reactive power and voltage. Leaving the comparison aside, Fig. 6.8 and 6.9 demonstrates that VSM can keep a stable voltage and frequency after the energization of the onshore network. It delivers a frequency variation that is 87 % lower than PSC and an adequate voltage profile, which settles into steady state after 0.16 s.

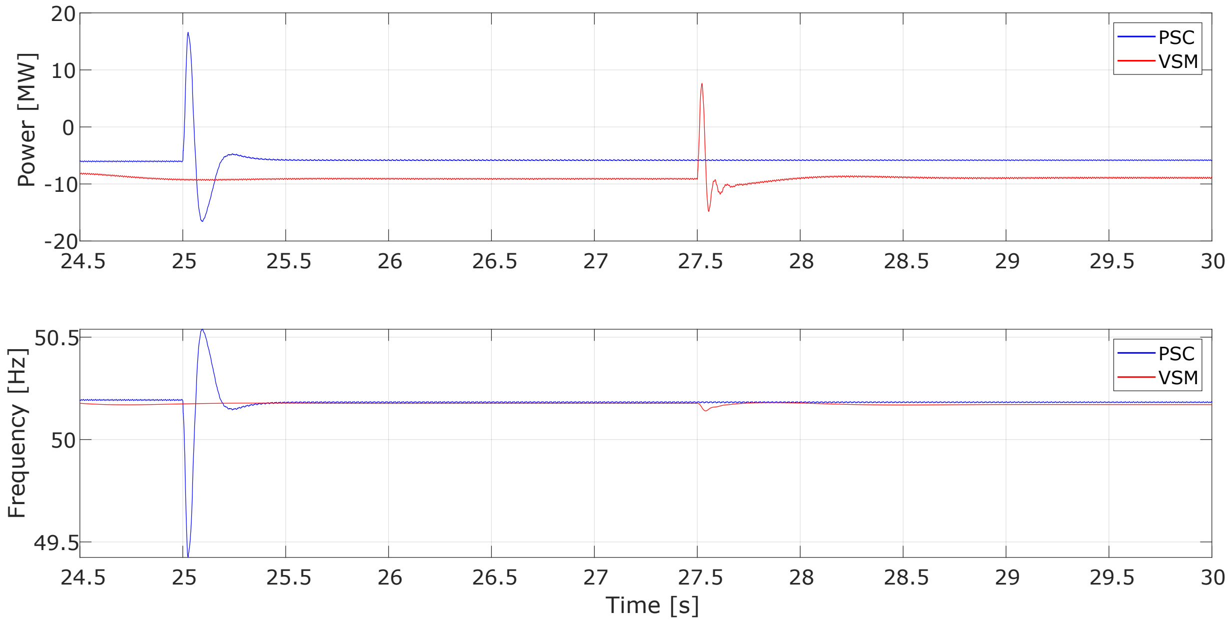

Figure 6.8: Active Power and frequency during energization of the onshore network. The figure shows the performance of PSC and VSM. Please recall that the time instants at which the switching is done are different.

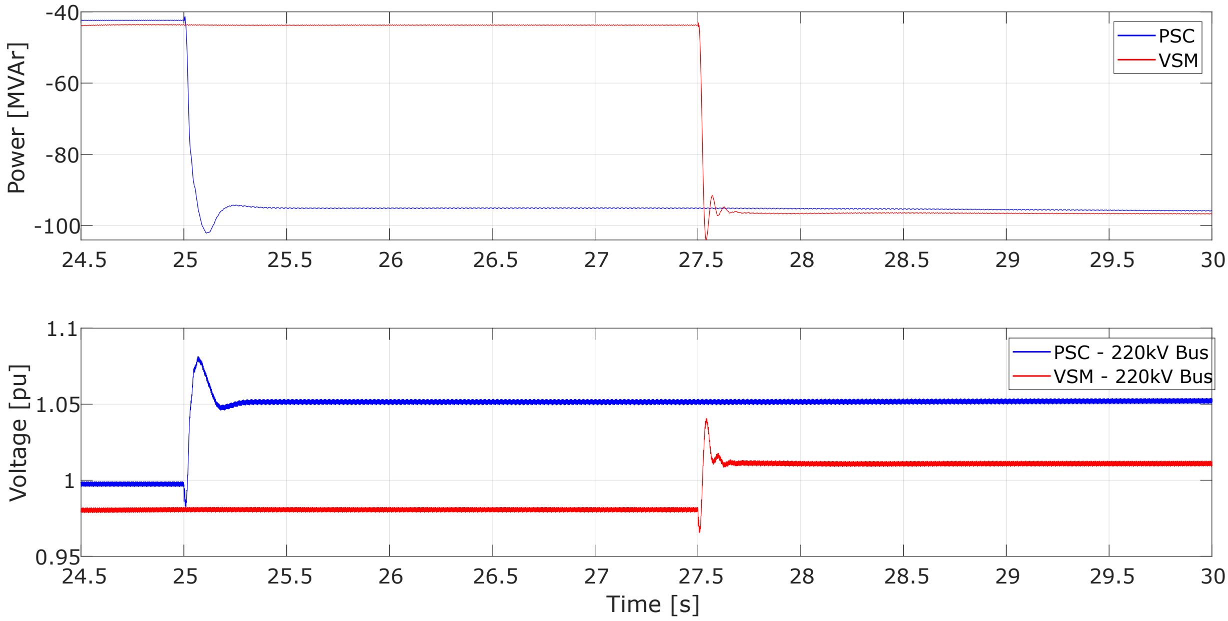

Figure 6.9: Reactive Power and onshore Bus voltage during energization of the onshore network. The figure shows the performance of PSC and VSM. Please recall that the time instants at which the switching is done are different.

6.6 Connection of Block-loads

The last step of the BS procedure presented in this project is the connection of block-loads. VSM is expected to present a better performance at this stage due to the virtual inertia and damping effect. That is what Fig. 6.10 is showing by plotting the IBESS active power and network frequency. The lack of inertia of PSC generates a high RoCoF and a frequency drop of 0.64 Hz. On the other hand, when VSM is implemented, a smooth change in frequency (low RoCoF) and a 0.2 Hz frequency drop is observed. However, the frequency settling time for the VSM is 1.16 s longer than for PSC because of the inertia effect of the former case. The difference in the shape of the IBESS power signals are caused by the effect of the inertia and damping terms that avoid a rapid change in the VSM delivered power. After both frequency signals settle, they present a similar steady state value of 50.07 Hz . Regarding the power support given by the WTs, it is also shown in Fig. 6.10. At the switching instant, the P-f droop does not supply any extra power, being the IBESS responsible for delivering the total power to the load. The reason is that the WT droop response time is slow and its effects become important at 30.1 s for PSC and 30.2 s for VSM. The contributions of the WTs are $\Delta P_{OWPP} = 19$ MW when IBESS is operated under PSC and $\Delta P_{OWPP} = 16$ MW for VSM.

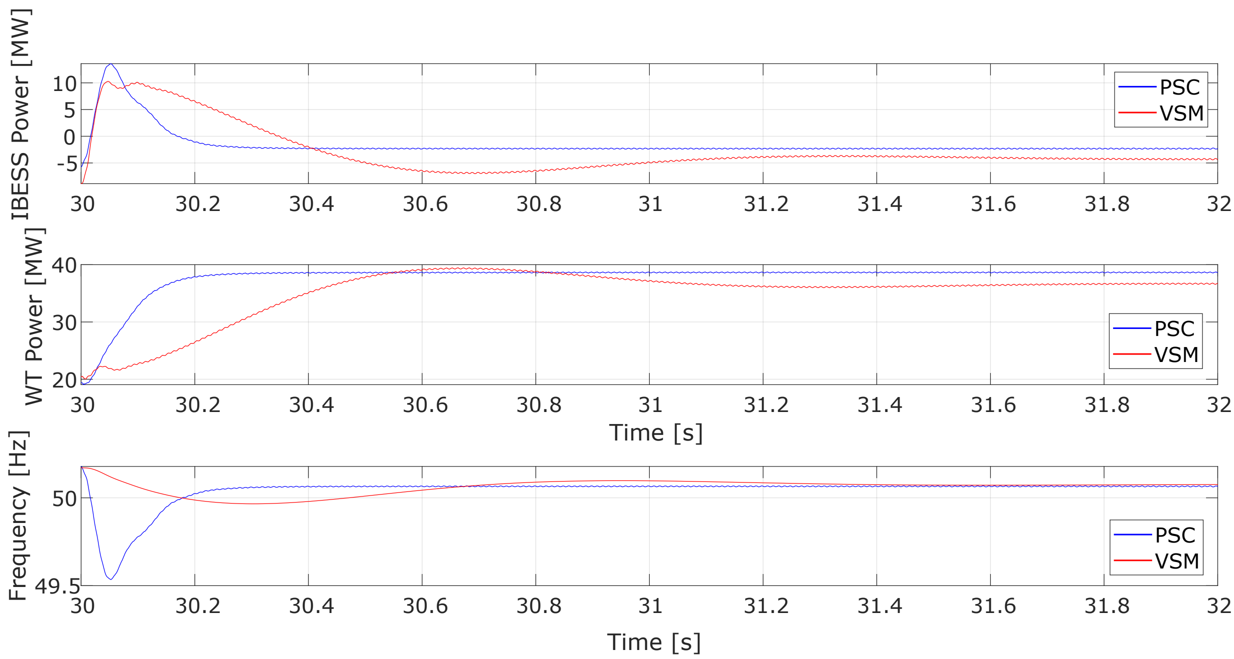

Figure 6.10: Active Power and frequency during connection of first block-load. The figure shows the performance of PSC and VSM.

Finally, the overall performance of the IBESS under VSM control is presented in Fig. 6.11. Active power and frequency follow an identical behaviour to the one showed in Fig. 6.10, repeated three times. Note how the IBESS generated power increases after each block-load connection. The OWPP power should be ramped-up during block-loading to reduce the burden of the IBESS. In this case, not doing so, does not represent a problem because the size of the loads is only 20 MW, but it could be an issue with higher loads as the IBESS needs to supply the total load power at the switching instant. However, after the first power transient, the P-f droops of the WT clusters are aiding the IBESS by supplying 16 MW. The observed behaviour of the frequency is successful, as it keeps its value in an interval of [49.8,50.18] Hz and presenting a RoCof of 0.64 Hz/s.

Concerning reactive power and voltage level at the onshore buses, the behaviour during block-loading is also stable, reaching steady state after 1.4 s. The reactive power that the IBESS needs to absorb after each block-load connection is reduced. This is due to the development of a sustained current in the transmission line that creates a voltage drop. A lower voltage in the OHL generates that the line shunt capacitance supplies less reactive power. In addition, the sustained current flowing through the line series reactance also causes the loss of reactive power. The voltage at the 220 kV onshore bus remains in an interval of [0.98,1.01] pu, which is considered successful. Finally, the converter terminal voltage has a lower amplitude, which denotes reactive power absorption.

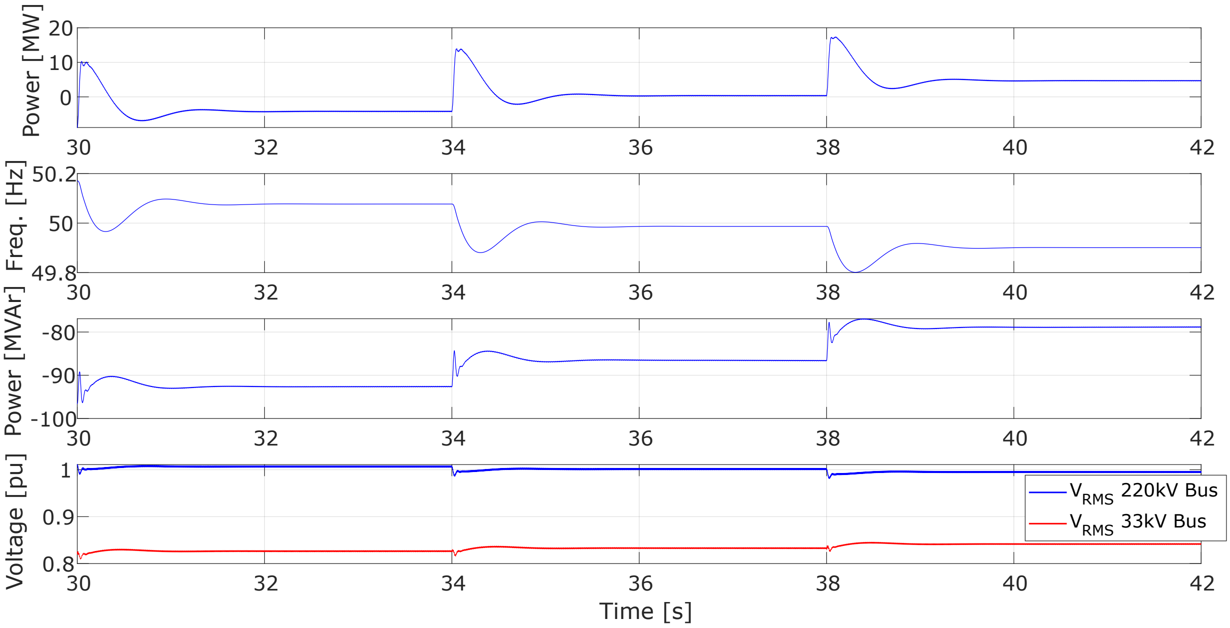

Figure 6.11: IBESS Performance during block-load connection. IBESS is operated under VSM.

6.7 Summary

This chapter presented an alternative GFM control scheme in order to achieve BS of an OWPP. The main feature of the controller was an enhancement of the power synchronization loop by adding virtual inertia and damping. Concerning, the voltage and current controllers, they were developed as cascaded regulators in order to implement a current limiter that avoids converter overloading. The development of the controllers was explained at the beginning of the chapter. Not only the different block-sets are described, but also the tuning principles are introduced.

The VSM demonstrated to be successful in the OWPP energization and following participation in the power system restoration. The success criteria was fulfilled as the frequency and voltage remain between [49.84,50.21] Hz and [0.94,1.04] pu, respectively.

Furthermore, a comparison between the performance of PSC and VSM was presented in various sections. VSM showed significant advantages in terms of frequency control, as the virtual inertia and damping effect reduce the oscillations that appear after switching. In addition, the voltage is regulated better, being its value at the 220 kV Bus closer to the reference in VSM if compared to PSC. When the onshore network was energized, the frequency signal of VSM presented a better performance. However, the voltage exhibits ringing, which is not perceptible in PSC. This goes in line with the reduction of the stability margins due to the cascaded controllers, that is mentioned in the literature, [16], and verified in the simulations. Finally, when block-loads are connected, the VSM demonstrates all its potential reducing the frequency drop a 67 % compared to PSC. In summary, the VSM performance is superior than PSC because frequency and voltage are maintained in a narrower interval.

Chapter 7

Conclusion and Future Work

Conclusion

Every year more actions are taken globally in order to move into a more sustainable power system. Many of them go in line with the gradual decommission of traditional power plants based on fossil fuels. However, these energy sources are the main BS providers at present, at least in locations where hydroelectric power is not abundant. A blackout is an unlikely, but impactful event that must be solved as fast as possible to reduce the socioeconomic problems that generates. Consequently, in a future scenario where renewable energy will be a primary power source, it is crucial to secure reliable sources of BS based on on wind power. In fact, OWPPs are good candidates as BS units because of their fast response and high power capability. Nevertheless, the intermittent character of wind, combined with the lack of energy storage threatens the availability of the service.

Furthermore, the main challenge to be addressed in order to enable a BS from an OWPP is the need of a self-start unit that can energize the export cable, substation transformers and enable the synchronization of the WTs. The IBESS is an appropriate self-start unit as it combines the functionalities of Energy Storage and STATCOM systems. Additionally, the operation of the IBESS as a GFM converter enables the creation of a voltage waveform to which the WTs can latch up. Therefore, the main objective of this project was to assess the capability of IBESS to BS the OWPP and following participation in the power system restoration.

Overall, the main contributions of the thesis are highlighted:

- **Modelling of a HVAC connected OWPP**. Based on the work of the researchers of the IBESS Project, [37], Hornsea II wind power plant was modelled in PSCAD. Furthermore, specific modelling guidelines of export cables and transformers for EMT simulations are given. A simple procedure for the aggregation of WTs and the development of an equivalent AC collector system is also presented. These guidelines are valid for any engineer who intends to model an OWPP.
- **Development of GFM and GFL controllers**. The IBESS is operated as a GFM converter to enable the energization of the OWPP and synchronization of the WTs. Two different GFM approaches are designed and their performance compared. They are based on the work done in [32] and [31], for PSC and VSM implementations respectively. Moreover, the controller development is complemented with tuning guidelines to increase the understanding and give more significance to the report as it can aid future modifications of the controller parameters. On the other hand, WTs are equipped with GFL converters. Traditional vector current controllers and associated droops are designed. Their tuning is also explained and the relevant references given.
- **Successful BS of the OWPP**. Relying on soft-charging, which consists on the gradual increment of the voltage amplitude, the export cable sections and transformers are charged without experimenting voltage or current transients. The soft-charge is allowed by the GFM converter that sets a ramp shaped reference for the voltage amplitude until it reaches its nominal value. Afterwards, the WTs are switched and synchronized. The WT switching causes inrush currents due to the transformer energization. When the transient has decayed, the WT generators are enabled and they support the islanded system through their droop controllers. This procedure

is performed successfully, as frequency and voltage remain in tight thresholds, both during energization and islanded operation.

- **Participation in the power system restoration**. The system formed by the IBESS and the OWPP is able to energize the onshore network and accept block-loads. The first stage is simulated by switching an OHL and a transformer, which creates a current transient. Concerning block-loading it is accomplished by the connection of three 20 MW resistive loads. Again, the process is successful as frequency and voltage are correctly regulated and remain inside the thresholds required by NGESO and ELIA.

In summary, this project has demonstrated that a wind power plant equipped with a self-start unit such as the IBESS is capable of conducting BS. This is an interesting observation as it introduces the techno-economic potential of the IBESS. It can be incorporated in many existent wind power plants in order to provide services such as BS, frequency response and virtual inertia provision, [10]. In addition, the IBESS is a device that is not powered by fossil fuels, instead its battery is charged by the wind power plant or the grid, so it contributes to the vision of future power systems.

Along the report, the performance of the different subsystems is assessed. The ES-STATCOM system behaviour is evaluated during the BS procedure by plotting its power contribution, together with the frequency and voltage at its converter terminal and substation Bus. The STATCOM part demonstrates its potential when the converter needs to absorb the reactive power generated by the export cable and transmission line. Its 112 MVAr rating is in line with the requirements of NGESO for reactive power capability of BS units. On the other hand, the ES part is especially important during soft-charge as it has to feed the losses of the OWPP, and during block-loading. At this final stage of the BS, it supplies the total load demand at first instance, being assisted by the OWPP after a short time. The size of the battery is 50 MW, which shows to be sufficient to BS the OWPP and enable block-loading.

There are several GFM control techniques in the literature. In this project two of them where evaluated for BS purposes. PSC demonstrated to be successful in regulating voltage and frequency during the process. However, the VSM implementation introduced some advantages such as the reduction of frequency oscillations after switching because of its inertia and damping terms. It showed improved voltage control at the onshore bus, as it is equipped with PI control in the voltage regulator. Moreover, during block-loading, the RoCoF was reduced due to virtual inertia. In conclusion, it is recommended to utilize a VSM for BS provision.

Future Work

Even though the BS capability of the IBESS and OWPP has been demonstrated, there are several tasks that should be accomplished in order to achieve a more detailed assessment of the concept. Some of these tasks are presented below as future work.

- **Battery management**. During the project, the battery of the ES-STATCOM was considered sufficiently charged. Thereby, there has not been any monitoring of the SOC and its control was disregarded. In future developments, the battery management needs to be considered from a plant control point of view, as it needs to keep a sufficient SOC to perform self-start. Furthermore, the converter control should be enhanced by adding the regulation of the voltage at the battery terminals (DC link).
- **MMC dynamics**. The converter has been treated as a controllable voltage source, while its internal dynamics were not considered. However, it is expected that the MMC needs to

be started and its multiple capacitors energized. Besides, during BS the converter PWM, capacitor balancing, or harmonic generation are neglected. Consequently, in following studies, the MMC should be modelled in detail to account to its internal characteristics and evaluate the performance during its own self-start and providing BS.

- **Power sharing among WTs**. The project has considered that the WTs were aggregated into groups of 9 turbines. This is convenient to reduce the computational burden. However, it is not considering the power sharing between them. During islanded operation a very small amount of power is delivered by the WT clusters. If this power is divided equally among the 9 WTs, an excessive use of pitch control would be needed to curtail the generation. It must be assessed what are the issues of this situation and consider that only some of the total number of WTs are operating. This would need a more detailed model of the AC collector system and aggregation of WTs into smaller groups.

- **Protection systems**. One of the unknowns of soft-charging is the fault detection and clearing. The settings for undervoltage protection have to be modified to perform soft-charge, as the voltage is gradually increasing. Therefore, the concept should be evaluated from a protection point of view, also considering what would be the damage to the different devices in the event of an uncleared fault.

- **Intermittent wind**. Wind intensity is presumed, so the whole assessment is done under the assumption that there is a sufficient and constant wind speed in the offshore site. It would be of interest to conduct simulations with fluctuating wind to evaluate the performance of the IBESS and OWPP during islanded operation. Moreover, these simulations would deliver how much wind is needed to participate of the power system restoration.

- **WT dynamics**. The WT converter is also treated as an averaged voltage source. Therefore, the DC link or rotor (mechanical) dynamics are neglected. The WT model could be enhanced considering these aspects. This goes in connection with the previous item, **Intermittent wind**, as the combination of wind fluctuations and WT dynamics would enable a better evaluation of the performance of the OWPP during islanded operation and following block-load connection.

- **Real timestamps**. In order to reduce the computational burden, the timestamps for the BS procedure are selected close to each other. In fact, the performed simulations do not last longer that 40 s. This may not be possible in a real energization due to reliability and safety reasons or even because of grid code requirements. Consequently, it would be necessary to analyze and decide what should be the switching time stamps in a real life scenario.

- **Plant controllers**. Plant controllers are not developed during the project. However it could be relevant to design high level regulators for SOC management or power sharing between the IBESS and OWPP. In addition, power allocation among WTs should be also regulated.

Bibliography

[1] F. Qiu and P. Li. An integrated approach for power system restoration planning. Proceedings of the IEEE, 105(7):1234–1252, 2017. doi: 10.1109/JPROC.2017.2696564.

[2] OFGEM. Report into the power outages on friday 9 august 2019. URL https://www.ofgem.gov.uk/publications-and-updates/companies-pay-105-million-over-9-august-power-cut.

[3] A. Jain, J. Sakamuri, K. Das, O. Goksu, and N. Cutululis. Functional requirements for black start and power system restoration from wind power plants. 2019. doi: 10.5281/zenodo.3460518.

[4] NGESO. Black start from non-traditional generation technologies. URL https://www.nationalgrideso.com/document/148201/download.

[5] ELIA. Study report on the review of black start services, . URL https://www.elia.be/-/media/project/elia/elia-site/electricity-market-and-system---document-library/restoration-services---rsp-and-emergency-situations/2018/2018-study-report-on-the-review-of-the-black-start-ancillary-service---non-confidential-version.pdf.

[6] D. Pagnani, Ł. H. Kocewiak, J. Hjerrild, F. Blaabjerg, and C. L. Bak. Overview of black start provision by offshore wind farms. In IECON 2020 The 46th Annual Conference of the IEEE Industrial Electronics Society, pages 1892–1898, 2020. doi: 10.1109/IECON43393.2020.9254743.

[7] ENTSO-E. Commission regulation (EU) 2016/631 of 14 april 2016 establishing a network code on requirements for grid connection of generators, . URL https://eur-lex.europa.eu/legal-content/EN/TXT/PDF/?uri=CELEX:32016R0631&from=EN.

[8] ENTSO-E. Commission regulation (EU) 2016/1447 of 26 august 2016 establishing a network code on requirements for grid connection of high voltage direct current systems and direct current-connected power park modules, . URL https://eur-lex.europa.eu/legal-content/EN/TXT/PDF/?uri=CELEX:32016R1447&from=EN.

[9] D. Pagnani, F. Blaabjerg, C. L. Bak, F. M. Faria da Silva, Ł. H. Kocewiak, and J. Hjerrild. Offshore wind farm black start service integration: Review and outlook of ongoing research. Energies, 13 (23), 2020. ISSN 1996-1073. doi: 10.3390/en13236286. URL https://www.mdpi.com/1996-1073/13/23/6286.

[10] S. K. Chaudhary, X. Wang, D. Yang, R. Teodorescu, Ł. Kocewiak, M. P. S. Gryning, P. Johnson, and C. Y. Chen. Techno-economic feasibility of a STATCOM with battery energy storage for the offshore wind power plants. In Proceedings of CIGRE Symposium Aalborg 2019. CIGRE (International Council on Large Electric Systems), Jun 2019. CIGRE Symposium Aalborg 2019 ; Conference date: 04-06-2019 Through 07-06-2019.

[11] A. Jain, O. Saborío-Romano, J. Sakamuri, and N. Cutululis. Blackstart from HVDC-connected offshore wind: Hard vs soft energization. I E T Renewable Power Generation, 15(1):127–138, 2021. ISSN 1752-1416. doi: 10.36227/techrxiv.12948737.v1.

[12] J. Rocabert, A. Luna, F. Blaabjerg, and P. Rodríguez. Control of power converters in AC microgrids. IEEE Transactions on Power Electronics, 27(11):4734–4749, 2012. doi: 10.1109/TPEL.2012.2199334.

[13] S. D'Arco and J. A. Suul. Virtual synchronous machines — classification of implementations and analysis of equivalence to droop controllers for microgrids. In 2013 IEEE Grenoble Conference, pages 1–7, 2013. doi: 10.1109/PTC.2013.6652456.

[14] Q. Zhong and G. Weiss. Static synchronous generators for distributed generation and renewable energy. In 2009 IEEE/PES Power Systems Conference and Exposition, pages 1–6, 2009. doi: 10.1109/PSCE.2009.4840013.

[15] ELIA. Design note in restoration services, . URL https://www.elia.be/-/media/project/elia/elia-site/electricity-market-and-system---document-library/restoration-services---rsp-and-emergency-situations/2018/2018-design-note---future-restoration-services.pdf.

[16] A. Jain, J. N. Sakamuri, and N. A. Cutululis. Grid-forming control strategies for black start by offshore wind power plants. Wind Energy Science, 5(4):1297–1313, 2020. doi: 10.5194/wes-5-1297-2020. URL https://wes.copernicus.org/articles/5/1297/2020/.

[17] A. Atputharajah and T. K. Saha. Power system blackouts - literature review. In 2009 International Conference on Industrial and Information Systems (ICIIS), pages 460–465, 2009. doi: 10.1109/ICIINFS.2009.5429818.

[18] S. Chaudhary, R. Teodorescu, J.R. Svensson, Ł. Kocewiak, P. Johnson, and B. Berggren. Islanded operation of offshore wind power plant using STATCOM with batteries. In 2021 IEEE Power Engineering Society General Meeting, 2021.

[19] T. Ackermann. Wind power in power systems. Wiley, Chichester, West Sussex ;, 2nd ed. edition, 2012. ISBN 1-283-71669-0.

[20] O. Anaya-Lara, J. Tande, K. Uhlen, and K. Merz. Offshore wind energy technology. John Wiley & Sons, Inc., Hoboken, NJ, elektronisk udgave. edition, 2018 - 2018. ISBN 9781119097808.

[21] Siemens Gamesa. Offshore wind turbine, SG 8.0-167 DD. URL https://www.siemensgamesa.com/products-and-services/offshore/wind-turbine-sg-8-0-167-dd.

[22] MHI Vestas Offshore Wind. V164 10 MW turbine. URL https://mhivestasoffshore.com/innovations/.

[23] General Electric Renewable Energy. Haliade-X offshore wind turbine, . URL https://www.ge.com/renewableenergy/wind-energy/offshore-wind/haliade-x-offshore-turbine.

[24] K. Eriksson and D. Wensky. System approach on designing an offshore wind power grid connection. URL https://library.e.abb.com/public/34ec041beda66334c1256fda004c8cc0/03MC0132%20Rev.%2000.pdf.

[25] W. P. Robbins N. Mohan, T. M. Undeland. Power Electronics. Hardcover. Wiley, 3rd edition, 2003. ISBN-13: 978-0-471-22693-2.

[26] Siemens Energy. SVC PLUS (STATCOM), . URL https://www.siemens-energy.com/global/en/offerings/power-transmission/facts/portfolio/svcplus.html.

[27] Hitachi ABB Power Grids. STATCOM - SVC Light. URL https://www.hitachiabb-powergrids.com/offering/product-and-system/facts/statcom/svc-light.

[28] Siemens Energy. SVC Plus (STATCOM) Frequency stabilizer, . URL https://www.siemens-energy.com/global/en/offerings/power-transmission/facts/portfolio/svcplus-frequency-stabilizer.html.

[29] S. K. Chaudhary, A. F. Cupertino, R. Teodorescu, and J. R. Svensson. Benchmarking of modular multilevel converter topologies for ES-STATCOM realization. Energies, 13(13), 2020. ISSN 1996-1073. doi: 10.3390/en13133384. URL https://www.mdpi.com/1996-1073/13/13/3384.

[30] Y. Chen, R. Hesse, D. Turschner, and H. Beck. Comparison of methods for implementing virtual synchronous machine on inverters. Renewable energy & power quality journal, pages 734–739, 2012.

[31] S. D'Arco, J. A. Suul, and O. B. Fosso. A virtual synchronous machine implementation for distributed control of power converters in smartgrids. Electric Power Systems Research, 122:180–197, 2015. ISSN 0378-7796. doi: https://doi.org/10.1016/j.epsr.2015.01.001. URL https://www.sciencedirect.com/science/article/pii/S0378779615000024.

[32] L. Zhang, L. Harnefors, and H. Nee. Power-synchronization control of grid-connected voltage-source converters. IEEE Transactions on Power Systems, 25(2):809–820, 2010. doi: 10.1109/TPWRS.2009.2032231.

[33] L. Yu, R. Li, and L. Xu. Distributed PLL-based control of offshore wind turbines connected with diode-rectifier-based HVDC systems. IEEE Transactions on Power Delivery, 33(3):1328–1336, 2018. doi: 10.1109/TPWRD.2017.2772342.

[34] Y. Gui, X. Wang, and F. Blaabjerg. Vector current control derived from direct power control for grid-connected inverters. IEEE Transactions on Power Electronics, 34(9):9224–9235, 2019. doi: 10.1109/TPEL.2018.2883507.

[35] Ørsted. Hornsea Two offshore wind farm. URL https://hornseaprojects.co.uk/hornsea-project-two.

[36] M. Lehmann, M. Pieschel, M. Juamparez, K. Kabel, Ł. Kocewiak, and S. Sahukari. Active filtering in a large-scale STATCOM for the integration of offshore wind power. 2018.

[37] Aalborg University, Ørsted Wind Power, and Hitachi-ABB AB Corporate Research. IBESS: Integrated battery energy storage and STATCOM for the optimal operation and control of wind power plant in power system. URL https://www.et.aau.dk/research-programmes/wind-power-systems/activities/IBESS/.

[38] Cigre WG C4.502. Power system technical performance issues related to the application of long HVAC cables. In Cigre Technical Brochure, Ref:556. CIGRE (International Council on Large Electric Systems), October 2013.

[39] A. Morched, B. Gustavsen, and M. Tartibi. A universal model for accurate calculation of electromagnetic transients on overhead lines and underground cables. IEEE Transactions on Power Delivery, 14(3):1032–1038, 1999. doi: 10.1109/61.772350.

[40] B. Gustavsen. Panel session on data for modeling system transients insulated cables. In 2001 IEEE Power Engineering Society Winter Meeting. Conference Proceedings (Cat. No.01CH37194), volume 2, pages 718–723 vol.2, 2001. doi: 10.1109/PESW.2001.916943.

[41] Cigre WG C4.307. Transformer energization in power systems: A study guide. In Cigre Technical Brochure, Ref:568. CIGRE (International Council on Large Electric Systems), October 2013.

[42] N. Chiesa, H. K. Høidalen, and M. Lambert. Calculation of inrush currents - benchmarking of transformer models. 2011.

[43] E. Muljadi, S. Pasupulati, A. Ellis, and D. Kosterov. Method of equivalencing for a large wind power plant with multiple turbine representation. 2008 IEEE Power Engineering Society General Meeting, 2008.

[44] L. Harnefors, M. Hinkkanen, U. Riaz, F. M. M. Rahman, and L. Zhang. Robust analytic design of power-synchronization control. IEEE Transactions on Industrial Electronics, 66(8):5810–5819, 2019. doi: 10.1109/TIE.2018.2874584.

[45] L. Harnefors, L. Zhang, and M. Bongiorno. Frequency-domain passivity-based current controller design. IET Power Electronics, 1(4):455–465, 2008. doi: 10.1049/iet-pel:20070286.

[46] EnergiNet. Technical regulation 3.2.5 for wind power plants above 11 kw, 2016.

[47] F. Blaabjerg M. Liserre and S. Hansen. Design and control of an LCL-filter-based three-phase active rectifier. IEEE Transactions on Industry Applications, 41(5):1281–1291, 2005. doi: 10.1109/TIA.2005.853373.

[48] R. Teodorescu, M. Liserre, P. Rodriguez, and F. Blaabjerg. Grid converters for photovoltaic and wind power systems. John Wiley & Sons, 2nd edition, 2011. ISBN 9780470057513.

[49] Hadi Saadat. Power system analysis. 1998.

[50] R. Turner and K. S. Smith. Transformer inrush currents. IEEE Industry Applications Magazine, 16:14–19, 2010.

[51] W. T. Wiechowski. Harmonics in transmission power systems. PhD thesis, 2006.

[52] C. Bajracharya, M. Molinas, J. Suul, and T. Undeland. Understanding of tuning techniques of converter controllers for VSC-HVDC. 06 2008.

[53] S. D'Arco, J. A. Suul, and O. B. Fosso. Automatic tuning of cascaded controllers for power converters using eigenvalue parametric sensitivities. IEEE Transactions on Industry Applications, 51(2):1743–1753, 2015. doi: 10.1109/TIA.2014.2354732.

[54] K. Sharifabadi, L. Harnefors, H. P. Nee, S. Norrga, and R. Teodorescu. Design, control and application of modular multilevel converters for HVDC transmission systems. John Wiley & Sons, 1st edition, 2016. ISBN 9781118851555. doi: 10.1002/9781118851555.

[55] ABB High Voltage Cables. XLPE Land cable systems, user's guide, . URL `https://library.e.abb.com/public/ab02245fb5b5ec41c12575c4004a76d0/XLPE%20Land%20Cable%20Systems%202GM5007GB%20rev%205.pdf`.

[56] ABB High Voltage Cables. XLPE Submarine cable systems, user's guide, . URL `https://new.abb.com/docs/default-source/ewea-doc/xlpe-submarine-cable-systems-2gm5007.pdf`.

[57] E. Twining and D. G. Holmes. Grid current regulation of a three-phase voltage source inverter with an LCL input filter. IEEE Transactions on Power Electronics, 18(3):888–895, 2003. doi: 10.1109/TPEL.2003.810838.

Appendix A

OWPP Parameters

A.1 Export Cable Parameters

The following subsections present the parameters of the different cable sections in the OWPP test model. The export cables are implemented as frequency dependant phase models. On the other hand, the collector equivalent circuit is modelled as a $\pi-$section as the longer cable length is $\leq 10\,\text{km}$ in the collector system.

A.1.1 Underground Cable

The underground transmission has a total length of 40 km. It consists on three single core 220 kV aluminium cables, which are laid in flat formation. The separation between the centers is equal to 80 cm. In addition, cross-bonding between sheaths is considered. The detailed cable parameters are given in Table A.1.

Table A.1: List of parameters of the underground cable, taken from [55]

Parameter	Value	Unit
Voltage	220	kV
Length	40	km
Cross-section	2000	mm^2
Type	Single core	
Core conductor		
Resistivity	3.29E-08	Ω.m
Relative permeability	1	
Outer radius	0.0272	m
First insulating layer + Semi-conductive layer		
Relative permittivity	2.5	
Relative permeability	1	
Insulation thickness	0.023	m
Semi-conductive layers thickness	0.001	m
Sheath (Wire screen)		
Resistivity	2.83E-08	Ω.m
Relative permeability	1	
Thickness	0.00056	m
Over-sheath (Second insulating layer)		
Electrical permittivity	2.5	
Relative permeability	1	
Thickness	0.002	m

A.1.2 Submarine cable

The submarine transmission has a total length of 120 km. It is divided into two equal sections of 60 km due to the need of reactive power compensation in the middle of the export cable.

It consists on a 220 kV three copper core piped cable, with a trefoil layout and lead sheath. The separation between the center of the pipe and the center of each cable is equal to 7.5 cm. The detailed cable parameters are given in Table A.2.

Table A.2: List of parameters of the submarine cables, taken from [56]

Parameter	Value	Unit
Voltage	220	kV
Length	60	km
Cross-section	1200	mm^2
Type	Piped cable	
Pipe data		
Inner insulator		
Outer radius	0.133	m
Relative permittivity	2.5	
Relative permeability	1	
Pipe Conductor		
Outer radius	0.135	m
Resistivity	2.00E-06	Ω.m
Relative permeability	1	
Core conductor		
Resistivity	2.00E-08	Ω.m
Relative permeability	1	
Outer radius	0.0206	m
First insulating layer + Semi-conductive layer		
Relative permittivity	2.5	
Relative permeability	1	
Insulation thickness	0.023	m
Semi-conductive layers thickness	0.001	m
Sheath (Wire screen)		
Resistivity	2.14E-07	Ω.m
Relative permeability	1	
Thickness	0.0031	m
Over-sheath (Second insulating layer)		
Electrical permittivity	2.5	
Relative permeability	1	
Thickness	0.002	m

A.1.3 Collector equivalent circuit

The collector equivalent circuit consists on a $\pi-$section. Its parameters are given in Table A.3.

Table A.3: Collector equivalent circuit, $\pi-$section.

Parameter	Value	Unit
Impedance, Z		
Resistance, R	0.68	Ω
Reactance, X	1.62	Ω
Admittance, Y		
Conductance, G	0	S
Susceptance, B	1.53	mS

A.2 Transformer Parameters

The OWPP test model is equipped with several transformers as there are several voltage levels in the power plant. The first transformer raises the export cable voltage, 220 kV, to the AC transmission system voltage, 400 kV. Thereby, it interfaces the OWPP with the grid. Besides the IBESS is connected through a 33/220 kV transformer, while the Offshore power collection is done at 66 kV. WT generators are normally operated at LV, thus each WT is equipped with a 0.690/66 kV step-up transformer. Table A.4 present the parameters for each of the transformers in the OWPP model.

Table A.4: Transformer parameters

Transformer	Grid	IBESS	Collector	WT
Voltage ratio [kV/kV]	400/220	33/220	220/66	66/0.690
Configuration	Y/Yn	Δ/Yn	Yn/Δ	Δ/Yn
Power rating [MVA]	475	112	270	72
Series resistance [pu]	0.002	0.002	0.002	0.002
Series reactance [pu]	0.1	0.12	0.1	0.09
Core losses [pu]	0.002	0.0025	0.002	0.007
Magnetizing current [pu]	0.005	0.005	0.005	0.005
Air core reactance [pu]	0.2	0.24	0.2	0.25
Knee point voltage [pu]	1.17	1.17	1.17	1.17

A.2.1 WT Transformer Magnetization Curves

Transformer saturation. The following saturation characteristic is obtained by measuring the magnetizing current and flux linkage at the LV side. Figure A.1 represents the saturation when measuring these magnitudes in phase "a", during energization with remanent flux (recall Section 4.5.4). The rest of the phases would follow a similar behaviour.

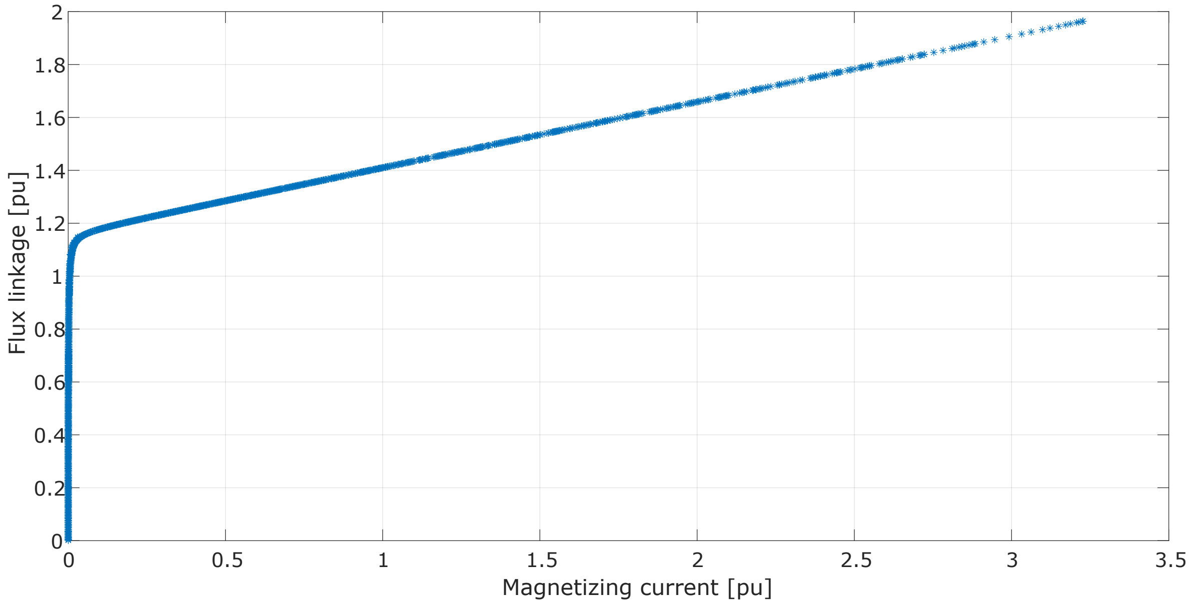

Figure A.1: Transformer saturation curve ($I_{base} = 85.2\,\text{kA}$ and $\Phi_{base} = 1.8\,\text{Wb} - \text{N}$)

Appendix B

GFL and GFM Controllers Design

In this appendix the development of the controllers that were utilized in the project is explained with more detail. It intends to serve as a guideline for students or engineers that pursue the design of these regulators.

B.1 Wind Turbine Controller

This controller is based on vector current control in the *dq*-frame. Figure B.1 shows an schematic of the WT model and the measuring points for voltage and current. Voltage is measured before the transformer, v_o while the current coincides with the converter current, i_c.

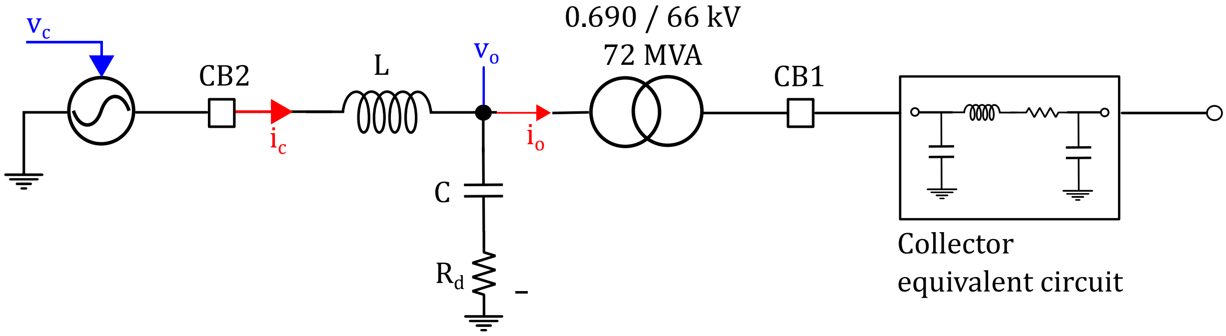

Figure B.1: WT Model and measuring points.

On the other hand, Fig. B.2 shows the block diagram of the controller and the plant. The plant is simply an *RL* circuit, where *L* is the filter inductance and *R* is a small resistance accounting for the losses in the main reactor of the filter.

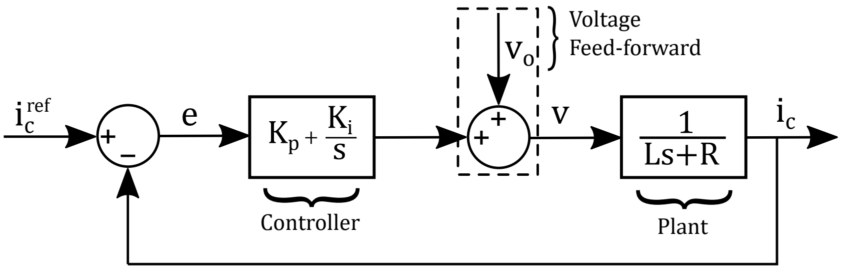

Figure B.2: Control diagram.

.

The design of the controller follows the pole cancellation technique. The objective is to get a critically damped closed loop transfer function, so it has the following expression:

$$G_{CL}(s) = \frac{\alpha_{CL}}{s + \alpha_{CL}} \tag{B.1}$$

being α_{CL} the desired closed loop bandwidth. Consequently, the open loop transfer function needs to be:

$$G_{OL}(s) = \frac{\alpha_{CL}}{s} \tag{B.2}$$

Considering the open loop transfer function of the system in Fig. B.2, and reordering terms,

$$G_{OL}(s) = \frac{K_p s + K_i}{s} \frac{1}{Ls + R} = \frac{K_p}{Ls} \cdot \frac{s + \frac{K_i}{K_p}}{s + \frac{R}{L}} \tag{B.3}$$

being K_p and K_i the proportional and integral gains of the controller. Therefore, to obtain (B.2), the gains should be:

$$K_p = \alpha_{CL} \cdot L \tag{B.4}$$

$$K_i = \alpha_{CL} \cdot R \tag{B.5}$$

At this point α_{CL} should be determined. The selection of this parameter is closely related to the converter switching frequency, f_{sw}, and should be defined as, [45]:

$$\alpha_{CL} \leq 0.2 \cdot 2\pi f_{sw} \tag{B.6}$$

Apart from (B.6), the designer has to consider the resonances of the LCL filter. In the case shown in Fig. B.1, the LCL filter resonances are damped by the resistance R_d, so it is safe to only utilize (B.6). If this resistance did not exist, it would be necessary to select a bandwidth sufficiently below the LCL resonant frequency to avoid oscillations. Other option is to utilize an active resistance in the controller as it is explained in [57].

Furthermore, the implementation presented in this project considered voltage feed-forward in the current controller output. Normally, with voltage feed-forward, the integral gain is not necessary or it is very small. The latter option is taken to avoid the steady state error that the small voltage drop in the filter resistance, R, would generate.

The calculation of the converter current reference is done by solving the power equations in the *dq*-frame.

$$P = \frac{3}{2}\left(v_{o,d} i_{c,d} + v_{o,q} i_{c,q} + 2 v_0 i_0\right) \tag{B.7}$$

$$Q = \frac{3}{2}\left(v_{o,q} i_{c,d} - v_{o,d} i_{c,q}\right) \tag{B.8}$$

The synchronization of the WTs is made through a PLL that sets $v_{o,d} = V$ and $v_{o,q} = 0$, being V the peak value of the phase to ground voltage. Considering that the voltage is balanced, thus the zero components are zero, $v_0 = i_0 = 0$, the reference currents are calculated as:

$$i_{c,d}^{ref} = \frac{2}{3} \frac{P^{ref}}{v_{o,d}} \tag{B.9}$$

$$i_{c,q}^{ref} = \frac{2}{3} \frac{Q^{ref}}{v_{o,d}} \tag{B.10}$$

where P^{ref} and Q^{ref} are the reference active and reactive power, respectively that result from the sum of the WT power reference set points and the P-f and Q-V droops.

Droop controllers

Finally, the last part of the WT controller is the P-f and Q-V droops that are useful to support the stability of the system both in grid-connected mode or in islanded mode. Both controllers are developed in per unit as a proportional gain and a first order transfer function than represents a delay:

$$Droop = \frac{K}{1+Ts} \tag{B.11}$$

For the P-f droop, K is taken similar to the one utilized for synchronous generators, $K = \frac{1}{R} = \frac{1}{0.05} = 20\,\mathrm{p\,u}$, [49]. If a synchronous generator wants to be imitated, then the time constant T has to resemble the time to move a mechanical valve or governor. Regarding the Q-V droop K is selected between 0.5 to 1 p u , which means that a change of 1 p u in the voltage amplitude would generate a change in reactive power of 0.5 or 1 p u respectively. The time constant for the Q-V droop can be faster than for the P-f droop as, taking the synchronous machine as reference, the speed of excitation control is not limited by mechanical devices.

Notice that the droops are in per unit, so their outputs must be multiplied by the base apparent power, S_b, so as to be utilized in the current controller. The output of the droops is summed to the WT power set points to obtain P^{ref} and Q^{ref}. Overall, the resulting controller is shown in Fig. B.3.

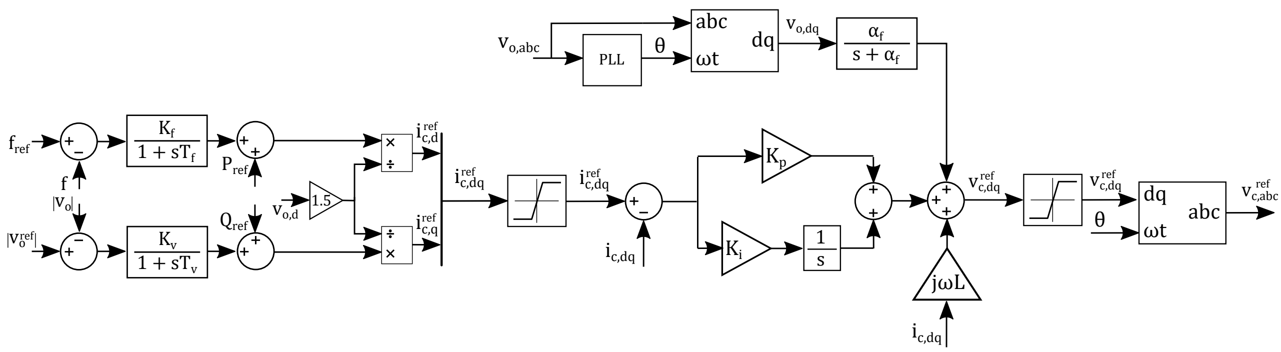

Figure B.3: Implemented WT controller.

.

B.2 IBESS Controller

The IBESS was operated under two different GFM control schemes: PSC and VSM. Nevertheless, the IBESS model was identical for both controllers, and it is shown in Fig. B.4. The measuring points for the controller implementation are v_o for the voltage and i_c for the current.

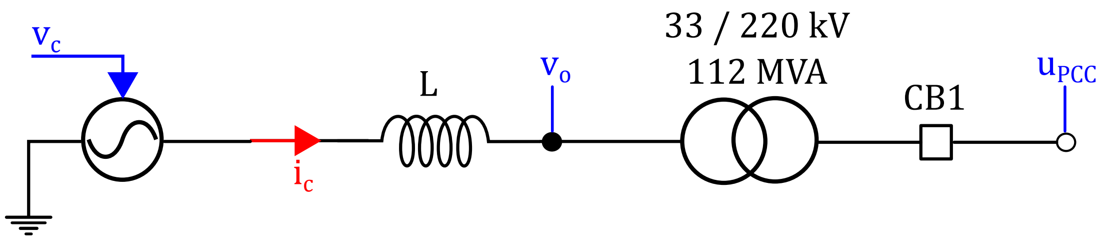

Figure B.4: IBESS model and measuring points.

In the following subsections a more detailed explanation of how to get the controller parameters is given. The AVC is not elaborated further as it consists on a simple droop, and was sufficiently explained in the main report.

B.2.1 Virtual Synchronous Machine

The VSM consists of the power synchronization loop and the cascaded PI controllers for the voltage and current control.

Power Synchronization Loop

The development of the power synchronization loop is tied to the swing equation, (B.12), which was explained in Section 6.2.1. Besides, the controller block diagram is depicted in Fig. B.5

$$M \cdot \frac{d\omega_g}{dt} = P_{ref} - P - K_d \cdot (\omega_g - \omega_f) - K_g \cdot (\omega_1 - \omega_g) \tag{B.12}$$

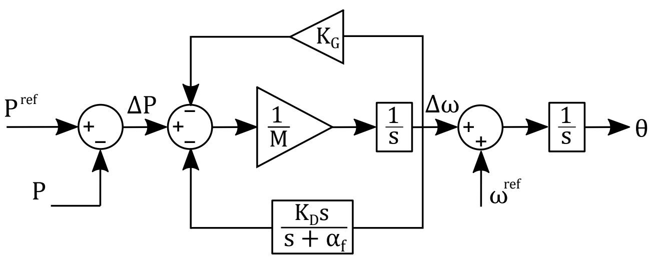

Figure B.5: Power synchronization loop, with virtual inertia and damping terms.

From (B.12) it is clear that M, K_g, K_d and α_f need to be defined. M is the virtual inertia scaled by ω_1, and it is determined by (B.13), [44]. The degree of freedom is the inertia constant, H that is measured in seconds. ω_1 corresponds to the nominal frequency of the system, while S_b is the base apparent power of the converter providing the virtual inertia. For the IBESS, it is considered that $S_b = 50\,\text{MW}$, which is the rating of the battery. This decision is based on the fact that the battery is responsible for the active power supply from the IBESS. Selecting an $H = 5\,\text{s}$, M is equal to:

$$M = \frac{2S_bH}{\omega_1} = \frac{2 \cdot 50 \cdot 5}{2\pi 50} = 1.59\,\text{MWs}^2/\text{rad} \tag{B.13}$$

The next parameter to determine is the frequency droop, K_g. It is defined as (B.14) and the degree of freedom is R. Typical for synchronous generators is, $R = 0.05$, [49]. However, for the purpose of BS, an $R = 0.02$ turned out to give faster settling time and lower overshoot. The risk of selecting $R = 0.02$ is the possible saturation of the battery, as a change in frequency of 1 Hz would lead to a change in power of $\Delta P = 50\,\mathrm{MW}$.

$$K_g = \frac{S_b}{R\omega_1} = \frac{50}{0.02 \cdot 2\pi 50} = 7.96\,\mathrm{MWs/rad} \tag{B.14}$$

Finally, the damping term must be selected. A compromise between RoCoF and settling time is needed. High values of K_d would help reducing the RoCoF, but it would extend the settling time. Besides, the cutoff frequency α_f should be sufficiently small to damp any oscillation at and above the fundamental frequency. Aiming to achieve both objectives, in this project $K_d = 8\,\mathrm{MWs/rad}$ and $\alpha_f = 20\,\mathrm{rad/s}$ are chosen.

Cascaded voltage and current controller

The controller block diagram is shown in Fig. B.6. The current controller is identical to the one shown in Section B.1, so the reader should follow exactly the same procedure to set the gains K_{pi} and K_{ii}.

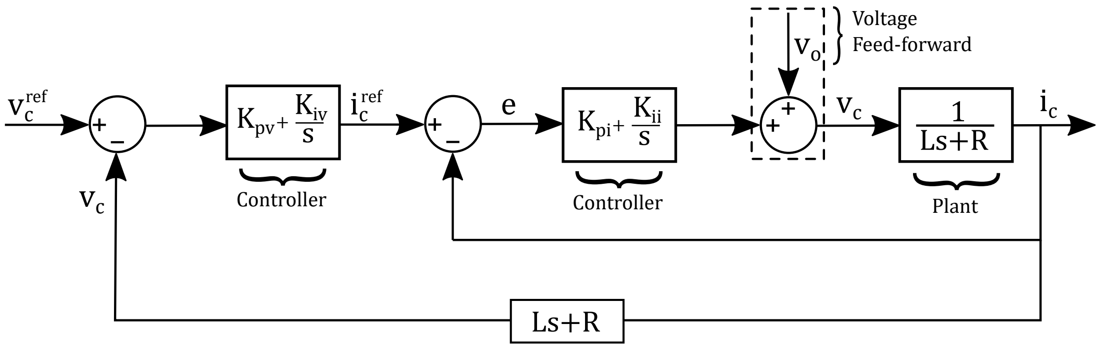

Figure B.6: Control diagram.

.

Regarding the voltage controller, it can be considered that its plant is the previously defined current regulator. Recall that the objective of the pole cancellation technique was to achieve a critically damped system with a closed loop transfer function as (B.1). Therefore, the open loop transfer function of the voltage controller is:

$$G_{OL}(s) = \frac{K_{pv}s + K_{iv}}{s}\frac{\alpha_{CL,i}}{s + \alpha_{CL,i}} \tag{B.15}$$

being $\alpha_{CL,i}$ the current controller bandwidth. Recall that this parameter was limited by the converter switching frequency as $\alpha_{CL,i} \leq 0.2 \cdot 2\pi f_{sw}$. The tuning criteria of the voltage controller is based on the Modulus optimum, [52], and consists in cancelling the dominant pole of the plant. In this case this is obtained for:

$$K_{pv} = \alpha_{CL,v} \cdot \frac{1}{\alpha_{CL,i}} \tag{B.16}$$

$$K_{iv} = K_{pv} \cdot \alpha_{CL,i} = \alpha_{CL,v} \tag{B.17}$$

where $\alpha_{CL,v}$ is the desired closed loop bandwidth of the voltage controller. To avoid unwanted interactions, it must be at least one decade below the current control bandwidth, therefore:

$$\alpha_{CL,v} \leq 0.02 \cdot 2\pi f_{sw} \tag{B.18}$$

Finally, the implemented controller is shown in Fig. B.7. To obtain the converter voltage reference, $v_{c,dq}$, an active resistance term, $R_a \cdot i_{c,dq}$ is subtracted. The recommended value for this parameter is given in Section B.2.2.

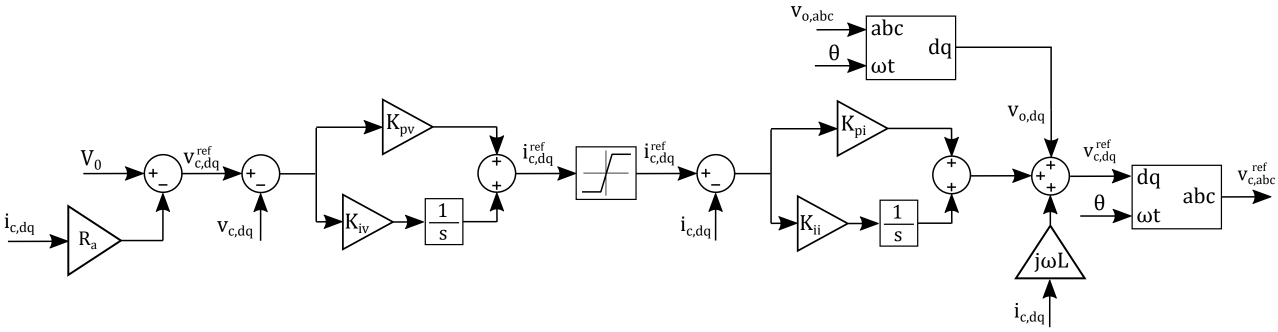

Figure B.7: Implemented cascaded controllers.

.

B.2.2 Power Synchronization Control

The PSC control scheme consist of a power synchronization loop and a current limiting control. The latter regulator utilizes an active resistance to damp oscillations and reduce the sensitivity to small disturbances (Recall Fig. 3.7). Its value, R_a, is tied to the bandwidth of the controller, achieving a slow convergence time if R_a is very large. The authors in [44] recommend,

$$R_a \leq 0.2\,\mathrm{p\,u} \tag{B.19}$$

Furthermore, in the implementation from [32] the active resistance consists in a high pass filter of gain R_a. In order to make the high pass filter converge to R_a for almost all the frequency range, the cutoff frequency has to be negligible. Therefore, it is recommended $\omega_b \leq 0.1 \cdot \omega_1$.

Power Synchronization Loop

In the GFM controller developed in [32], the power synchronization loop consists in a droop gain and a single integrator to obtain the phase angle θ. Figure B.8 shows this implementation.

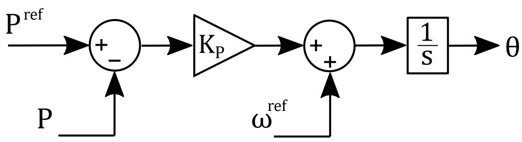

Figure B.8: Power Synchronization Loop.

The degree of freedom is the droop K_p which determines the frequency change, $\Delta\omega$ when there are power variations ΔP. Its value is also tied to the stability of the closed loop system. To obtain a sufficiently stable system, the authors in [44], recommend to select K_p as:

$$K_p = \frac{\omega_1 R_a}{\kappa V^2} \tag{B.20}$$

where V is the amplitude of the converter phase voltage. κ is the scaling factor, which for peak value vector scaling is equal to $\frac{3}{2}$. Note that if R_a is given, K_p is determined, as ω_1, κ and V are intrinsic parameters of the model than cannot be modified by the designer. In the project, an $R_a = 0.075\,\mathrm{p\,u}$ was selected ($S_b = 112\,\mathrm{MVA}$ and $V_b = 33\,\mathrm{kV}$, which gives an $R_a = 0.73\,\Omega$). So, the power synchronization loop gain is:

$$K_p = \frac{2 \cdot 2\pi 50 \cdot 0.73}{3 \cdot 26.944^2} = 0.21\,\mathrm{rad/MWs} \tag{B.21}$$

Current limiting controller

The design of the current limiting controller proposed in [32] is special as it is designed to act only when the converter is overloaded. This is evident from the voltage control law, (B.24) and the current reference calculation (B.23).

$$v_{c,dq}^{ref} = \alpha_{CL} L(i_{c,dq}^{ref} - i_{c,dq}) + j\omega_1 L i_{c,dq} + v_{o,dq} \tag{B.22}$$

$$i_{c,dq}^{ref} = \frac{1}{\alpha_{CL} L}\left(V_0 - v_{o,dq} - j\omega_1 L i_{c,dq} - \frac{R_a s}{s+\omega_b} i_{c,dq}\right) + i_{c,dq} \tag{B.23}$$

If $i_{c,dq}^{ref}$ does not get limited, most of the terms in (B.24) get cancelled, remaining only:

$$v_{c,dq}^{ref} = V_0 - \frac{R_a s}{s+\omega_b} i_{c,dq} \approx V_0 - R_a i_{c,dq} \tag{B.24}$$

From these equations, it is evident that the only degree of freedom is the closed loop bandwidth, α_{CL}, as the rest of the terms are parameters of the model or the system that cannot be changed. Therefore, α_{CL} is selected following (B.6). Finally, the implemented controller is depicted in B.9

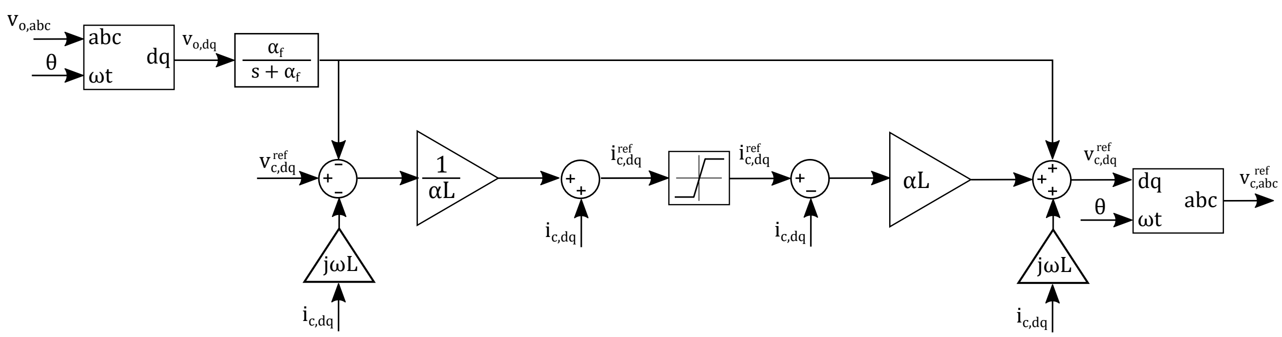

Figure B.9: Current Limiting Controller.